
Noise Induced Processes in Neural Systems



Peter Roper

Ph.D. in Mathematics
Nonlinear and Complex Systems Group
Department of Mathematical Sciences
Loughborough University - 1998

Noise Induced Processes in Neural Systems

by

Peter Roper

A Doctoral Thesis

Submitted in partial fulfillment of the requirements

for the award of

Ph.D. in Mathematics of Loughborough University

November 1998

©by Peter Roper 1998

Certificate of Originality

This is to certify that I am responsible for the work submitted in this thesis, that the original work is my own except as specified in acknowledgments or in footnotes, and that neither the thesis nor the original work contained therein has been submitted to this or any other institution for a higher degree.

..... (Signed)

..... (Date)

“Let this voluntary confession forestall any future criticism: I am writing about things entirely outside my own experience or anyone else’s, things that have no reality whatsoever.”

Lucien – The True History

Abstract

Real neurons, and their networks, are far too complex to be described exactly by simple deterministic equations. Any description of their dynamics must therefore incorporate noise to some degree. It is my thesis that the nervous system is organized in such a way that its performance is optimal, subject to this constraint. I further contend that neuronal dynamics may even be enhanced by noise, when compared with their deterministic counter-parts.

To support my thesis I will present and analyze three case studies. I will show how noise might (i) extend the dynamic range of mammalian cold-receptors and other cells that exhibit a temperature-dependent discharge; (ii) feature in the perception of ambiguous figures such as the Necker cube; (iii) alter the discharge pattern of single cells.

Acknowledgements

Unfortunately it is traditional at this point to thank one's partner and one's supervisor. I say unfortunate since tradition tends to become trite and so limits my ability to express the overwhelming gratitude that I now feel toward them both.

Michelle: it's been a long time since we sat in the sun on Fountain's Fell and decided that maybe programming for a bunch of cowboys wasn't all it was cracked up to be. If it wasn't for you I'd still be humming "Rawhide" and fighting the Cambridge rush hour every morning – thanks for the past four years, and most importantly thanks for the past six months. It's now time to turn the tables!

Paul: the only Ph.D. supervisor that I've ever encountered who truly comprehends what it means to 'supervise'. Thank you for all of the inspiration, the guidance, and for the friendship that you've shown me. But most importantly thank you for giving me enough rope (but not too much).

Three years have left more debts of gratitude than will fit on a couple of sides of A4. However, further thanks (in no particular order) are due to Steve Coombes (as always), to Martin Elliffe (for C that verges on prose), to Ras Petersen (for curbing the worst excesses of my thesaurus use), to Keith Watling (a man whose blind devotion to Mac's doesn't get in the way of running the best damned computer network that I've ever had the pleasure of relying on – something that I come to appreciate even more with distance), to Hazel, Jo, Helen and the rest of the staff in room W183 (the people who really run this department), to André Longtin (for answering dumb questions with good grace), and to David Brown and the Babraham Institute (for allowing me enough leeway to finish this thing).

My two previous theses were written under the *aegis* of my four parents and my brother. Once more all five have listened patiently to three years of complaints and have unstintingly supported me, and I'm more grateful to them than ever. I now have another two parents: Marie and Bill – welcome to my acknowledgements page, thank you for all of the late night (GMT) email encouragement over the past months, and also for your very generous

hospitality during my visits.

I want too to extend my thanks to Loughborough University for funding my studies via a University studentship, to the trustees of the John Phillips Guest Travel Scholarship for paying for a trip across the Atlantic to complete chapter three, and to Clive Pugh for rustling up occasional sums to cover trips when all other avenues had been exhausted. I spent almost five years trying to find funding for this thesis, and am fully aware that in this current economic climate a willingness to fund any academic endeavour is an admirable thing indeed.

I'd also like to take this opportunity to wish a plague on the first-born of each of the team responsible for 'developing' Adobe Illustrator 7¹ and 'porting' it to NT. It is the worst piece of software that I have ever been unlucky enough to use. Unfortunately I'm unlikely to get my wish, but a good alternative would be to re-locate the company to Reykjavik. If only they knew how much late-night profanity (and how little postscript) their product has generated.

In contrast, I'd like to sing the praises of 'WinEdt', the \LaTeX front-end written by Alexander Simonic. A masterpiece!

¹Version 8 isn't much better, if you were wondering.

Contents

0	Preface	1
1	A review of concepts and tools	4
1.1	Noise	4
1.2	The master equation	7
1.3	The Fokker–Planck equation	10
1.3.1	Stationary solutions	12
1.4	Kramers’ rate theory	13
1.4.1	Escape in multi–dimensional potentials	16
1.5	Stochastic Resonance	16
1.5.1	A <i>bona–fide</i> resonance	19
1.5.2	The inter–spike interval histogram	22

1.5.3	Biological SR	22
2	The origins of neuronal noise	24
2.1	Neuronal structure and function	24
2.1.1	Cellular physiology	24
2.1.2	Electro-physiology	25
2.1.3	Cytology	26
2.1.4	Chemical messengers and synaptic transmission	28
2.1.5	Action potential generation	29
2.2	Neuronal noise	32
2.2.1	Aleatory synaptic function	33
2.2.2	Fluctuations of the membrane potential	33
2.2.3	Randomness in spike generation	35
2.3	Discussion	38
3	A temperature-dependent cold receptor model	39
3.1	Introduction	39
3.2	A summary of the neuro-physiology of cold receptors	41
3.3	A temperature-dependent phase model of a cold receptor	48
3.3.1	Ermentrout and Kopell's canonical bursting model	48

3.3.2	A temperature–dependent phase model	52
3.3.3	Modeling temperature dependence and fluctuations	55
3.4	Analysis of bursting and beating	56
3.4.1	The deterministic limit ($D \rightarrow 0$) – the Strutt map	59
3.4.2	Stochastic dynamics of bursting and beating – smoothing the Mathieu staircase	65
3.5	Analysis of the near–threshold regime – noise enhanced stability and resonance	68
3.5.1	Stability and trapping for $T < T_1$	69
3.5.2	Resonance for $T > T_1$	71
3.6	Discussion	74
3.6.1	Paths for other receptors	74
3.6.2	Chaos	74
3.6.3	Noise distributions	74
3.6.4	Asymmetric burst patterns	75
3.7	Conclusions	75
4	The perception of ambiguous images	76
4.1	Introduction	76
4.2	Stochastic resonance in cognition	79

4.2.1	Riani and Simonotto's experiment	80
4.2.2	Chialvo and Apkarian's experiment	81
4.3	A cognitive model of the perceptual process	82
4.4	Haken's competitive network	84
4.4.1	Network dynamics	84
4.4.2	Stochastic dynamics of the Haken model	88
4.5	The diffusive Haken model	92
4.5.1	Stochastic dynamics of the driven diffusive model	95
4.6	Discussion	100
5	Neuronal dynamics with intrinsic noise	102
5.1	A deterministic leaky-integrate-and-fire neuron	102
5.1.1	Continuous time formalism	102
5.1.2	Discrete time formalism	104
5.1.3	Single neuron dynamics	106
5.2	Intrinsic noise	107
5.2.1	Synaptic noise	108
5.2.2	Threshold noise	109
5.3	Stochastic dynamics	109

5.3.1	Heuristic results	110
5.3.2	Fokker–Planck analysis	112
5.4	Noisy dynamics in an effective potential	115
5.4.1	Deterministic sub–system and the critical temperature	115
5.4.2	The effective potential	116
5.5	Periodic Modulation and Response	119
5.6	Discussion	122
6	Conclusions	124
A	A Few Theorems	128
A.1	Floquet’s theorem	128
A.2	Multistability in networks of weakly coupled bistable units – the anti–continuum limit	131
A.2.1	Continued solutions of the diffusive Haken model	132
B	Numerical Issues	134
B.1	Random and pseudo–random number generators	134
B.1.1	Transformation methods and non–uniform deviates	136
B.2	Numerical simulation of noisy dynamical systems	139

Chapter 0

Preface

“**noise** (*Telecomm.*). (1) In general, any unwanted disturbance super-imposed on a useful signal and tending to obscure its information content.” [Wal91]

Most definitions of noise tend to the negative. Noise is too often seen as disruptive and as something to be minimized or restricted. It is my contention that this narrow view is often not applicable to neural systems. The theme that runs through this thesis is that noise can assist the entrainment of a dynamical system to a weak periodic forcing, and a *leitmotif* is the quantification of this phenomena by a measure due to Gammaitoni *et al.* [GMS95].

Outline

After a preliminary discussion of some relevant techniques and neuro-physiology, this thesis tackles three topics, which represent three levels of the hierarchy by which information processing may be supposed to occur in the brain.

Noise and the single cell: In chapter 3 I present a tractable stochastic phase-model of the temperature sensitivity of a mammalian cold receptor. These cells are free nerve endings that exhibit a highly temperature-dependent discharge pattern. The neuro-physiological evidence supports a simple model that comprises a slow oscillation of the neuronal mem-

brane potential coupled to some noise source. I first show how this simple model may derive from more complete models, such as those based on the dynamics of ion channels. Using simple linear dependencies on temperature of the model's parameters, I then show that this model can reproduce the experimentally observed transitions between bursting, beating and stochastically phase-locked firing patterns. I analyze the model in the deterministic limit and predict, using Floquet theory and the Strutt map, the number of spikes-per-burst for a given temperature. The inclusion of noise produces a variable number of spikes-per-burst, and also extends the dynamic range of the neuron, both of which are analyzed in terms of the Strutt map. I also characterize the noise-induced trapping and stochastic resonance effects that appear near the onset of deterministic firing.

Noise at the network level: Chapter 4 represents my work on a model for the perceptual interpretation of ambiguous figures. An ambiguous figure is one that admits two or more perceptual alternatives (a common example is the Necker cube). It is known that an observer studying such a figure over a long time period, finds that his (or her) interpretation of the figure randomly and continually switches between the possible alternatives. This phenomena is called reversal. I introduce a simple model, due to Haken [Hak91], that may be considered as a model for the interpretive process and I examine how this model may be extended to describe reversal. When the ambiguous figure is periodically modulated in some manner, reversal can become entrained to the modulation in a way that resembles stochastic resonance. I show how a similar noisy-resonance phenomenon can occur in Haken's model, and I further show that at resonance, the theoretical transition rate between states matches the driving frequency. I further show that this effect persists when a diffusive coupling is introduced into the network, a technique that leads to a more robust system.

Sub-cellular processing in the presence of noise: I develop, in chapter 5, a simple model of a spiking neuron that displays threshold and quantal synaptic noise. I show analytically that there are parameter regimes for which these two types of noise generate an effective asymmetric-bistable potential function for the dynamics. The two stable states of the potential correspond to a de-polarized bursting state and to a hyper-polarized quiescent state, and the membrane potential of the neuron executes a random walk between them.

Thus, noise can fundamentally alter the neuronal discharge from a simple spiking regime to a regime of highly-correlated bursts. The parameters of the noise distributions alter the shape of the generalized potential, and hence also characteristics of the discharge pattern. Increasing synaptic noise increases the length of the burst, while increasing the threshold noise increases the interval between bursts. Finally I show that a weak periodic modulation of the system induces stochastically phase-locked transitions from the quiescent to the bursting state, and the transition rate exhibits a form of stochastic resonance.

Theory should never be presented without some form of supportive experimental evidence. In this work, such evidence is provided by numerical simulations and so the thesis concludes with an appendix that discusses the numerical techniques that I have used.

Chapter 1

A review of concepts and tools

To avoid disrupting the thread of a later narrative, I wish to review here some useful mathematical tools and concepts.

1.1 Noise

The term *noise* describes fluctuations in some parameter that derive from non-deterministic behaviour¹. To indicate briefly possible physical origins of noise, I wish to sidestep a philosophical red herring and to draw an analogy with the equilibrium thermodynamics and statistical physics of a classical, ideal gas².

Each individual atom of an ideal gas may be considered as a point particle that moves chaotically but deterministically. A mole of such a gas comprises $\sim 10^{23}$ atoms, all of which are in motion. The equilibrium properties of the gas are well described by a small number of macroscopic parameters such as the pressure and temperature. These state variables derive from the collective motion of the atoms, and their equilibrium values are functions

¹The spin-glass paradigm of neural systems [Hop82] has fostered the terminology of ‘fast’ and ‘slow’ noise. All fluctuations considered by this thesis operate on similar time-scales to that of their corresponding system’s dynamics and so are fast noise.

²The extension to a quantum description merely includes a further source of randomness.

of the mean positions and momenta of the atomic ensemble. However, close examination of the state variables shows that they are not truly constant but in fact fluctuate rapidly about some average value. These statistical distribution of these fluctuations is generally well-defined, with a variance D that is given by Einstein's fluctuation-dissipation relation

$$D = \frac{2kT}{f} \quad (1.1)$$

where T is the absolute temperature, and f the viscosity of the gas. Therefore, even though fluctuations in the state variables might have a deterministic origin at the atomic level, their macroscopic effects can only be analysed statistically.

To continue the analogy, biological systems such as neurons comprise many interacting subsystems. Facets of their behaviour may be also described by macroscopic state variables, *e.g.* neurotransmitter release rate. Neural description based on these state variables either neglects or approximates much of the sub-cellular processing and so it is unsurprising that such coarse-grained approximations must incorporate noise to some degree.

Noise falls naturally into two categories: external and internal noise³. External noise is caused by some force acting upon the system under investigation. Its archetype is Brownian motion, whereby the collective, stochastic motions of microscopic molecules cause the random trajectory of a macroscopic pollen particle. External noise acts as an imposed force, and it is not affected by the system's dynamics. Mathematically, it enters the dynamical equations via additive coupling and (in principle) can be switched off. Internal noise derives from fluctuations inherent to the system. It is intimately related to the system's evolution, and is best described mathematically by a multiplicative term.

Within this thesis I will consider non-inertial systems subject to an external noise, $\zeta(t)$, and so described by Langevin equations of the general form

$$\frac{d}{dt}x(t) = F(x, t) + \zeta(t) \quad (1.2)$$

³More properly, the distinction between external and internal noise is somewhat artificial and depends upon how one designates the boundaries of the system.

where $x(t)$ is some state variable.

A randomly fluctuating variable $\zeta(t)$ is completely specified by its temporal correlation⁴ and by its probability distribution $P(\mathcal{X}) \equiv P(\zeta(t) = \mathcal{X})$. Where $P(\mathcal{X})$ is the probability that at a time t , ζ takes the value \mathcal{X} . The determination of the probability distribution of a real, physical system is generally achieved by fitting a curve to a set of measurements taken from different realizations of the system. However, such a technique is not always reliable or accurate, and more often all that can be ascertained about the distribution are its moments, *e.g.* the mean, the variance and the kurtosis. These quantities are not very informative about the underlying dynamics, instead a more useful object is the auto-correlation function, defined by

$$G(t' - t) = \lim_{T \rightarrow \infty} \frac{1}{T} \int_0^T dt x(t)x(t') \quad (1.3)$$

this is the temporal average of a two time product, measured over an arbitrary time T which is then allowed to become infinite. There exist many techniques for measuring approximations to the auto-correlation (see *e.g.* [DeF81]). Furthermore, from the Wiener-Khinchin theorem (see *e.g.* [vK92]), the power spectral density (PSD), $S(f)$, of a stationary process⁵ is given by the Fourier transform of its auto-correlation function, so that

$$S(f) = \frac{2}{\pi} \int_0^\infty dt \cos(ft)G(t) \quad (1.4)$$

(since the auto-correlation function is an even function, the Fourier transform may be replaced by a cosine transform). The PSD describes the frequency distribution of the power in the random signal $x(t)$. The simplest (and hence possibly the least physical) noise source is Gaussian noise: at a time t , $\zeta(t)$ is drawn from the distribution

$$\mathbb{N}(\zeta, \sigma) = \frac{1}{\sqrt{(2\pi\sigma^2)}} \exp\left(-\frac{(\zeta - m)^2}{2\sigma^2}\right) \quad (1.5)$$

⁴Extended systems may also display spatially correlated noise but this will not be considered here.

⁵*i.e.* a system whose fluctuations are drawn from a distribution with time-invariant moments.

Gaussian noise therefore has mean m and is delta-correlated, so that

$$\langle \zeta(t) \rangle = m \quad \text{and} \quad \langle \zeta(t)\zeta(t') \rangle = \sigma^2 \delta(t - t') \quad (1.6)$$

a Fourier transform of its auto-correlation function is therefore a constant over the entire spectrum. By analogy with light, Gaussian noise is therefore also called *white* noise.

1.2 The master equation

A stochastic process, $\zeta(t)$, is called Markovian if the probability that is in a given state at a time t_2 is deducible from the knowledge of its state at a previous time t_1 , but is independent of its history before t_1 (see appendix B.2 for a more rigorous definition).

Some definitions for the stochastic process $\zeta(t)$

- $p_1(\mathcal{X}_1, t_1)$ is the probability density that $\zeta(t)$ takes the value \mathcal{X}_1 at a time t_1 .
- $p_2(\mathcal{X}_1, t_1; \mathcal{X}_2, t_2)$ is the joint probability density that $\zeta(t)$ takes the value \mathcal{X}_1 at a time t_1 , and the value \mathcal{X}_2 at a time t_2 .
- $p_n(\mathcal{X}_1, t_1; \mathcal{X}_2, t_2; \dots; \mathcal{X}_n, t_n)$ is the joint probability density that $\zeta(t)$ takes the value \mathcal{X}_1 at a time t_1 , the value \mathcal{X}_2 at a time t_2 , ... and the value \mathcal{X}_n at a time t_n .
- $p_{1|1}(\mathcal{X}_2, t_2 | \mathcal{X}_1, t_1)$ is the conditional probability density that $\zeta(t)$ takes the value \mathcal{X}_2 at a time t_2 , given that it takes the value \mathcal{X}_1 at a time t_1 .
- $p_{1|n-1}(\mathcal{X}_n, t_n | \mathcal{X}_1, t_1, \dots, \mathcal{X}_{n-1}, t_{n-1})$ is the conditional probability density that $\zeta(t)$ takes the value \mathcal{X}_n at a time t_n , given that it takes the value \mathcal{X}_{n-1} at a time t_{n-1} , ... and the value \mathcal{X}_1 at a time t_1 .

where the conditional probability density $p_{1|1}(\dots | \dots)$ is defined by

$$p_{1|1}(\mathcal{X}_2, t_2 | \mathcal{X}_1, t_1) = \frac{p_2(\mathcal{X}_1, t_1; \mathcal{X}_2, t_2)}{p_1(\mathcal{X}_1, t_1)} \quad (1.7)$$

and is also referred to as the ‘transition probability’ from state \mathcal{X}_1 to \mathcal{X}_2 .

The Markov property may therefore be abbreviated to

$$p_{1|n-1}(\mathcal{X}_n, t_n | \mathcal{X}_{n-1}, t_{n-1}, \dots, \mathcal{X}_1, t_1) \equiv p_{1|1}(\mathcal{X}_n, t_n | \mathcal{X}_{n-1}, t_{n-1}) \quad (1.8)$$

and so given the temporal hierarchy $t_3 > t_2 > t_1$ and using equation (1.7)

$$\begin{aligned} p_3(\mathcal{X}_1, t_1; \mathcal{X}_2, t_2; \mathcal{X}_3, t_3) &= p_2(\mathcal{X}_1, t_1; \mathcal{X}_2, t_2) p_{1|2}(\mathcal{X}_3, t_3 | \mathcal{X}_2, t_2, \mathcal{X}_1, t_1) \\ &= p_1(\mathcal{X}_1, t_1) p_{1|1}(\mathcal{X}_2, t_2 | \mathcal{X}_1, t_1) p_{1|1}(\mathcal{X}_3, t_3 | \mathcal{X}_2, t_2) \end{aligned} \quad (1.9)$$

Integration over all intermediate states \mathcal{X}_2 and division by $p_1(\mathcal{X}_1, t_1)$ gives the Chapman–Kolmogorov equation

$$p_{1|1}(\mathcal{X}_3, t_3 | \mathcal{X}_1, t_1) = \int d\mathcal{X}_2 p_{1|1}(\mathcal{X}_2, t_2 | \mathcal{X}_1, t_1) p_{1|1}(\mathcal{X}_3, t_3 | \mathcal{X}_2, t_2) \quad (1.10)$$

Subject to time–ordering, *i.e.* that t_2 lies between t_1 and t_3 , the Chapman–Kolmogorov equation states that the transition probability density from state \mathcal{X}_1 to state \mathcal{X}_3 is the integral (or sum) over all possible intermediate states of the probability of transition $\mathcal{X}_1 \rightarrow \mathcal{X}_2 \rightarrow \mathcal{X}_3$.

A differential equation for the probability density can be found by first integrating the Chapman–Kolmogorov equation w.r.t. \mathcal{X}_1 and re–labeling its indices, so that

$$p_1(\mathcal{X}_2, t_2) = \int d\mathcal{X}_1 p_{1|1}(\mathcal{X}_2, t_2 | \mathcal{X}_1, t_1) p_1(\mathcal{X}_1, t_1) \quad (1.11)$$

setting $t_2 = t_1 + \delta t$, then the time derivative of $p_1(\mathcal{X}, t)$ is given by

$$\frac{\partial}{\partial t} p_1(\mathcal{X}, t) = \lim_{\delta t \rightarrow 0} \frac{p_1(\mathcal{X}, t + \delta t) - p_1(\mathcal{X}, t)}{\delta t} \quad (1.12)$$

Evaluation of equation (1.12) requires computation of $p_{1|1}(\mathcal{X}_2, t_1 + \delta t | \mathcal{X}_1, t_1)$. Taylor expanding in powers of δt , and ensuring that normalization is preserved

$$p_{1|1}(\mathcal{X}_2, t_1 + \delta t | \mathcal{X}_1, t_1) = p_{1|1}(\mathcal{X}_2, t_1 | \mathcal{X}_1, t_1) + \delta t \frac{\partial}{\partial t} p_{1|1}(\mathcal{X}_2, t_1 | \mathcal{X}_1, t_1) + \dots \quad (1.13)$$

truncate at first order, and use the fact that $p_{1|1}(\mathcal{X}_2, t_1 | \mathcal{X}_1, t_1) = \delta(\mathcal{X}_2 - \mathcal{X}_1)$. Furthermore, note that the second term on the RHS, $\partial p_{1|1} / \partial t$, is made up of two parts – transitions **into** the state, and transitions **out** of the state. Define the transition probability density per–unit–time, $W_{t_1}(\mathcal{X}_1, \mathcal{X}_2)$, that the system changes from \mathcal{X}_1 to \mathcal{X}_2 within the time interval $t_1 \rightarrow t_1 + \delta t$, so that

$$\begin{aligned} p_{1|1}(\mathcal{X}_2, t_1 + \delta t | \mathcal{X}_1, t_1) &= \delta(\mathcal{X}_2 - \mathcal{X}_1) + W_{t_1}(\mathcal{X}_1, \mathcal{X}_2) \delta t \\ &\quad - \delta t \int d\mathcal{X} W_{t_1}(\mathcal{X}_1, \mathcal{X}) \delta(\mathcal{X}_2 - \mathcal{X}_1) \end{aligned} \quad (1.14)$$

substituting (1.14) into (1.11) and then into (1.12), one obtains

$$\frac{\partial}{\partial t} p_1(\mathcal{X}_2, t) = \lim_{\delta t \rightarrow 0} \frac{\delta t \int d\mathcal{X}_1 [p_1(\mathcal{X}_1, t_1) W_{t_1}(\mathcal{X}_1, \mathcal{X}_2)] - \delta t \int d\mathcal{X} [p_1(\mathcal{X}_2, t_1) W_{t_1}(\mathcal{X}_2, \mathcal{X})]}{\delta t}$$

re-labeling the second integral, so that $\mathcal{X} \rightarrow \mathcal{X}_1$, to arrive at the master equation

$$\frac{\partial}{\partial t} p_1(\mathcal{X}_2, t) = \int d\mathcal{X}_1 [p_1(\mathcal{X}_1, t_1) W_{t_1}(\mathcal{X}_1, \mathcal{X}_2) - p_1(\mathcal{X}_2, t_1) W_{t_1}(\mathcal{X}_2, \mathcal{X}_1)] \quad (1.15)$$

The master equation has the form of a balance equation. It gives the rate of change of the probability density due to transitions into the state \mathcal{X}_2 from all other states \mathcal{X}_1 , and transitions out of \mathcal{X}_2 into any other state \mathcal{X}_1 . The master equation is not only more tractable than the corresponding Chapman–Kolmogorov equation, but it is also easier to interpret physically.

1.3 The Fokker–Planck equation

A description that complements the Langevin approach of equation (1.2) is that of the Fokker–Planck equation. This partial differential equation is the equation of motion of the probability distribution $P(\mathbf{x}, t)$ of the state vector \mathbf{x} , and it derives from the master equation.

Express the transition probability $W(\dots)$ as a function of the size of the jump

$$W(\mathcal{X}', \mathcal{X}) \rightarrow W(\mathcal{X}'; r), \quad \text{with } r \equiv \mathcal{X} - \mathcal{X}' \quad (1.16)$$

so that the master equation becomes

$$\frac{\partial}{\partial t} p(\mathcal{X}, t) = \int dr W(\mathcal{X} - r; r) p(\mathcal{X} - r, t) - p(\mathcal{X}, t) \int dr W(\mathcal{X}; -r) \quad (1.17)$$

Assume that **only** small jumps occur, *i.e.* $\exists \delta > 0$, s.t.

$$W(\mathcal{X}'; r) \simeq 0 \quad \forall |r| > \delta \quad (1.18)$$

$$W(\mathcal{X}' + \Delta\mathcal{X}; r) \simeq W(\mathcal{X}; r) \quad \forall |\Delta\mathcal{X}| < \delta \quad (1.19)$$

and so the transition probability $W(\mathcal{X}'; r)$ is a strongly peaked function of r , but varies only slowly with \mathcal{X}' . Furthermore, assume that $p(\mathcal{X}, t)$ also varies slowly with \mathcal{X} . Consequently, the first integral of equation (1.17) can be dealt with by a Taylor expansion. To second order:

$$\begin{aligned} W(\mathcal{X} - r; r) p(\mathcal{X} - r, t) &\simeq W(\mathcal{X}; r) p(\mathcal{X}, t) - r \frac{\partial}{\partial \mathcal{X}} [W(\mathcal{X}; r) p(\mathcal{X}, t)] \\ &\quad + \frac{r^2}{2} \frac{\partial^2}{\partial \mathcal{X}^2} [W(\mathcal{X}; r) p(\mathcal{X}, t)] \end{aligned} \quad (1.20)$$

and so equation (1.17) becomes

$$\frac{\partial}{\partial t} p(\mathcal{X}, t) = \int dr W(\mathcal{X}; r) p(\mathcal{X}, t) - \int dr r [W(\mathcal{X}; r) p(\mathcal{X}, t)]$$

$$+ \int dr \frac{r^2}{2} \frac{\partial^2}{\partial \mathcal{X}^2} [W(\mathcal{X}; r)p(\mathcal{X}, t)] - p(\mathcal{X}, t) \int dr W(\mathcal{X}; -r) \quad (1.21)$$

the first and last terms on the RHS cancel, leaving the second–order Kramers–Moyal expansion of the master equation⁶.

Now introduce the ‘jump moments’ (*i.e.* the mean and variance of the fluctuations)

$$D^{(n)} = \int_{-\infty}^{\infty} dr r^n W(\mathcal{X}; r) \quad (1.22)$$

such that Kramers–Moyal expansion may be written

$$\frac{\partial}{\partial t} p(\mathcal{X}, t) = -\frac{\partial}{\partial \mathcal{X}} \left[D^{(1)}(\mathcal{X})p(\mathcal{X}, t) \right] + \frac{1}{2} \frac{\partial^2}{\partial \mathcal{X}^2} \left[D^{(2)}(\mathcal{X})p(\mathcal{X}, t) \right] \quad (1.23)$$

which is the one–dimensional Fokker–Planck equation. The coefficients, $D^{(1)}(\mathcal{X})$ and $D^{(2)}(\mathcal{X})$ are termed the *drift* and the *diffusion*, and since they are moments of the fluctuation distribution, the Fokker–Planck equation may be specified without any knowledge of the kernel $W(\dots)$. Thus, a Langevin system (1.2) subject to a Gaussian noise (1.6) has drift and diffusion

$$D^{(1)}(x) = \langle x \rangle = F(x) \quad \text{and} \quad D^{(2)}(x) = \langle x^2 \rangle = \sigma^2 \equiv D \quad (1.24)$$

In fact, for any one–dimensional system, there exists [Ris89] a change of variables, say $\mathcal{X} \rightarrow \mathcal{Y}$, that transforms any Fokker–Planck equation into one with a constant diffusion term, *i.e.* $D^{(1)}(\mathcal{X}) \rightarrow D^{(1)}(\mathcal{Y})$, $D^{(2)}(\mathcal{X}) \rightarrow D$.

The Smoluchowski equation

The Smoluchowski equation is a special case of the Fokker–Planck equation and describes the motion of an over–damped particle in a potential $U(x)$. It has drift and diffusion

⁶A theorem due to Pawula [Ris89] states that either the Kramers–Moyal expansion terminates at first or second order, or it does not terminate at all.

coefficients

$$D^{(1)}(x) = -\frac{d}{dx}U(x) \quad \text{and} \quad D^{(2)} = \sigma^2 \quad (1.25)$$

The multi-variate Fokker-Planck equation

For the case of M random variables, the Fokker-Planck equation generalizes to its multi-dimensional form [Gil96b]

$$\begin{aligned} \frac{\partial}{\partial t}P(\mathbf{x}, t) = & \sum_{i=1}^M \frac{\partial}{\partial x_i} \left[D_i^{(1)}(\mathbf{x}, t)P(\mathbf{x}, t) \right] + \frac{1}{2} \sum_{i=1}^M \frac{\partial^2}{\partial x_i^2} \left[D_i^{(2)}(\mathbf{x}, t)P(\mathbf{x}, t) \right] \\ & + \sum_{i,j=1, i < j}^M \frac{\partial^2}{\partial x_i \partial x_j} \left[D_{ij}^{(3)}(\mathbf{x}, t)P(\mathbf{x}, t) \right] \end{aligned} \quad (1.26)$$

1.3.1 Stationary solutions

The uni-variate Fokker-Planck equation (1.23) may be re-written as a continuity equation

$$\frac{\partial}{\partial t}p(x, t) = \frac{\partial}{\partial x} \left(-D^{(1)}(x) + \frac{1}{2} \frac{\partial}{\partial x} D^{(2)}(x) \right) p(x, t) = -\frac{\partial}{\partial x} \mathcal{J}(x, t) \quad (1.27)$$

where $\mathcal{J}(x, t)$ is a probability current.

Stationary solutions have a constant probability current. First, suppose that the current vanishes, so that $\mathcal{J}(x, t) = 0$. Integration of (1.27) yields

$$p_{st}(x) = \frac{2\mathcal{N}_0}{D^{(2)}(x)} \exp \left(2 \int_x \frac{D^{(1)}(x')}{D^{(2)}(x')} dx' \right) \equiv 2\mathcal{N}_0 \exp(-\Xi(x)) \quad (1.28)$$

where \mathcal{N}_0 is a normalization constant, and $\Xi(x)$ a generalized potential with

$$\Xi(x) = \ln D^{(2)}(x) - 2 \int^x \frac{D_1(x')}{D_2(x')} dx' \quad (1.29)$$

Any stationary state with a non-zero (but constant) \mathcal{J} can now be written in terms of this generalized potential, so that

$$p_{st}(x) = 2\mathcal{N}_0 \exp[-\Xi(x)] - 2\mathcal{J} \exp[\Xi(x)] \int_x \frac{\exp[-\Xi(x')]}{D^{(2)}(x')} dx' \quad (1.30)$$

1.4 Kramers' rate theory

A Brownian particle trapped in a deep potential well (figure 1.1), resides there for a time that exceeds all of the system's relaxation times, and that has an Arrhenius (*i.e.* exponential) dependence upon the height of the barrier. The mean escape rate⁷, r_A , is given by the Van't Hoff–Arrhenius formula [HTB90]

$$r_A = \Pi \exp\left(-\frac{2\delta U}{D}\right) \quad (1.31)$$

where δU is the height of the barrier separating the minima, $D = \sigma^2$ is the noise variance and Π is some pre-factor.

To evaluate this pre-factor, consider a Brownian particle obeying Langevin dynamics of the form (1.2), and trapped in a meta-stable state of the potential, $U(x)$ (figure 1.1). Furthermore, suppose that the barrier height δU is very large and the noise is weak, *i.e.* D small. Thus, both of the probability current, \mathcal{J} , at the summit of the barrier, and the variation with time of $p(x, t)$ will be very small and so the particle will be in a quasi-stationary state.

The probability density of the particle's position, $p(x, t)$, obeys a Smoluchowski equation (1.25) and so this quasi-stationary solution has a generalized potential (equation (1.29))

$$\Xi(x) = 2\frac{U(x)}{D} \quad (1.32)$$

⁷The mean escape rate is the reciprocal of the mean escape time from the well.

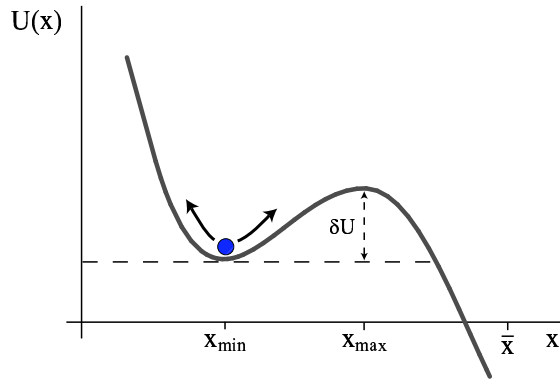


Figure 1.1: *Brownian escape from a potential well: a particle obeying Langevin dynamics typically resides close to the minimum of the meta-stable state, but will occasionally traverse over the barrier at x_{max} with a mean rate that depends exponentially upon both the noise strength, D , and the barrier height, δU .*

Furthermore, assume that if the particle escapes beyond the barrier (say to the point \bar{x} , see figure 1.1), it escapes to infinity and does not return (consequently put $p(\bar{x}, t) \simeq 0$).

Following Risken [Ris89], integrate (1.27) and so write the probability current $\mathcal{J}(x, t)$ as

$$\mathcal{J}(x, t) = -\frac{D}{2} e^{-\Xi(x)} \frac{\partial}{\partial x} \left[e^{\Xi(x)} p(x, t) \right] \quad (1.33)$$

For a stationary state, the flux over the barrier is small, as is $\partial p / \partial t$, and so assume that \mathcal{J} is independent of spatial position. Integrate between x_{min} and \bar{x} , and use $p(\bar{x}, t) \simeq 0$, to obtain

$$\mathcal{J} = \frac{\frac{D}{2} \exp[\Xi(x_{min})] p(x_{min}, t)}{\int_{x_{min}}^{\bar{x}} dx' \exp[\Xi(x')]} \quad (1.34)$$

For a high barrier (*i.e.* large $\delta U/D$), the probability density close to the minimum is approximately given by

$$p(x, t) \simeq p(x_{min}, t) \exp \left[-2 \frac{U(x) - U_{min}}{D} \right] \quad (1.35)$$

The probability of finding the particle in a region of width $2\delta x$, centered on x_{min} is

$$\begin{aligned} P(x=x_{min}, t) &= \int_{x-\delta x}^{x+\delta x} p(x', t) dx' \\ &= p(x_{min}, t) \exp\left[2\frac{U_{min}}{D}\right] \int_{x-\delta x}^{x+\delta x} \exp\left[-2\frac{U(x')}{D}\right] dx' \end{aligned} \quad (1.36)$$

for small D , the probability density (1.35) is sharply peaked and so the actual value of δx need not be specified.

The probability current, \mathcal{J} , is equal to the product of the probability P and the escape rate over the barrier r , and so from (1.34) and (1.36)

$$r \equiv \frac{\mathcal{J}}{P} = \left(\frac{2}{D} \int_{x_{min}-\delta x}^{x_{min}+\delta x} \exp\left[-\frac{2U(x)}{D}\right] dx \int_{x_{min}}^{\bar{x}} \exp\left[\frac{2U(x)}{D}\right] dx \right)^{-1} \quad (1.37)$$

the main contribution to the first integral is from a region about x_{min} , while the main contribution to the second is due to a region close to x_{max} . Therefore, Taylor expand the potential $U(x)$ to second order

$$U(x) \approx U(x_{min}) + \frac{1}{2}U''(x_{min})(x - x_{min})^2 \quad (1.38)$$

$$U(x) \approx U(x_{max}) - \frac{1}{2}|U''(x_{max})|(x - x_{max})^2 \quad (1.39)$$

substituting both of these into (1.37), and integrating over $\pm\infty$ gives the Kramers' rate

$$r_K = \frac{1}{2\pi} \sqrt{U''(x_{min})|U''(x_{max})|} \exp\left(-2\frac{\delta U}{D}\right) \quad (1.40)$$

note that the Arrhenius factor ($\exp(\dots)$) depends only upon the noise strength and the barrier height, while the pre-factor depends only upon properties of the potential's stable and unstable fixed points.

1.4.1 Escape in multi-dimensional potentials

Generalization of Kramers' rate equation (1.40) to more than one dimension is far from trivial, and can only be computed exactly for a small class of potentials [HTB90]. However, to briefly indicate how Kramers' theory may be extended to compute an approximation to the rate of escape over a saddle-point, of a damped particle confined to a two-dimensional potential, and subject to an isotropic noise source. The method proceeds as for the one-dimensional case of the preceding section, and again Taylor expansions for the probability current at the saddle-point, and the probability density at the minima must be computed. The resulting *generalized Kramers' rate* (also known as the Eyring formula [MS96a]) is given by

$$r_K = \frac{\lambda}{2\pi} \sqrt{\frac{\det \mathbf{H}(\mathbf{x}_{min})}{|\det \mathbf{H}(\mathbf{x}_s)|}} \exp\left(-\frac{2\delta U}{D}\right) \quad (1.41)$$

where the Hessian \mathbf{H} of the potential has components

$$H_{ij} = \frac{\partial^2 U}{\partial x_i \partial x_j} \quad (1.42)$$

and is evaluated at the minima, \mathbf{x}_{min} , and the saddle, \mathbf{x}_s . λ is the positive eigenvalue of the Hessian of the potential at the saddle, and $\delta U = U_s - U_{min}$ is the height of the potential barrier at the saddle.

1.5 Stochastic Resonance

Stochastic resonance (SR) [MW89, BG96, MPO94, WM95] is a phenomenon whereby random fluctuations and noise can enhance the detectability and/or the coherence of a weak signal in certain nonlinear dynamical systems. The classic paradigm is one of a particle obeying gradient (*i.e.* in the limit of high friction) dynamics, such that

$$\frac{d}{dt}x(t) = -\frac{d}{dx}U(x) \quad (1.43)$$

and confined to a symmetric, bi-stable potential $U(x)$, *e.g.* of the form

$$U(x) = \frac{1}{4}x^4 - \frac{1}{2}x^2 \quad (1.44)$$

In the absence of any external perturbations, the particle relaxes to an equilibrium state at the bottom of one of the wells. When the particle is driven stochastically by some weak, additive noise source (figure 1.2a) then it will spend most of its time executing a random walk centred upon one of the potential minima. Occasional transitions between the two wells occur with a mean rate, r_K , that is given by (1.40). If, instead, the particle is subject to a sub-threshold⁸ periodic forcing, say of the form $A \cos(\Omega t)$, then it will oscillate about one of the minima. Such a forcing may be interpreted as rocking the potential back and forth. However, if both types of driving are present, the dynamical equation (1.43) becomes

$$\dot{x} = -U'(x) + A \cos(\Omega t) + \zeta(t) \quad (1.45)$$

The system now displays noise-assisted switching (figure 1.2b): the transition rate (1.31) becomes modulated by the periodic forcing, increasing when the barrier is lowered and decreasing when it is raised. Thus, the particle has a greater tendency to switch when it is aided by the periodic bias (*i.e.* after a residence time close to half a period) and a lesser tendency when it is hindered.

Consider now how varying the noise strength D affects the switching process.

- In the limit $D \rightarrow 0$, then $\tau_A \gg \mathcal{T}$, where $\mathcal{T} = 2\pi/\Omega$ is the time period of the regular forcing and $\tau_A = r_A^{-1}$ is the mean *residence time* of a potential well. Thus even though escape is most likely when the barrier is low, actual switching events will be rare and occur on a time-scale much greater than that of the periodic forcing.
- For large D , transitions have little dependence on the barrier height. Thus, $\tau_A \ll \mathcal{T}$ and so switching occurs much more rapidly than the period of driving. The particle

⁸*i.e.* too weak to cause transitions between potential wells in the absence of noise.

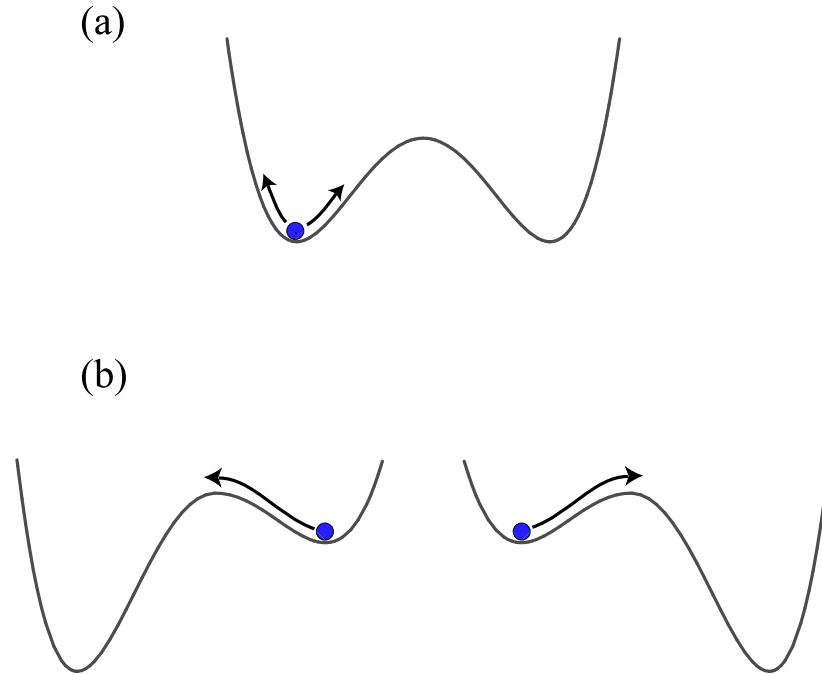


Figure 1.2: *Forced and stochastic motion in a bi-stable well: (a) stochastic motion, the particle executes a random walk about one of the minima, (b) stochastic and periodic forcing combine, causing noise-assisted switching.*

oscillates wildly between minima and with a trajectory that has little coherence with the forcing.

- Moderate noise results in behaviour intermediate to these two regimes and so the assisted switching can become strongly correlated with the biasing. In fact, for a given driving frequency Ω , there is an optimal noise strength D_{opt} for which the transition rate is maximally correlated with the periodic driving. Below D_{opt} transitions occur less frequently, and above D_{opt} the system is too noisy and transitions occur at random.

The description of this effect as stochastic *resonance* implies that there is some matching of time-scales. Benzi *et al.* [BPSV82] coined the name SR, and justified it by noting that the maximal correlation between noisy-switching and driving occurs when the mean waiting

time between two noise-induced transitions is comparable with half of the period, \mathcal{T} , of the biasing. Thus yielding the time-scale matching condition for stochastic resonance

$$\tau_A = \frac{1}{2}\mathcal{T} \tag{1.46}$$

1.5.1 A *bona-fide* resonance

It is easy to visualize this co-operation between noise and signal; what is often more problematic is a quantification of this effect. The original study by Benzi *et al.* [BPSV82] first observed SR as corresponding to a peak in the power spectra of switch times. McNamara and Wiesenfeld [MW89] shifted the focus of investigation and predicted that SR would appear as a maximum in a plot of the output signal-to-noise ratio (SNR) versus the noise strength. Methods for SNR computation are still under contention⁹, but a general technique [MW89] is to compute the power spectrum of the output signal (the barrier crossing rate) and divide it by the power spectrum of the noise signal. For the bi-stable system (1.44) the output power spectrum typically comprises a narrow peak, located at the driving frequency and riding upon a broad-band Lorentzian background. The SNR may therefore be computed by dividing the height of the peak by the height of the Lorentzian background at the same frequency. This measure is now widely considered to be the true signature of stochastic resonance, and has direct application in the signal processing analysis of devices such as SQUIDS [BJS90]. In fact, Heneghan *et al.* [HCC⁺96] have shown the equivalence between this quantity and one that optimizes the Shannon information transfer rate (trans-information) of a memory-less channel.

To characterize SR in a system, it must be examined over a long time. Spectral computation can therefore be awkward for SR studies, since it will involve Fourier transforming large arrays. Furthermore, even though the SNR does depend non-monotonically upon the noise strength, the noise intensity D_{SNR} for maximal SNR does not coincide with the optimal noise D_{opt} for time-scale matching (1.46) (see *e.g.* [GHJM98] and references therein). Thus, SNR measures are erroneous when considering entrainment and phase-locking effects, and

⁹A debate which, to quote Ronald Fox, has “generated much heat but little light”.

furthermore the lack of time–scale matching makes the name ‘resonance’ inappropriate.

For periodically–driven bistable systems an alternative, and visually more compelling, SR measure depends upon the histogram of barrier crossing times [ZMJ90] in which a sequence of residence times of one of the minima is recorded, binned and histogrammed. Depending on the noise level, such a residence time histogram (RTH) typically consists of several narrow peaks super–imposed upon an exponentially decaying envelope (figure 1.3). Each peak is centred at an half–odd–integer multiple of the driving period, such that the j^{th} peak is located at a time

$$\mathcal{T}_j = \left(j - \frac{1}{2}\right) \mathcal{T}, \quad j \in \mathbb{Z} \quad (1.47)$$

To measure the area, or “strength”, of a peak introduce the quantity [GMS95]

$$\mathcal{P}_n = \int_{\mathcal{T}_n - a\mathcal{T}}^{\mathcal{T}_n + a\mathcal{T}} \mathcal{H}(t) dt \quad (1.48)$$

where¹⁰ $a = \frac{1}{3}$ and $\mathcal{H}(t)$ is the normalized distribution of transition times. With increasing noise, \mathcal{P}_n for the n^{th} harmonic peak first rises and then falls, reaching a maximum at some critical value of the noise. For high noise levels a new peak close to the origin is observed (figure 1.3d), representing transitions that are caused solely by noise, and that have no correlation with the driving. The harmonic peaks do not reach their maxima simultaneously, but instead each has a unique critical noise. Recall the relation (1.46): resonance takes place when the driving frequency “matches” the mean transition rate due to noise of the un–forced system. In [GMS95] it was suggested that this would occur when the first (harmonic) peak is maximal. This is because, at this time, very few transitions occur at the sub–harmonics and so this peak dominates the histogram. Under these conditions, the mean first passage time, which is equal to the first moment of the histogram, is close to the driving period. This measure therefore recovers the original interpretation of SR as being a true resonance phenomenon.

¹⁰In fact, the systems considered by this thesis generally have strongly defined peaks with low–background distributions, and so the actual value of the parameter a is immaterial.

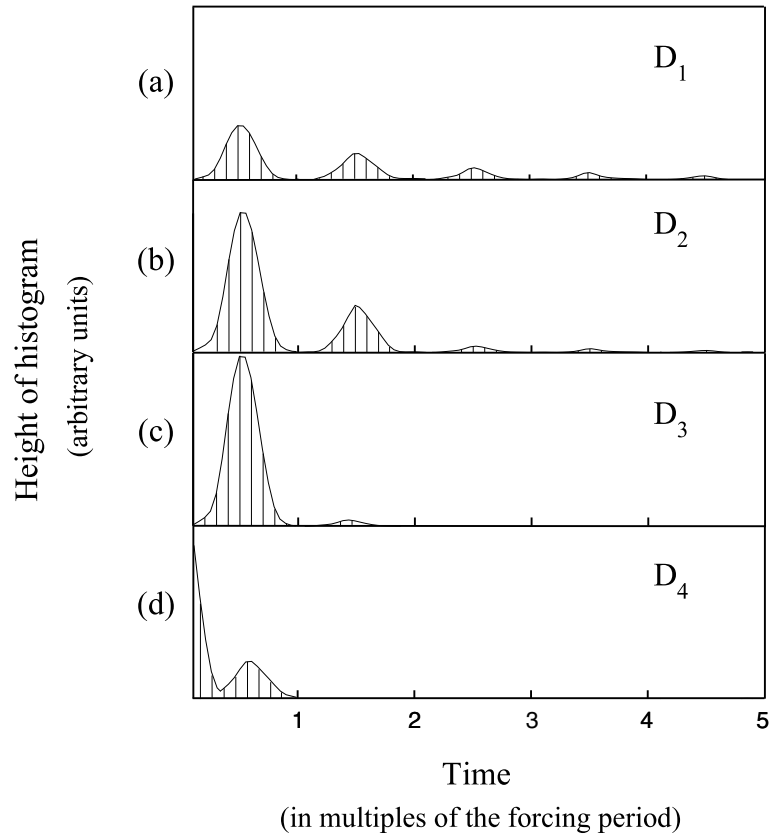


Figure 1.3: *Residence time histograms (RTH) for a particle subject to both stochastic and periodic forcing and moving in a bi-stable potential. Various noise levels are shown, with $D_1 < D_2 < D_3 < D_4$ and $D_3 \approx D_{opt}$.*

Note also that each peak strength \mathcal{P}_n is a function of both the noise and of the driving frequency, and further from (1.46) that each driving frequency Ω has a different critical-value of the noise. Thus, each \mathcal{P}_n goes through a maximum as either the noise intensity or the frequency is increased.

An analytical connection between the RTH measure and the SNR one has yet to be proven, and may not even exist [CFJ98]. However it would appear that if a system exhibits SR according to the RTH measure, then it will also exhibit a non-monotonic SNR. Choi *et al.* [CFJ98] have recently criticized the use of residence time histograms. Their argument is that

in the limit of vanishingly small amplitude driving (*i.e.* $A \rightarrow 0$), the quantities \mathcal{P}_n (equation (1.48)) will still go through a maximum as a function of the noise, even though the system does not display a multi-modal residence-time histogram. This is of course correct, since in the absence of periodic forcing the histogram of residence times is essentially a decaying exponential (such a histogram should be contrasted with the ones shown in figure 1.3). If one now determines the variation with noise of the histogram height at any arbitrary point (*e.g.* at a time equal to a period of the forced case), one does see the height pass through a maximum. However, this occurs at much lower noise levels (*i.e.* there is no matching of time-scales) and is simply an artefact of the sampling. However, such vanishingly small amplitude driving rarely has relevance in the real world and so I take the pragmatic view that Gammaitoni's measure is only pertinent to periodically-driven systems and should only be used to quantify those that display discernible, multi-modal residence time histograms.

1.5.2 The inter-spike interval histogram

A technique, resembling the RTH, for analysing neural spike data is the inter-spike interval histogram (ISIH), which is a histogram of the time intervals between successive spikes. An important distinction between these two measures is that the RTH is a histogram of times for a single escape from a well, *i.e.* it is an ensemble measure, while the ISIH is a histogram of a series of "switching" times of a single neuron/oscillator (*i.e.* it is a renewal process). Thus the residence time histogram exhibits peaks centred at half-odd integer multiples of the driving frequency, while the ISIH will show peaks centred at integer multiples of the driving frequency (recall equation (1.47)).

1.5.3 Biological SR

What is the relevance of SR to biological and neural systems? There is now growing neuro-physiological evidence that noise might aid the transduction of small sub-threshold signals by various sensory neurons. Furthermore, the efficacy of these neurons appears to exhibit a non-monotonic dependence on the noise strength. SR-type effects have recently been indicated in: the cricket cercal system [LM96], human tactile sensation [CIG96], hair

mechano-receptors in the tail fan of the crayfish [DWPM93], and mammalian cold receptors (see chapter 3). At the network level, the application of an electric field containing both a periodic and a noise component has been shown to pacify a (chemically induced) epileptic seizure in an *in vitro* hippocampal slice [GNN⁺96]. It has also been suggested that SR could feature at higher levels of brain function such as in the perceptual interpretation of ambiguous figures (see chapter 4). Good descriptions of many of these experiments may be found in the review articles [Mos94, MPO94, WM95, WJ98].

Chapter 2

The origins of neuronal noise

“Our science has always desired to monitor, measure, abstract, and castrate meaning, forgetting that life is full of noise and that death alone is silent: work noise, noise of man, and noise of beast. Noise bought, sold, or prohibited. Nothing essential happens in the absence of noise.” [Att85]

Neuronal noise is difficult both to categorize and measure. However, it is an important facet of the behaviour of biological neurons that is frequently neglected in theoretical and modeling studies. As a prelude to a discussion of its origins, I wish to give a short description of neuronal structure and function.

2.1 Neuronal structure and function

2.1.1 Cellular physiology

Neurons are eukaryotes. They contain a cell nucleus and cytoplasmic organelles, and are enclosed by a thin (< 10 nm) double layer (bi-layer) of phospho-lipid molecules. The most important of the organelles are mitochondria, which are found throughout the neuron. These small, cigar-shaped structures convert the glucose and oxygen delivered by the bloodstream

into ATP, which is then used as a store of energy. The lipid bi-layer's function is twofold: it prevents the cell's contents mixing with extra-cellular material, and it acts as an (imperfect) electrical insulator.

2.1.2 Electro-physiology

Neuronal cytoplasm consists mostly of water, proteins and inorganic salts such as Na^+ , K^+ , Cl^- and Ca^{2+} . When the cell is at rest, the intra-cellular and extra-cellular fluids differ in both ionic composition and concentration. In consequence there is a charge imbalance, and hence a potential difference, across the membrane. Neuronal operation is effected by the manipulation of this potential difference by the controlled movement of ions across the lipid membrane. Glyco-protein macro-molecules are scattered throughout, and protrude through, the membrane. These macro-molecules function either as sites for the reception of specific chemical messengers, or they facilitate trans-membrane ionic currents. Such ionic currents are either due to diffusion through a channel and **along** a chemical gradient, or to enzymes, known as *active pumps*, which metabolize ATP to move ions **against** their concentration gradient.

Diffusive ionic transport through a channel is a *passive* process, and the current through a single channel can involve the transmission of up to 10^8 ions per second [KSJ91]. Channels are typically highly selective to a single ionic type, and may be sub-classified into non-gated and gated channels. Non-gated channels are water-filled pores which allow a continual ionic flux. The rate of flux depends on the concentration gradient, and these channels are responsible for maintaining the resting potential. Gated channels are allosteric proteins that have (at least) two stable conformal states, open and closed, and are modulated by certain stimuli. Voltage-gated channels are sensitive to the electrical potential across the membrane, while chemically-gated channels respond to the presence of certain chemical messengers. Recordings of the current flowing through a single channel indicate that gated channels can fluctuate rapidly between open and closed states.

Channels allow ions to flow along concentration gradients, and the resulting chemical equi-

librium dissipates the trans-membrane potential difference. To restore it, ions must be pumped against their concentration gradients to balance the passive flux. Such *active* transport requires energy, which is provided by the hydrolysis of ATP. There are many different enzyme pumps, but the sodium-potassium pump, $\text{Na}^+\text{-K}^+$ ATPase, is ubiquitous and accounts for a third of all energy consumed by each neuron. Its function is to restore the intra- and extra-cellular concentrations of sodium and potassium. $\text{Na}^+\text{-K}^+$ ATPase is preferentially biased with a stoichiometric ratio 3:2, extruding more sodium from the cell than is replaced by potassium.

When the cell is at rest it exhibits a trans-membrane potential, the *resting potential*, in the range -40mV to -90mV. If the cell's potential becomes less negative, the cell is said to be *depolarized*; if it becomes more negative, the cell is *hyper-polarized*. Recall that the origin of the resting potential is a disparity between the intra- and extra-cellular fluids. Each ionic species is subject to two pressures controlling its passage through the membrane: an electric one due to charge build up, and an osmotic one which tends to equalize chemical concentrations. In the resting state, the $\text{Na}^+\text{-K}^+$ ATPase pump maintains high concentrations of intra-cellular potassium and extra-cellular sodium. Even though the lipid membrane at rest is permeable to K^+ ions, an electrical gradient opposes their efflux and subsequent chemical equilibration. The resulting potassium distribution therefore derives from a balance between the osmotic and electric forces. Similarly, the membrane is permeable to Cl^- ions but a chloride influx is opposed by the electric gradient and so the extra-cellular concentration high. In contrast, there is a high extra-cellular concentration of sodium since it is continually pumped out of the cell, and therefore both the chemical and the electric gradients favour a Na^+ influx. However, when the neuron is at rest, the lipid membrane is impermeable to Na^+ and thus its distribution is maintained.

2.1.3 Cytology

A neuron may be partitioned both functionally and morphologically into four sections: the *soma*, the *dendrites*, the *axon* and the *pre-synaptic terminals*.

- **The soma** is the metabolic centre of the cell. It is typically pyramidal in shape and contains the cell nucleus and hence the cell's genetic material. The primary function of the soma is protein synthesis. There are usually two distinct structures which extend from the soma: the dendrites and the axon.
- **The dendrites** are an arborised structure which extend the receptive surface of the cell. They generally receive input from other neurons, and are considered to be the information gathering region of the cell. Inter-neuron communication occurs at specialized junctions called synapses, and can be either chemically or electrically promoted. Chemical synapses employ the release of transmitter substances by the signalling cell to cause the transient opening of gated channels on the dendrites of the receptive cell. In contrast, electrical synapses are non-gated channels of low electrical resistance through the cell membrane. The resulting ionic flux through the dendrites is summed in the soma, and the net change in the ionic composition of the cytoplasm determines the neuron's response to its input. The role of the dendrites in information processing and computation has been extensively reviewed in [Mel94, BC97].

Dendritic morphology differs greatly between cell types, and defies general classification. Shepherd [She94] therefore defines dendrites as,

“... all those branches which do not fulfill the criteria of being an axon”.

- **The axon** is a thin, tubular structure which projects from a specialized region of the soma called the axon hillock. Axonal lengths vary between several micrometres and a metre, and diameters vary between one micrometre and one millimetre. The axon has a dual function: chemical transport from the soma to the pre-synaptic terminals, and the propagation of information to other neurons. Information is communicated by means of an action potential (AP), or ‘spike’.¹ An AP is a brief stereotypical electrical impulse which travels with a constant velocity along the axon, away from the soma and toward the pre-synaptic terminals. At its distal end the axon divides into fine branches, called telodendria.
- **The pre-synaptic terminals**, or *boutons*, are specialized swellings that occur on

¹In this thesis I will use the terms ‘action potential’, ‘AP’ and ‘spike’ interchangeably.

the axonal telodendria. They are the transmitting elements of the neuron, and are used to disseminate information about the neuron's activity to the receptor surface of other neurons. The point of contact is known as the synapse, and a neuron can have more than one synapse with another neuron. The pre-synaptic terminals of chemical synapses contain small, spherical membranes, called *vesicles*. Each vesicle contains a small amount (≈ 5000 molecules) of chemical transmitter, and is anchored to a cytoskeletal matrix called the vesicular grid.

2.1.4 Chemical messengers and synaptic transmission

The synapse is the point of functional contact between the axon terminals of one neuron and the dendrites of another. The two neurons do not make physical contact, but are separated by a fluid filled gap of about 20nm, called the synaptic cleft.

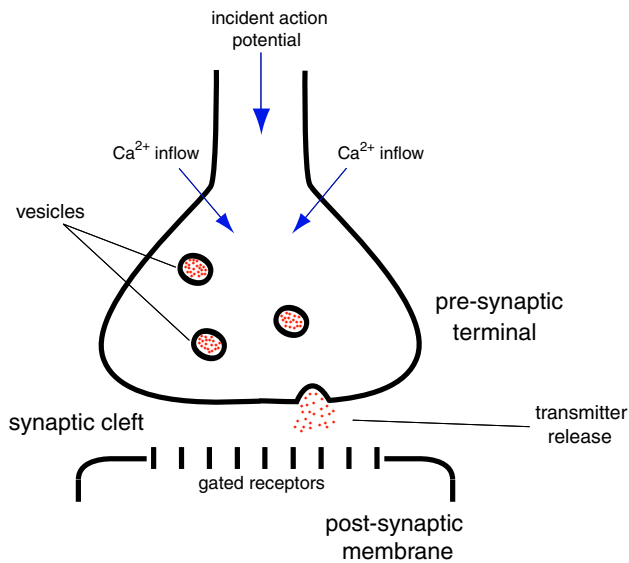


Figure 2.1: *Synaptic function: an incident AP causes vesicular release into the synaptic bouton. The vesicles subsequently fuse to the pre-synaptic membrane and spill neurotransmitter into the synaptic cleft. Transmitter molecules bind to receptors on the post-synaptic membrane, and open chemically gated ion channels (see text).*

When an incident axon potential invades the pre-synaptic terminal it activates voltage-gated Ca^{2+} channels, thus allowing calcium entry. The transient Ca^{2+} influx triggers vesicle release from the grid, and subsequently causes them to fuse to the pre-synaptic membrane. The neurotransmitter contained within each vesicle is spilt into the synaptic cleft and diffuses toward the post-synaptic membrane. At the post-synaptic membrane the transmitter binds to receptor molecules, and opens chemically-gated ion channels. The resulting ingress of charge into the dendrites is termed a post-synaptic potential (PSP). If the ionic inflow is positively charged (*e.g.* Na^+) the PSP depolarized the membrane and is termed *excitatory*; if it is negative (*e.g.* Cl^-) then the membrane becomes hyper-polarized and the PSP is *inhibitory*.

Transmitter release is therefore quantal. In lower animals a single action potential will typically release $10^3 - 10^4$ vesicles. However, for neurons in the mammalian central nervous system this drops to 1 – 10 vesicles per AP [KF87].

Vesicles are regenerated in the pre-synaptic terminals by a process called *endocytosis* [KSJ91].

2.1.5 Action potential generation

The excitatory and inhibitory PSP's all diffuse via the dendrites to the soma, where they are non-linearly combined. If there is an excess of positive charge then the soma becomes depolarized and charge builds up at a region close to the axon hillock, called the trigger zone. The membrane of this initial axonal segment contains many voltage-gated Na^+ channels. If the total charge at the trigger zone exceeds a threshold (usually in the region of -40mV) then these sodium channels open to allow a large Na^+ inflow along the chemical gradient. The inter-cellular sodium concentration increases until the osmotic and electric forces balance, which occurs at about +50mV. At this point the sodium channels become inactive. Since the membrane potential is now positive, there is an inward flow of Cl^- and an outward one of K^+ . This resets the trans-membrane potential to its resting value. The intra- and extra- cellular cytoplasm are now returned to their original compositions by the

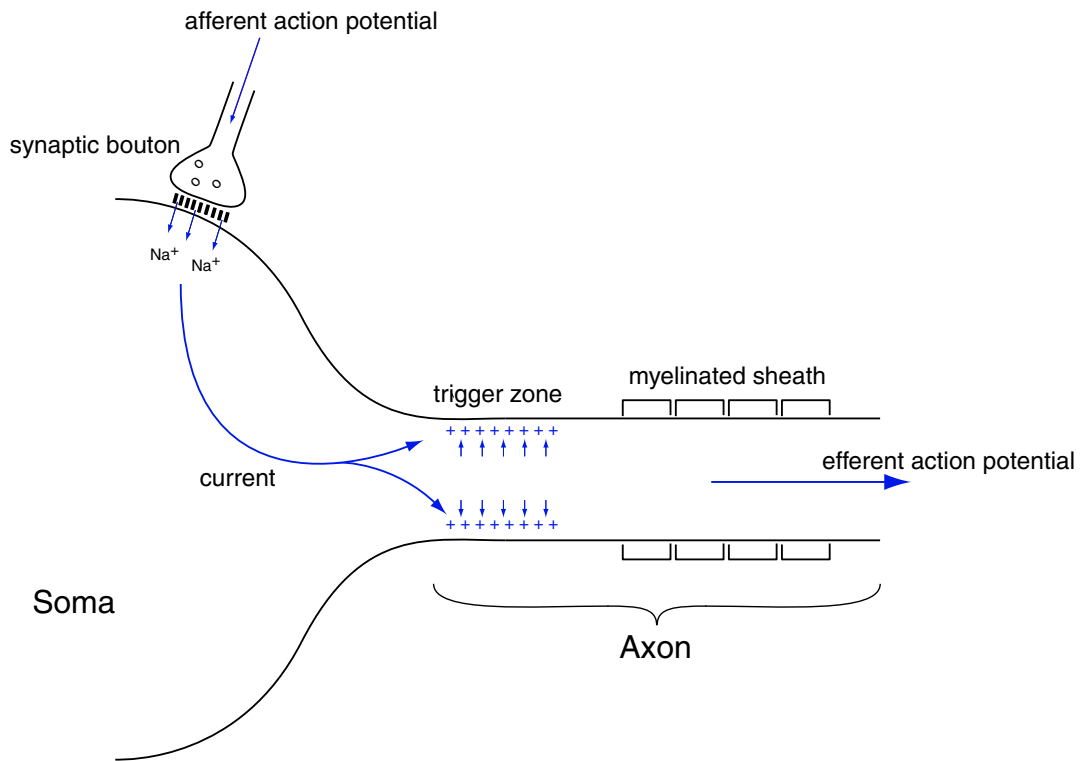


Figure 2.2: An incident pre-synaptic action potential causes an excitatory PSP. The PSP diffuses to the soma, and charge builds up at the trigger zone. The membrane becomes depolarized, and if the threshold is exceeded, an action potential is generated. The AP propagates along the axon, away from the soma.

sodium-potassium pump. Resetting of the membrane potential is not instantaneous but has a finite time course.

This brief excitation is the action potential. Propagation of the AP is achieved by the diffusion of the initial sodium influx to the neighbouring axonal membrane. This portion of membrane now becomes super-threshold, thus its Na⁺ channels open – and the process repeats.

Following spike generation, there is a short time (3 – 4ms) during which the neuron is unable to initiate a further action potential [KSJ91]. This is the *absolute refractory period*

(ARP), and it is a consequence of the residual in-activation of the Na^+ channels and opening of the K^+ channels. However, if the membrane remains depolarized beyond this refractory period, a second spike may ensue. The ARP therefore places an upper bound on the spiking frequency.

If instead the initial PSP summation is sub-threshold, Na^+ - K^+ ATPase and the non-gated channels slowly return the soma to its resting state without the generation of an action potential.

The Hodgkin–Huxley equations

Hodgkin and Huxley's [HH52] model of spike generation in the giant-squid axon captures well the biophysics of current flow at the trigger zone. The starting point for its derivation is the conservation of electrical charge

$$C \frac{d}{dt} V = -\mathcal{F} + I \quad (2.1)$$

where C is the capacitance, \mathcal{F} the membrane current, and I any external or synaptic current entering the cell. The membrane current depends upon V and upon three conductances: g_L , g_{Na} and g_K

$$\mathcal{F}(V, g_L, g_{\text{Na}}, g_K) = g_L(V - V_L) + g_{\text{Na}}(V - V_{\text{Na}}) + g_K(V - V_K) \quad (2.2)$$

where V_L , V_{Na} and V_K are the leakage, the sodium and the potassium reversal potentials respectively. The passive leakage conductance g_L is independent of both time and voltage, however the active sodium and potassium conductances, g_{Na} and g_K , are given by

$$g_{\text{Na}} = \bar{G}_{\text{Na}} m_{\text{Na}}(t)^3 h_{\text{Na}}(t) \quad \text{and} \quad g_K = \bar{G}_K n_K(t)^4 \quad (2.3)$$

where \bar{G}_{Na} and \bar{G}_K are the maximal channel conductances. The conductance variables, m_{Na} , h_{Na} and n obey

$$\frac{d}{dt}m_{Na} = \frac{m_{\infty}(V) - m_{Na}}{\tau_m(V)} \quad \frac{d}{dt}h_{Na} = \frac{h_{\infty}(V) - h_{Na}}{\tau_h(V)} \quad \frac{d}{dt}n_K = \frac{n_{\infty}(V) - n_K}{\tau_n(V)} \quad (2.4)$$

with $m_{Na}, h_{Na}, n_K \in [0, 1]$, and the asymptotic values, $m_{\infty}(V), h_{\infty}(V), n_{\infty}(V)$ depend sigmoidally upon the voltage. The τ_m, τ_n and τ_h are time constants, with $\tau_m \ll \tau_h, \tau_n$. All of the reversal potentials, the maximal conductances, the conductance variables and the time constants, were experimentally obtained from patch-clamp measurements on the giant squid axon.

Integration of the Hodgkin–Huxley equations shows that for zero input current ($I = 0$) the neuron remains at its resting-potential ($V_{rest} \approx -40$ mV). An action potential is generated when a large enough current is applied: the cell rapidly depolarizes to +50mV, before slowly returning to V_{rest} . The fast upstroke is caused by the rapid increase of m_{Na} (inward Na^+), its rise is halted by the slower h_{Na} (Na^+ inactivation) and n_K (outward K^+). Hyperpolarization is due to the increase of n_K . During the recovery, h_{Na} and n_K reset to their asymptotes.

2.2 Neuronal noise

Stochastic neural activity is apparent at all levels of recording: from single ion channels to spike trains [Hol76]². Some of this randomness is no doubt due to noisy input, either as signals from other neurons (*e.g.* [GM64, Ric95]) or as direct sensory input (*e.g.* [DWPM93, LM96]). However, there is a large component which derives internally to the cell.

²The presence of chaos in neural systems has also been indicated by many theoretical studies, and is supported by the neuro-physiological evidence. For a discussion, and also techniques for distinguishing between noise and chaos, see *e.g.* [Gla95], and also the discussion at the end of chapter 3

2.2.1 Aleatory synaptic function

In vitro recordings from neuro-muscular synaptic junctions shows the continuous and spontaneous generation of small (about 0.5mV) post-synaptic potentials. These miniature PSP's (termed miniature end-plate-potentials, mepps) are evoked at a mean rate of about 1Hz, even in the absence of stimulation [Kat66]. Single mepps are generally too small to cause the post-synaptic neuron to spike, but otherwise, apart from their size, they are indistinguishable from those triggered by an afferent action potential. mepp magnitudes suggest that each one is caused by transmitter release from a single vesicle, and therefore discharge in the pre-synaptic bouton has a stochastic component. The inter-mepp histogram is fitted well by an exponential, implying that random vesicle release is Poisson distributed. This further suggests that vesicles are released independently of each other, and with constant probability. Similar spontaneous discharge has been observed in other preparations [KSJ91].

Vesicular release probability depends strongly on the membrane potential of the pre-synaptic terminal, rapidly increasing with bouton depolarization [Hol76]. Consequently, vesicular discharge by an afferent action potential is also Poisson distributed, but with a much higher release probability than when the cell is at rest. Typically, the release probability due to an action potential is $p \approx 0.6$ [Per92]. Therefore, if there are n vesicles available for release, the mean transmitter released by an afferent spike will be $m = pn$ vesicles.

Measurement of m-PSP amplitudes demonstrates that vesicle size is not fixed, but is Normally distributed with a wide variance [HLQ69]. Furthermore, the mean and variance of this distribution is common to all synapses.

2.2.2 Fluctuations of the membrane potential

The interplay between neurotransmitter molecules, receptors, channels, and ions may only be described statistically due to the large numbers concerned. Several spectral densities arise:

- **Johnson–Nyquist noise.** Fatt and Katz [FK50, FK52] estimated the thermally induced voltage fluctuations in the membrane potential. Such fluctuations are analogous to the Johnson–Nyquist (JN) noise observed in electronic components. For an RC circuit of resistance R and capacitance C , JN noise has a band-limited Gaussian distribution³, with mean $4kTR$ and variance kT/C [DeF81], where k is the Boltzmann constant and T the absolute temperature. It therefore has a power spectral density (PSD):

$$S(f) = \mathcal{C} \tag{2.5}$$

with \mathcal{C} constant.

- **Shot noise.** Although current flow through a channel involves many ions, the transition probability of a single ion is low and is Poisson distributed. Channels are relatively sparse over the membrane and so ion movement through them is likely to be independent. Furthermore, the transit time for each ion will be similar for all ions, and therefore so too will be the current carried by a single ion. The current flow through the ion channel will therefore have the form

$$I_s(t) = \sum_{t_k} \mathcal{G}(t - t_k) \tag{2.6}$$

where t_k represents the time of passage of the k^{th} ion which contributes $\mathcal{G}(t - t_k)$ to the total current $I_s(t)$. The spectral density of the current will therefore be that of shot noise [Ric54, Hol76], and its precise form will depend on the function $\mathcal{G}(t)$.

- **Excess noise.** The low frequency r.m.s. noise level of a non-equilibrium system is often greater than can be accounted for by either JN or shot noise [Hol76]. Empirically, such noise often has a spectral density which varies as

$$S(f) = \frac{\mathcal{B}}{f^\zeta} \tag{2.7}$$

³A signal is said to be band limited if its Fourier transform vanishes outside of some finite interval. Quantum corrections to Nyquist's derivation of the spectrum mean that JN noise is only flat up to 7×10^{13} Hz [Gar85].

where \mathcal{B} is some constant which depends on the experiment, and the exponent ς is close to 1. Such excess noise is named flicker- or $1/f$ noise. Its origins are poorly understood, but Verveen *et al.* [VD68] have shown that the intensity of the $1/f$ spectrum is related to passive K^+ flux, but is unaffected by either sodium transport or metabolic processes. Lundström *et al.* [LM74] therefore suggest that it may be a consequence of current modulation due to the vibrational modes of the glyco-protein channels.

- **Current noise.** The number of receptors activated by the presence of neurotransmitter in the synaptic cleft is not constant, but instead rapidly fluctuates as transmitter molecules collide with receptor sites [KM72]. The resulting current flow through the membrane is therefore noisy, with statistics that reflect the gating fluctuations. Recall that the arrival of a single transmitter molecule at a receptor site on the post-synaptic membrane causes the channel to open. If the activation probability of a channel is p_a , and its inactivation probability is $(1 - p_a)$, then the population statistics of N channels are binomially distributed with mean Np_a and variance $Np_a(1 - p_a)$. The power spectral density of these fluctuations therefore follow a Lorentz distribution [DeF81, Hol76] with a time constant τ , *i.e.*

$$S(f) = \frac{\tau \mathcal{E}^2}{1 + f^2 \tau^2} \quad (2.8)$$

where the parameters τ and \mathcal{E} are empirically determined, and τ is a relaxation time [LN71a].

2.2.3 Randomness in spike generation

If a low intensity stimulus is applied to a neuron, no response occurs; if a high intensity one is used, the cell will spike. Intermediate to these two regimes is a range of stimuli for which firing is probabilistic. Verveen [Ver61, DeF81] repeatedly applied a constant stimulus to a frog nerve preparation, and measured the neuron's response. To avoid habituation, stimuli were applied at two second intervals. It was found (figure 2.3) that the firing probability varies monotonically between 0 and 1 over a range of stimuli, and further that the firing

probability is approximately Gaussian. Pecher [Pec39] compared the firing variance of two fibres taken from the same preparation to show that these fluctuations derive internally to the neuron and have no external origin.

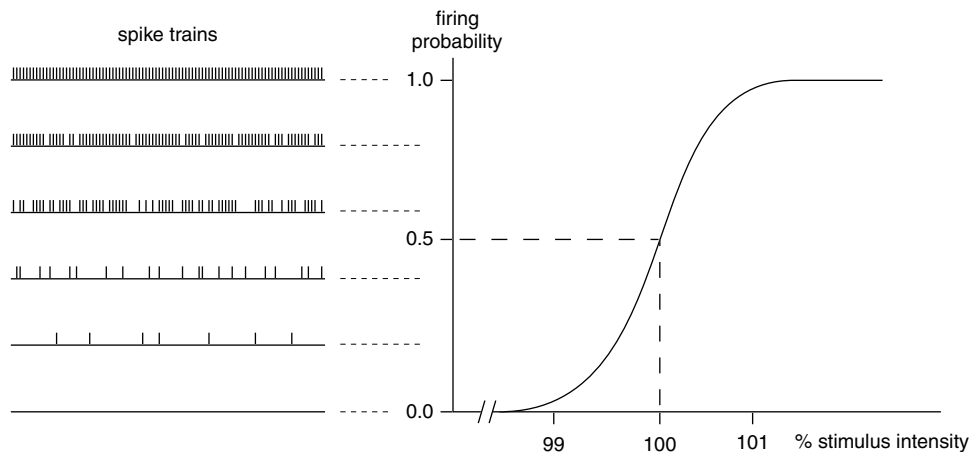


Figure 2.3: (left) Action potentials from a frog nerve in response to a repeated constant stimulus. Proceeding from top to bottom represents a reduction in stimulus intensity. (right) Firing probability for a given stimulus intensity. Stimulus strength is normalized about the threshold stimulus: threshold is defined as that stimulus for which the neuron fires on average once out of every two trials. (After [Ver61]).

Since such probabilistic firing effectively corresponds to a stochastic threshold, it is referred to as *threshold noise*.

Lecar and Nossal [LN71b] have studied threshold noise in a simplified Hodgkin–Huxley model, due to FitzHugh [Fit61]. FitzHugh noted that V and m_{Na} vary more rapidly (by an order of magnitude) than do h_{Na} and n_K , and further that the main properties of the Hodgkin–Huxley model could be reproduced by setting h_{Na} and n_K equal to their resting values, *i.e.* $h_{Na} = h_\infty$ and $n_K = n_\infty$, so that

$$\begin{aligned} C \frac{d}{dt} V &= -g_L(V - V_L) - \bar{G}_K n_\infty^4 (V - V_K) - \bar{G}_{Na} m_{Na}(t)^3 h_\infty (V - V_{Na}) + I \\ \frac{d}{dt} m_{Na} &= \frac{m_\infty(V) - m_{Na}}{\tau_m(V)} \end{aligned} \quad (2.9)$$

In the absence of noise, FitzHugh's reduced equations exhibit three fixed points: two stable and one saddle-point, as shown in the phase-plane in figure 2.4. The stable point at a represents a resting potential, while that at c is an excited state. If the dynamical equations are supplemented by a reset condition, then arrival at c represents spike generation. The saddle-point separatrix therefore divides the phase plane into two basins of attraction: trajectories with initial points to the left of the separatrix relax to the resting potential, while those with starting points to the right (ultimately) trigger a spike. The separatrix is therefore a threshold for spike-generation.

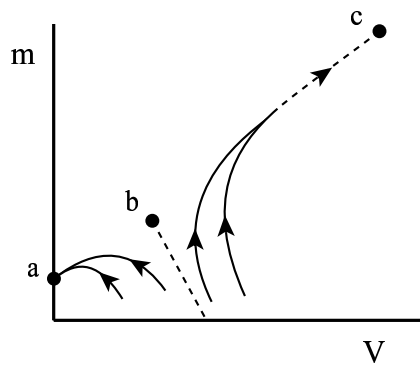


Figure 2.4: *Trajectories in the phase plane for the FitzHugh's reduced equations. a and c are stable fixed points, respectively corresponding to a resting potential and to spike generation. b is a saddle-point and the dotted line represents the separatrix. Trajectories starting to the left of the separatrix terminate at a , while those starting to the right of the separatrix terminate at c .*

The inclusion of neuronal noise causes V and m to fluctuate, and means that trajectories must be replaced by probability distributions for the position of the state vector in the (V, m) plane. More importantly, if the neuron is prepared at an initial point close to the separatrix, then the noise can propel the state vector over it. Thus, the noise can either cause the neuron to fire when the corresponding deterministic system would not, or *vice versa*: it can be prevented from firing when it otherwise would.

The consequences of this have been examined by the inclusion of additive noise to each

of equations (2.9). By identifying the probability of firing with the probability of having crossed the separatrix in the limit $t \rightarrow \infty$, Lecar and Nossal [LN71b] derive the general expression for the firing probability due to threshold noise

$$P(\text{fire}|I) = \frac{1}{2} \left[1 + \operatorname{erf} \left(\frac{I - I_\theta}{\mathcal{S}I_\theta} \right) \right] \quad (2.10)$$

where I is the stimulating current, I_θ is the threshold current, \mathcal{S} measures the spread of the transition region where the probability of firing varies from 0 to 1. $\operatorname{erf}()$ is the error function, defined by

$$\operatorname{erf}(x) = \frac{2}{\sqrt{\pi}} \int_0^x \exp(-z^2) dz \quad (2.11)$$

In a companion paper, Lecar and Nossal [LN71a] compute \mathcal{S} for various sources of membrane noise (see section 2.2.2) and compare their predictions with the experimental data. They find that the Verveen's data is best explained when the sodium channel fluctuations are the dominant contribution to threshold noise.

2.3 Discussion

In this chapter I have reviewed neuronal operation and have identified several sources of noise. For neuronal firing dynamics, the most potent of these are synaptic and threshold noise. In chapter 5 I will further show how these two noise sources affect the behaviour of a neuron.

Chapter 3

A temperature-dependent cold receptor model

3.1 Introduction

Bursting is the rhythmic generation of several action potentials during a short time, followed by a period of inactivity during which the membrane hyper-polarizes. The limiting case of a single spike per burst is termed *beating*. There are a wide variety of burst phenomena, but it appears that many are due to a similar underlying mechanism. First note that the various chemical and electrical dynamics of the neuron operate on many time-scales, and so some neurons are amenable to Rinzel and Lee's [RL87] treatment: their dynamics may be *dissected* into a fast system coupled to a slowly oscillating sub-system. Typically the fast system has a time-scale of milliseconds and models the membrane potential, and hence spike generation. The slow sub-system operates on a time-scale of tens of seconds and models trans-membrane ionic currents. The fast system is modulated by the slow one, and has two parameter regimes: a stationary state or *resting potential*, and a periodic state during which action potentials are generated. Thus, for bursting to occur, the slow variable must parameterize bifurcations in the fast system. Bursting phenomena may be sub-classified

[WR95, Rin87], according to the underlying wave form of the oscillatory component, *e.g.* triangular bursting: feline thalamo-cortical relay neurons exhibit brief spike bursts riding on a slow triangular wave [WR95].

An important class of bursting neurons are the mammalian cold receptor cells. These cells are free nerve endings [SBR90] that transduce patterns of heat energy into neuronal signals. They are found sub-cutaneously at every layer of the skin and tongue, but are relatively sparsely distributed over the skin [Iva90]. As a consequence of their small size, intra-cellular recordings of the various ionic processes contributing to excitability are not available. Instead the only quantity that can be measured directly is the spike train, however other cellular properties may be inferred by the use of pharmacological agents. Temporal firing patterns and inter-spike interval histograms (ISIH) from these neurons show that the bursting dynamics is highly temperature-dependent and further imply the existence of a slowly-oscillating temperature-dependent current that has a frequency that increases with temperature [BSW90].

In this chapter I present a canonical model for a thermally-dependent cold receptor neuron with noise, which exhibits bursting, beating and skipping. The model is a simplified version of an ionic slow wave bursting neuron, and can be obtained from the latter by following a phase reduction procedure due to Ermentrout and Kopell [EK86]. My goal is to better understand the paths in parameter space which yield the sequences of discharge patterns observed in cold receptors. My approach here is a general one, I take the specific example of a cold-receptor but this phase model also has applicability to other temperature-dependent, slow-wave bursting neurons such as those discussed in [BSWH84]. The model contains biologically motivated parameters and exhibits behaviour that is consistent with experiment. Moreover, it has the advantage of being mathematically tractable so that if these parameters were to be quantified, analytic predictions about the behaviour of real receptors could be made.

I analyse the model in the limiting case of zero-noise (the deterministic limit) and also when subject to a finite amount of thermal noise. For the former I am able to predict how many action potentials are generated per burst for a given temperature, and I also

derive the transition temperature from bursting to beating. For the latter I shall show how to estimate the skipping rate (*i.e.* the mean number of slow-wave cycles for which the neuron does not fire) at a given temperature. I demonstrate that skipping is a noise-induced effect that can occur for both the supra-threshold and the sub-threshold dynamics. Below threshold, spikes become deleted as a consequence of *noise-induced trapping* [AGMS94], while above threshold the firing pattern becomes augmented by *noise-induced spiking*. I further show that the phase-locking behaviour of the neuron in these two regimes displays a non-monotonic dependence on the noise level, consistent with the notions of *resonant trapping* and *autonomous stochastic resonance* [Lon97].

The chapter is organized as follows. Section 3.2 is a brief review of cold receptor physiology, a subject covered more completely in [LH96]. The model is introduced in section 3.3. In section 3.4 I first consider the limiting case of zero noise and analyse the simulated firing patterns via Floquet theory, I then examine how noise can alter the deterministic discharge pattern. In section 3.5 I consider how changing the level of noise can lead to resonant trapping and stochastic resonance in this phase model.

3.2 A summary of the neuro-physiology of cold receptors

Figure 3.1 shows characteristic discharge patterns at various static temperatures from receptors in the cat tongue. Not every cell has this repertoire of discharge, some exhibit only a few of these patterns when the temperature is varied. Furthermore the temperature at which a given discharge pattern occurs varies between receptors. Although it is unclear as to the extent to which the nervous system utilizes the temporal structure of such regular discharge, it is known [Lis97] that bursts are an efficient way to drive certain higher neurons. This is because, during a burst, the relatively high firing rates release higher levels of transmitter than would be the case if the individual spikes were more broadly distributed in time.

At low temperatures the neuron bursts repetitively with a uniform burst length and with bursts that are synchronized to the slow oscillation. However the timing of individual spikes

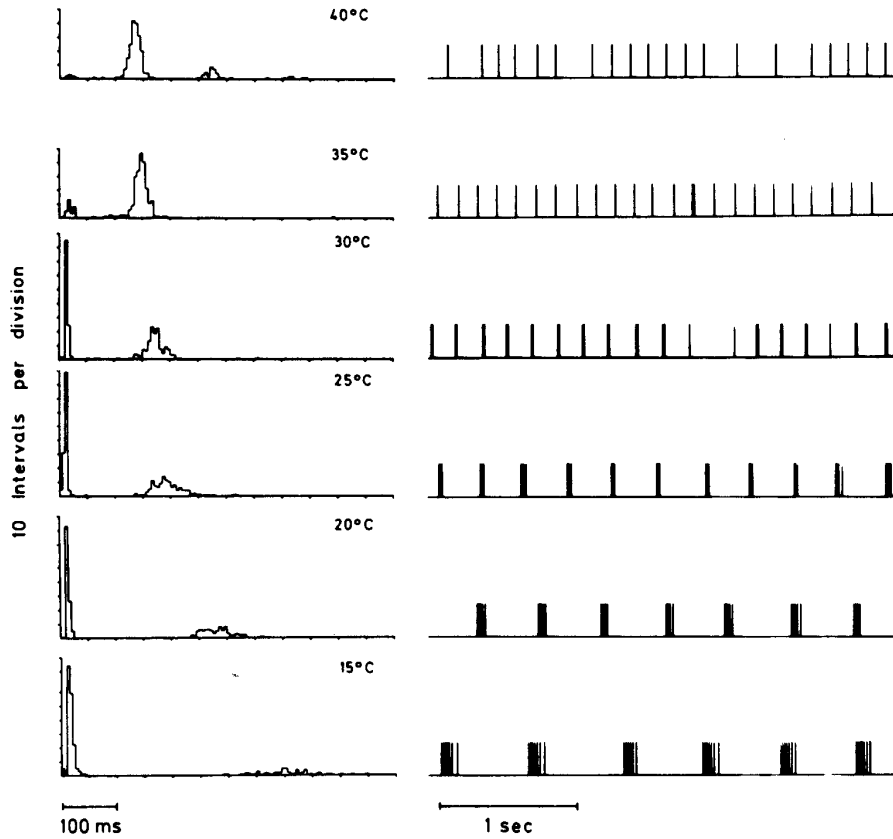


Figure 3.1: *Characteristic discharge patterns of bursting cold receptors of the cat lingual nerve at various constant temperatures. Left diagrams: interval distribution; right diagrams, impulse activity. The mean discharge rates (in s^{-1}) are 5.4 ($40^{\circ} C$); 7.2, ($35^{\circ} C$); 9.2, ($30^{\circ} C$); 10.4 ($25^{\circ} C$); 12.0 ($20^{\circ} C$); 11.0 ($15^{\circ} C$). Intervals shorter than 100 ms are intra-burst intervals. Reproduced from figure (1) of [SBR88] and methods are described in references therein, (reproduced with permission).*

within the burst is non-uniform [BBH80], a feature shared with *parabolic* bursting neurons [RL87]¹. When the temperature is quasi-statically increased, the burst length and inter-

¹A burst is termed parabolic if the spiking frequency is lower at both the beginning and the end of the burst compared with that during the middle of the burst.

burst period both diminish, until at the middle of its operating range the neuron emits a regular spike train with phase-locked spikes.

If the temperature is increased still further, the spike train becomes aperiodic so that occasional double spikes appear and skipping occurs: the spike train is still synchronized to some underlying rhythm, but between spikes a random integer number of oscillation cycles may be skipped [BSW90]. The origin of this randomness is uncertain. However, due to the cell's lack of synapses and its small size, it is thought that thermal and conductance fluctuations might be important. The skipping rate is also thermally-dependent, increasing with temperature, and above 40°C skips of up to eight cycles have been observed [SBR88]. Static temperature is therefore unambiguously encoded by both the discharge pattern and the oscillation period of the slow wave and not by a rudimentary firing rate code.

Cold receptors also exhibit a dynamic response to rapid (*i.e.* non-quasistatic) temperature changes [BBH80]. Figure 3.2 clearly shows this dynamic response when a cold receptor is exposed to cooling steps of 5°C. There is a rapid transient **increase** of the slow-wave frequency, which then slowly relaxes to the new steady state (*i.e.* to a frequency that is lower than the original one). As previously noted, the number of spikes-per-burst (SB) increases with a quasi-static temperature reduction. However, for a rapid temperature change SB overshoots the new steady-state value before slowly relaxing to it. Thus, there is a transient period during which the cell emits longer, and more frequent, bursts than would be dictated by the steady-state conditions. The frequency of spikes within a burst remains approximately constant. It further appears that there are two time-scales for this transient behaviour, with the SB-transient evolving more slowly than the frequency transient.

I wish to introduce some nomenclature for describing the discharge pattern. The number of action potentials in a given burst (*i.e.* SB) is N , and the mean number of spikes per burst, \bar{N} is the temporal average of N . Ω is the frequency of the slow oscillatory cycle, and is the reciprocal of the sum of the inter- and intra- burst durations. A single receptor at a fixed temperature does not always generate a constant number of spikes during every burst, but can instead vary by one or two spikes [BBH80]. The occurrence of additional spikes is

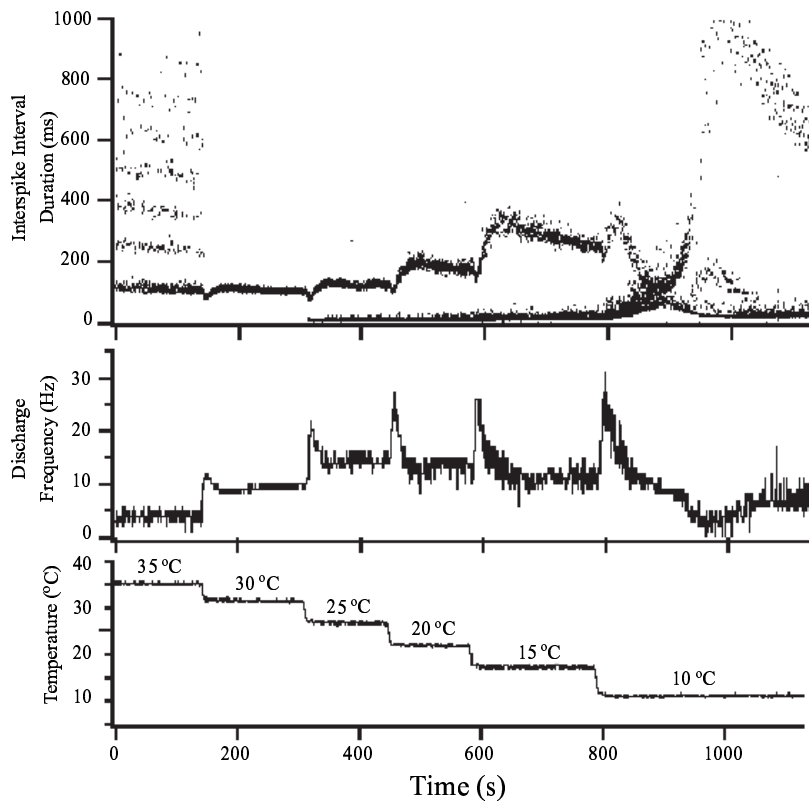


Figure 3.2: *Temperature response characteristic of a peripheral cold receptor of the cat skin during reduced extra-cellular calcium concentration (0.5 mM, control 1.5 mM) which enhances the rhythmicity of the impulse activity. Impulse activity was recorded during temperature changes from 35°C to 10°C in steps of 5°C as indicated in the lowest trace (T). The discharge frequency (F) is shown in the trace above by means of a conventional peri-stimulus-time histogram (bin width: 1s). The interval duration plot in the upper trace shows the corresponding distributions of the interspike-intervals (comprises about 11,000 intervals). Each dot represent a single interspike-interval. Note that temperature changes are abrupt rather than quasi-static, and so the cell exhibits transient behaviour. Furthermore, observe the abrupt transition to skipping (shown in the upper trace) which suggests the presence of a phase-transition (or bifurcation) in the cell's dynamics. (Reproduced from [BHD⁺ 98] with permission)*

statistically distributed, suggesting that a degree of stochasticity is present in the dynamics, however one cannot exclude the possibility of chaotic bursting [LH96]. The breadth of the ISIH peaks indicates that at a fixed temperature, the slow-wave frequency $\Omega(T)$ in fact fluctuates weakly but with a mean that is determined only by T and is independent of the spike number variability. Examination of the spike trains of several cells at different static temperatures reveals [BSWH84] that both Ω and \bar{N} depend monotonically (and sometimes approximately linearly [BBH80]) upon the temperature T , with Ω increasing and \bar{N} decreasing with T .

The thermo-sensitivity and regular discharge of cold-receptors has been likened to that of *Aplysia*² R15 neurons. In normal sea-water the *Aplysia* R15 cells exhibit an irregular endogenous bursting discharge caused by interactions between an internal pacemaker and synaptic inputs from other cells [AB85]. This discharge may be made periodic by perfusing with an artificial sea-water solution containing increased Mg^{2+} or low Ca^{2+} to block neurotransmitter release [WC82]. Under these conditions the activity of the cell depends only upon its pacemaker mechanisms. Even though the *Aplysia* organism does not thermo-regulate, the discharge from these pacemaker cells displays a temperature-dependence similar to that of mammalian cold receptors. It is thought that the bursting patterns and thermo-sensitivity of both cold receptors and of *Aplysia* R15 neurons derive from similar mechanisms, and so it has been proposed [WGC74, WC82] that these pacemaker cells could serve to model thermo-receptors. Studies of R15 neurons proved insightful for the understanding of slow wave bursting since it is possible to record intra-cellularly. In particular, the blocking agent TTX has been shown to prevent action potential generation while still leaving the slow-wave relatively intact. (The rhythmic behaviour of *Aplysia* is well reviewed in [AB85] and more recently in [CCB91].)

The effect of temperature on *Aplysia* R15 cells has been investigated [Car67]. The firing threshold was found to remain constant, but the membrane resting potential was observed to become more negative with increasing temperature, decreasing by 1.5mV for each degree

²*Aplysia Californica*: a large marine snail also known as the sea hare, see [Kan89] for a review of *Aplysia* neuro-physiology.

warmed. Further investigation [CA68] has shown that the cause of the change in resting potential is a biasing of the $\text{Na}^+\text{-K}^+$ pump with temperature. Such a biased pump is termed an electrogenic pump, and its overall effect is the generation of a constant current across the membrane. As temperature increases the pump becomes preferentially active toward sodium, extracting more Na^+ than is replaced by K^+ , and making the membrane potential more negative. The presence of an $\text{Na}^+\text{-K}^+$ pump in the cold receptor has been confirmed [SB90] by application of ouabain, a poison that blocks the pump's activity and so prevents the cell's return to its normal stable state. It was found that ouabain initially induces a short vigorous increase in cellular discharge, followed by a permanent cessation of activity. During the initial period Ω accelerates and \bar{N} increases to peak values, and these peak values increase monotonically with temperature. Inhibition of the electrogenic $\text{Na}^+\text{-K}^+$ pump causes a depolarizing imbalance of the membrane potential since positive charge is not removed from the cell, and it is therefore thought that Ω is controlled by both temperature and by the membrane potential.

The physiology of the cold receptor slow oscillation mechanism is uncertain, however it is thought [GHT82] that the *Aplysia* pacemaker involves two coupled slow trans-membrane currents. A slow inward voltage-dependent calcium current and an outward Ca^{2+} dependent potassium current which activates at an intermediate rate. The inward current is thought to be conveyed by a transient (T) [TLM⁺88] calcium channel, and the importance of T-channels in cold receptor oscillation has been investigated by Schäfer *et al.* [SBH82, SBR88]. In general T-channels activate (open) at low thresholds, in the range -70mV to 0mV, and become completely inactivated (closed) by a voltage-dependent inactivation gate as the voltage increases beyond -60mV. During the first part of the cycle Ca^{2+} accumulates in the cell and depolarizes the membrane. The depolarization inactivates the T-channel but the accumulation activates outward K^+ channels. When the outward current exceeds the inward, the membrane potential becomes more negative, initializing the hyper-polarizing part of the cycle. The amassed Ca^{2+} is now sequestered by another ATP driven pump. This in turn inactivates the outward K^+ current and begins to depolarize the membrane again, reactivating the T-channels. In *Aplysia* the overall amplitude of the oscillation is of the order of 15mV. At low temperatures the calcium T-current is blocked [WW74],

weakly reducing the oscillation amplitude. As a consequence of the reduced Ca^{2+} influx, the outward K^+ channel becomes activated more slowly, increasing the total oscillation period.

Skipping occurs in other preparations in which there is no apparent periodic stimulation. For example, a related thermo-responsive preparation is the ampullae of Lorenzini of the dogfish. These mandibular sensory afferents are used for prey detection, and are primarily electro-responsive but also respond to thermal stimuli. They exhibit a similar temperature-dependent slow wave, but although skipping occurs they do not burst in the same manner. They are much larger than cold-receptors and so are a simpler preparation to study. Recent data [BWSH94] suggests that their skipping is a consequence of noise internal to the neuron, and a similar mechanism has been suggested to operate in the cold-receptor [BBH80]. An electrical stimulus has no effect on the oscillatory period of the ampullae, but instead determines the skipping rate: a positive electric field increases the skipping probability, while a negative field reduces it. It has been suggested [BWSH94] that the oscillatory wave periodically brings the neuron close to its threshold for firing, but that actual action potentials are caused by inherent noise pushing the membrane potential over the threshold. Such a mechanism should be compared with that of stochastic resonance (recall section 1.5). The effect of an imposed field is to shift the baseline of the oscillation, so that the neuron becomes biased toward (negative field) or away (positive field) from the threshold, thus altering the firing probability. In this manner a single neuron is able to encode two sensory modes: a thermal one and an electrical one.

Aplysia R15 evidence further suggests the origin of the transient \bar{N} -overshoot during rapid temperature changes. It is known that the Na^+ - K^+ pump responds much more quickly to temperature changes than do the passive ion channels [WC82]. Therefore, before equilibration, the resting potential temporarily becomes much more positive and so more spikes can be fired during a burst.

In summary, a cold-receptor model based on the *Aplysia* data has a high resting potential at low temperatures, and so the slow wave causes depolarization for a large part of the cycle. The neuron therefore bursts. As the temperature increases, so too does the oscillation

frequency of the slow wave. In addition the resting potential becomes more negative and so the depolarization time due to the slow wave, and hence the burst length, is reduced. At high temperatures, the slow wave is no longer able to generate spikes by depolarization, instead all spikes must be noise driven.

3.3 A temperature-dependent phase model of a cold receptor

Longtin and Hinzer [LH96] have recently studied bursting and skipping in a cold-receptor model based upon an extension to Plant's model [Pla81]. Plant's model is a slow-wave, parabolic-bursting neuron that derives from the Hodgkin-Huxley equations (section 2.1.5). Although ionic models of this type allow much insight into cellular function, they involve a set of five coupled differential equations and so are difficult to treat analytically. Consequently I turn to a simpler canonical model.

3.3.1 Ermentrout and Kopell's canonical bursting model

Ermentrout and Kopell [EK86] consider a general parabolic bursting model of the form

$$\begin{aligned}\dot{\mathbf{u}} &= f(\mathbf{u}) + \varepsilon^2 g(\mathbf{u}, \mathbf{v}, \varepsilon) \\ \dot{\mathbf{v}} &= \varepsilon h(\mathbf{u}, \mathbf{v}, \varepsilon)\end{aligned}\tag{3.1}$$

where the vector $\mathbf{u} \in \mathbb{R}^p$ is identified with the vector of potentials contributing to the spiking mechanism (compare with the Hodgkin-Huxley model of section 2.1.5) and $\mathbf{v} \in \mathbb{R}^q$ describes the vector of potentials associated with the slow wave (*e.g.* the inward voltage-dependent Ca^{2+} and outward Ca^{2+} -dependent K^+ currents).

The $f()$, $g()$, $h()$ are smooth functions of their arguments, and have the following properties

- (i) $\dot{\mathbf{u}} = f(\mathbf{u})$ has an attracting invariant circle with a single critical (saddle-) point at $\mathbf{u} = 0$
- (ii) $\dot{\mathbf{v}} = \varepsilon h(0, \mathbf{v}, 0)$ has a stable limit cycle

As an example of (i), consider the reduced Hodgkin–Huxley equations

$$C \frac{d}{dt} V = -\mathcal{F}(V, m_{Na}, n_K) \quad \frac{d}{dt} m_{Na} = \frac{m_\infty(V) - m_{Na}}{\tau_m(V)} \quad \frac{d}{dt} n_K = \frac{n_\infty(V) - n_K}{\tau_n(V)} \quad (3.2)$$

and set $h_{Na} = h_\infty$ (compare with FitzHugh’s reduction, equation (2.9)). Typical null-clines for these equations are shown in figure 3.3.1, and from them it is clear that the system undergoes a saddle–node bifurcation. Below the bifurcation (figure 3.3.1a), there is a single fixed–point and the dynamics are excitable: small perturbations of V decay away, while those which cross the saddle–point separatrix cause a large excursion in V (*i.e.* an action potential). At the saddle–node bifurcation (figure 3.3.1b), a pair of critical points are created and the dynamics exhibit an invariant circle. This invariant circle persists when the system is taken beyond the bifurcation (figure 3.3.1c) and the dynamics then becomes oscillatory. Furthermore, note that since $g(\mathbf{u}, \mathbf{v}, \varepsilon)$ depends on both of \mathbf{u} and \mathbf{v} , there are regions of parameter space for which a non–zero ε can cause either excitable or periodic behaviour.

In the weak–coupling limit, *i.e.* $\varepsilon \rightarrow 0$, the invariant circle may be parameterized by a new variable $u \in \mathbb{S}^1$. The system (3.1) can therefore be reduced from $\mathbb{R}^p \times \mathbb{R}^q$ to $\mathbb{S}^1 \times \mathbb{R}^q$, and so to the form

$$\begin{aligned} \dot{u} &= \bar{f}(u) + \varepsilon^2 \bar{g}(u, \mathbf{v}, \varepsilon) & u &\in \mathbb{S}^1 \\ \dot{\mathbf{v}} &= \varepsilon \bar{h}(u, \mathbf{v}, \varepsilon) & \mathbf{v} &\in \mathbb{R}^q \end{aligned} \quad (3.3)$$

The invariant circle parameterized by u can now be mapped onto the unit circle by a change of variables $u = \mathcal{K}(\vartheta, \varepsilon)$. Under this second re–parameterization, (3.3) converges uniformly (except in some neighbourhood of $\vartheta = \pi$), in the limit $\varepsilon \rightarrow 0$, to the following canonical form

$$\frac{d\vartheta}{dt} = [1 - \cos(\vartheta)] + [1 + \cos(\vartheta)] \bar{g}(0, \mathbf{v}, 0) \quad (3.4)$$

$$\frac{d\mathbf{v}}{dt} = \frac{1}{c} \bar{h}(0, \mathbf{v}, 0) \quad (3.5)$$

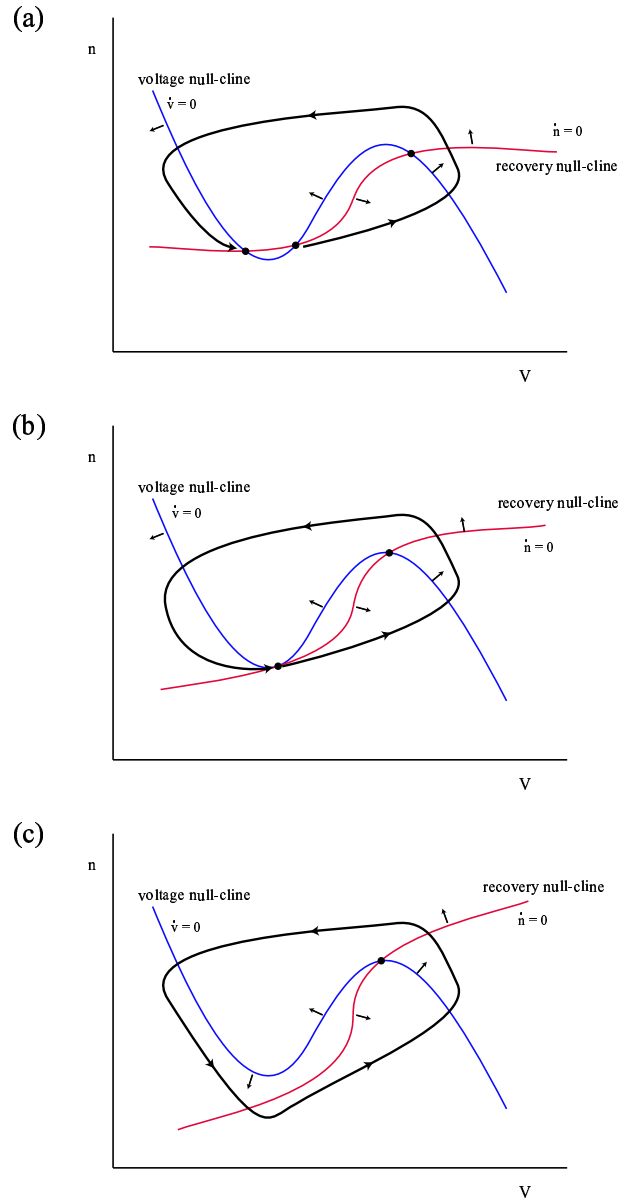


Figure 3.3: *Null-clines for the reduced Hodgkin–Huxley equations (3.2). (a) excitable dynamics: small perturbations of V decay away, while those which cross the saddle–point separatrix generate an action potential. (b) the saddle–node bifurcation and the creation of an invariant circle. (c) persistence of the invariant circle: a limit–cycle solution corresponding to repetitive firing.*

for all $\vartheta \neq \pi$. Where $\vartheta \in [-\pi, \pi]$ is the transformed membrane potential, $\iota = \varepsilon ct$, and c is a constant.

Furthermore, since (3.5) has a stable limit-cycle solution $v(\iota)$, the system (3.4),(3.5) may be replaced by

$$\frac{d\vartheta}{d\iota} = [1 - \cos(\vartheta)] + [1 + \cos(\vartheta)] \bar{g}(0, v(\iota), 0) \quad (3.6)$$

This canonical form has been named the *atoll* model [HI97] since the set of equilibria of the fast sub-system is a circle, and the vector of activity $(\vartheta, v(\iota))$ avoids it (see figure 3.4).

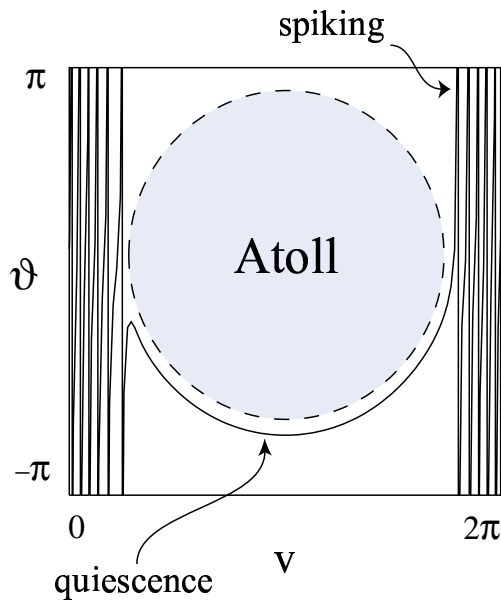


Figure 3.4: The *atoll* model [HI97] for $\bar{g}(0, v(\iota), 0) = \cos(v(\iota))$: the set of equilibria of the fast sub-system, equation (3.4), is a circle, and the vector of activity $(\vartheta, v(\iota))$ avoids it.

3.3.2 A temperature-dependent phase model

I have modified the canonical form (3.6) to account for temperature effects. However, this new model obeys similar dynamics and bifurcations. Specifically, I consider the following

$$\begin{aligned}\frac{d\theta}{dt} &= [b + \cos(\theta)] - A \cos(\Omega t) [1 - \cos(\theta)] \\ &= [b - A \cos(\Omega t)] + [1 + A \cos(\Omega t)] \cos(\theta)\end{aligned}\tag{3.7}$$

where $\theta \in [0, 2\pi]$ is defined on the unit circle \mathbb{S}^1 , and is identified with the (transformed) neuronal membrane potential at the trigger zone. Each time $\theta(t)$ completes a full rotation around the unit circle the neuron generates an action potential. The parameter b characterizes the activity of the electrogenic Na^+ - K^+ pump. The time-dependent term $A \cos(\Omega t)$ models the slow-wave dynamics, and I have chosen a cosine for its analytic simplicity. The up-stroke of the slow wave corresponds to the inward Ca^{2+} current, and the down-stroke to the outward K^+ current. Note, however, that the experimental data shows that the intervals between successive firings inside a burst typically increase monotonically through the burst [BBH80]. This suggests that if indeed the bursting is of slow-wave type, then the wave has an asymmetric shape. Thus, a more complex wave-form may better reproduce the finer details of the discharge pattern. In ionic models such as Plant's, the slow-wave depends on the membrane potential *via* voltage gating. However, recall that under the assumption of a weak coupling, the transformed equations (3.6) exhibit slow dynamics that de-couple from the membrane potential.

Longtin [RBL98] has shown that the frequency Ω of the slow-wave can be related to biophysical parameters of a conductance-based model of slow-wave bursting. The specific model chosen was the Plant model of the R15 cell of *Aplysia*, and his analysis predicts the approximate frequency of the slow-wave as a function of temperature.

The system displays a saddle-node bifurcation from a stable fixed point, resulting in a

stable limit cycle when

$$b - A \cos(\Omega t) = 1 + A \cos(\Omega t) \quad (3.8)$$

each excursion around the limit cycle corresponds to the generation of an action potential. Note that time appears here explicitly and so for certain parameter values, the bifurcation can occur periodically in first one direction and then the other. Thus, if the slow oscillation is of such magnitude that for part of the cycle

$$A \cos(\Omega t) < \frac{(b-1)}{2} - \epsilon \quad (3.9)$$

where ϵ is some small positive number, then the neuron bursts. This oscillatory behaviour across the saddle-node is much simpler than the corresponding bifurcations undergone by ionic models. For example, the Plant model has a two-dimensional slow sub-system that drives the fast, three-dimensional spiking dynamics through degenerate-homoclinic bifurcations between steady-state and limit-cycle solutions.

Close to the bifurcation the phase model exhibits *critical slowing down*, *i.e.* relaxation to a fixed point (the resting potential) becomes polynomial in time rather than exponential, thus increasing the time for $\theta(t)$ to traverse the unit circle. Such behaviour has also been described as passage through a bottleneck [Str94]. Therefore, within a burst there is a non-uniform distribution of spikes: an indicator of parabolic bursting. Critical slowing down and an associated bifurcation has been observed experimentally [MK78] in recordings from the membrane of a squid giant axon. Below the bifurcation point, a periodic electrical stimulus causes sub-threshold oscillations of the membrane potential which exponentially decay to the resting potential. However, as the bifurcation point is attained (either from above or below), the decay slows and is no longer exponential. Above the bifurcation point, stimulation results in a regular oscillation of the membrane potential.

Equation (3.7) may be made more tangible by graphing $1 + A \cos(\Omega t)$ and $b - A \cos(\Omega t)$, as in figure 3.5a. A saddle-node bifurcation occurs when the sinusoids cross, and bursting

occurs (with a mean number of spikes per burst, $\bar{N} \propto \Delta$) when the overlap, Δ , between them is large. Δ is a function of all of A, Ω and b , in fact

$$\Delta = \frac{2}{\Omega} \left(\pi - \cos^{-1} \left(\frac{b-1}{2A} \right) \right) = \frac{1}{\Omega} \left(\pi + \frac{b-1}{A} \right) + O \left[\left(\frac{b-1}{2A} \right)^3 \right] \quad (3.10)$$

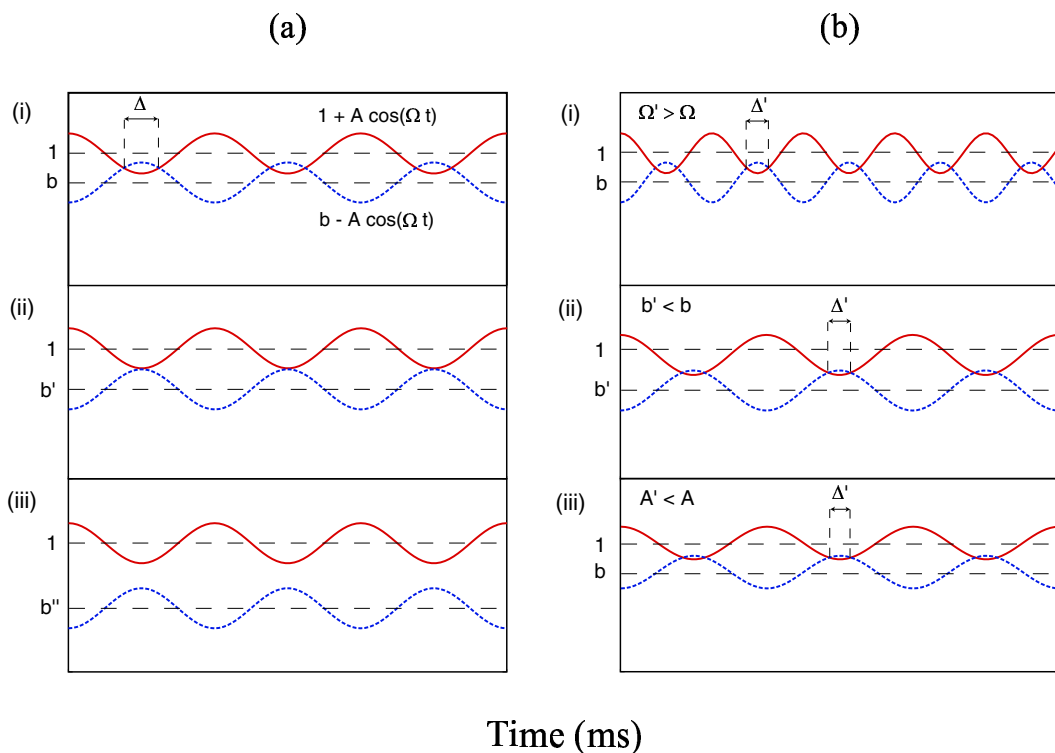


Figure 3.5: (a) The saddle-node bifurcation and bursting criteria for three different parameter regimes, with $b > b' > b''$, and $b' = 1 - 2A$ (see text). (i) when the overlap is large the neuron bursts: i.e. for a time Δ . (ii) bursting has ceased, any spiking activity must be noise driven and the neuron skips (i.e. it does not fire at every slow wave cycle). (iii) all spiking has ceased and the neuron is silent. (b) There are three possible mechanisms by which the burst length can be reduced ($\Delta' < \Delta$) (compare with (a)). (i) increasing slow wave frequency, $\Omega' > \Omega$ (ii) decreasing pump parameter $b' < b$ (iii) decreasing slow wave magnitude, $A' < A$

3.3.3 Modeling temperature dependence and fluctuations

The main effect of a temperature change is a variation in the rate constants of the biochemical processes occurring within the cell. There is evidence that the hyper-polarizing effect of the electrogenic pump becomes more pronounced [CA68] and that the amplitude of the slow wave increases [LH96] with warming. Furthermore, inspection of the spike-trains and corresponding ISIHs of figure 3.1 indicates that the slow wave frequency is also an increasing function of temperature. To maintain the simplicity of this model, I therefore introduce thermal dependence with linear functions of the magnitude of the pump coefficient, and of the magnitude and frequency of the slow wave.

$$b \rightarrow b(T) = b_0 - b_T T \quad A \rightarrow A(T) = A_0 + A_T T \quad \Omega \rightarrow \Omega(T) = \Omega_0 + \Omega_T T \quad (3.11)$$

where $\Omega_0, \Omega_T, A_0, A_T, b_0$ and b_T are constants. Here I am only concerned with the phenomenology of temperature-dependent cellular operation, however note that more complex relationships could be used if required. Figure 3.5b shows how the individual variation of each of these parameters can alter the burst length (however, it is likely that the discharge patterns observed are due to some combination of these mechanisms). I furthermore confine my interest to the temperature range for which $A(T), \Omega(T) > 0$.

The problem of quantifying the amount of neuronal noise present (see chapter 2) is exacerbated by the lack of intra-cellular recordings from these neurons. In the absence of synaptic input, its main components are due to (chapter 2 and [DeF81]) thermal ionic movement; to conductance fluctuations in the ion channels; and to pump noise. It is known (recall the fluctuation-dissipation relation (1.1) and see *e.g.* [DeF81]) that thermal noise, $\xi_T(t)$, is proportional to the *absolute* temperature and so varies only slightly over the temperature range of interest. Pump noise could be modeled by making $b(T)$ a random variable, $b(T) \rightarrow b(T)\xi_m(t) + \xi_a(t)$. Here $\xi_m(t)$ and $\xi_a(t)$ represent multiplicative and additive random noises respectively, and are drawn from some, as yet undetermined, distribution. However, any one-dimensional multiplicative Langevin equation may be transformed into an additive one [Ris89]. Thus, for simplicity these noise terms can be lumped together and so model

neuronal noise by the simple addition of a random term $\zeta(t) = \sigma\xi(t)$ to the dynamical equation (3.7). Furthermore, for concreteness we will choose $\xi(t)$ to be drawn from a zero-mean Gaussian distribution, such that

$$\langle \xi(t) \rangle = 0 \quad \text{and} \quad \langle \xi(t)\xi(t') \rangle = \delta(t - t') \quad (3.12)$$

Such a choice for the distribution aids analysis, but the qualitative aspects of my conclusions generalize to other distributions. I will refer to the noise variance $D = \sigma^2$ as the noise strength. Thus write

$$\frac{d\theta}{dt} = b - A(T) \cos(\Omega(T)t) + [1 + A(T) \cos(\Omega(T)t)] \cos(\theta) + \zeta(t) \quad (3.13)$$

from now on I will assume that $b(T)$, $A(T)$ and $\Omega(T)$ depend implicitly on temperature.

Now examine the system numerically for different temperatures (figure 3.6) and choose b_0 , b_T , A_0 and A_T such that at low temperatures there is a part of the cycle for which (3.9) is satisfied so that the neuron bursts (inset to figure 3.6f). As T increases $\Omega(T)$ and $A(T)$ both increase while $b(T)$ decreases. However, for a given temperature change the increase in $A(T)$ is smaller than and is counteracted by the larger change in $b(T)$. In this way both the intra- and inter-burst periods also decrease with temperature (insets to 3.6d and 3.6e). For high T equation (3.9) is never satisfied, and thus bursting does not occur, instead all spikes are noise driven (inset 3.6a). At low temperatures the histogram (main figures) is dominated by the time between successive spikes in a burst: the intra-burst period. As the temperature increases, the burst length decreases and the inter-burst period dominates (figures 3.6b and 3.6c). For noise-driven beating (figure 3.6a) skipping occurs: higher sub-harmonics of the slow wave begin to appear in the histogram.

3.4 Analysis of bursting and beating

The neuron's behaviour depends strongly on both the noise strength and the temperature. A graph of the mean number of spikes per burst, $\bar{N}(T)$, versus T for a neuron subject

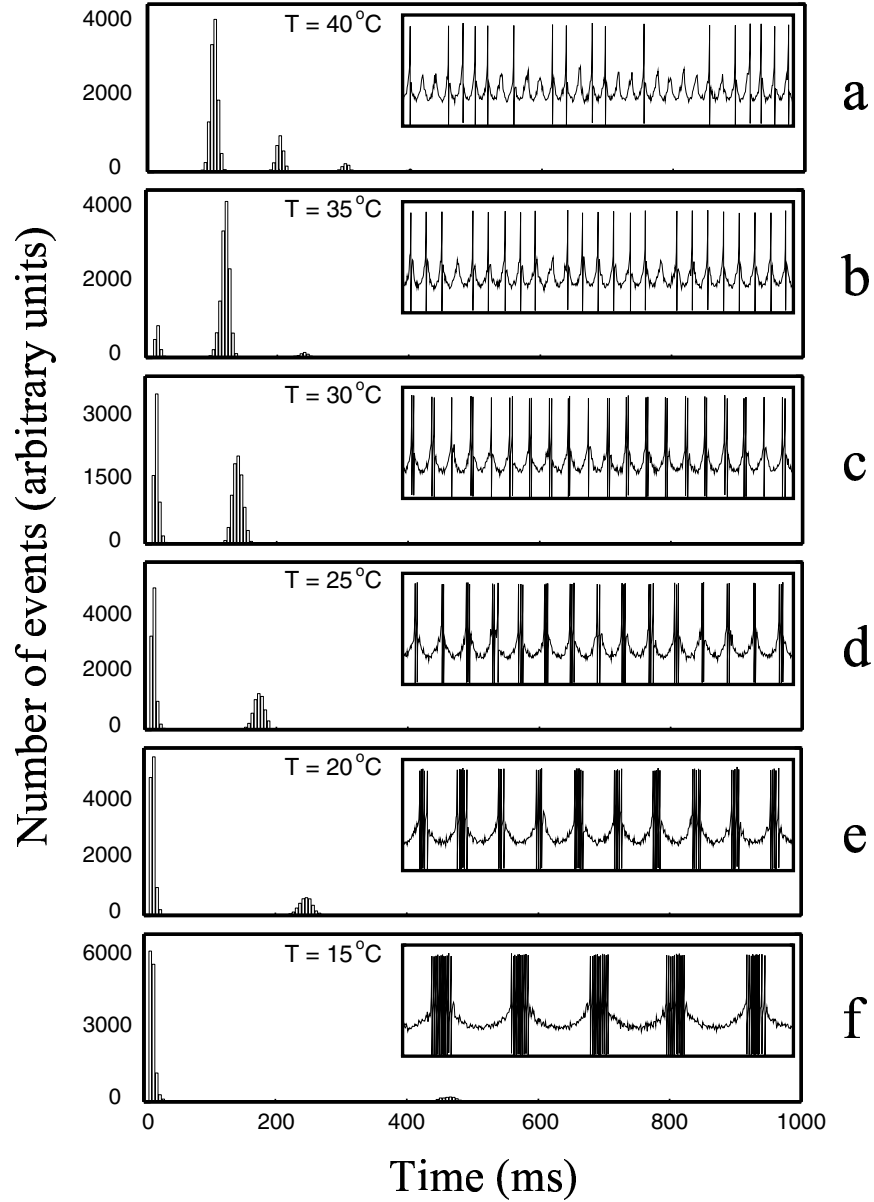


Figure 3.6: *Spikes trains (inset figures) and corresponding inter-spike interval histograms (main figures) for increasing temperatures. Parameters are: $A_0 = 0.3$, $A_T = 0.001$, $b_0 = 0.675$, $b_T = 0.007$, $\Omega_0 = -\pi/150$, $\Omega_T = \pi/1500$, and $D = 5.0$.*

to a vanishingly small level of noise, shows the staircase depicted in figure 3.7. Note that $\bar{N}(T)$ is constant over each plateau, but between adjacent plateaus changes by a single

spike per burst. Each plateau is labeled by its respective value of $\bar{N}(T)$, and the transition temperature between the n^{th} and $(n - 1)^{\text{th}}$ plateaus by T_n . If a low level of noise is now introduced, the staircase retains its shape but the steps become rounded, however as D increases the plateaus disappear and $\bar{N}(T)$ approaches a smoothly decreasing function of temperature.

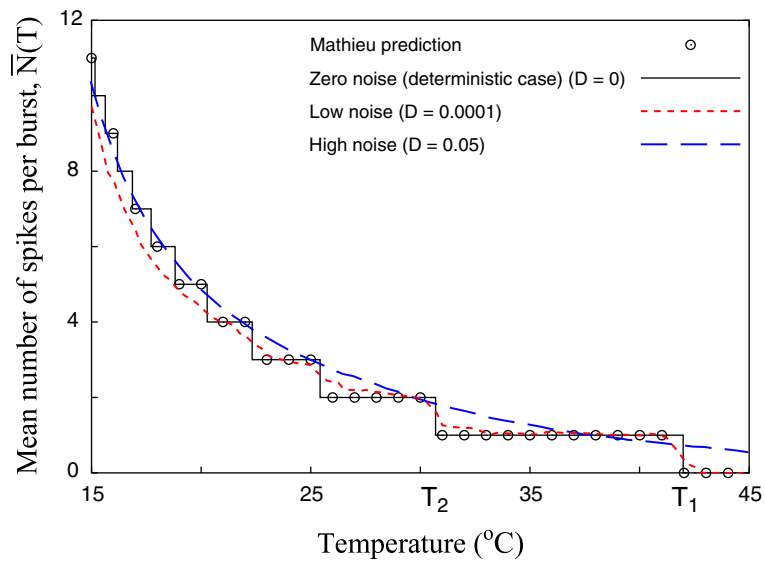


Figure 3.7: Mean number of action potentials per burst, \bar{N} , versus temperature, T . Simulation results with several noise levels are shown, and the circles (o) mark the corresponding Mathieu predictions for the deterministic neuron. Parameters are: $A_0 = 0.3$, $A_T = 0.001$, $b_0 = 0.675$, $b_T = 0.007$, $\Omega_0 = -\pi/150$, $\Omega_T = \pi/1500$, and $D = 0.05$. Two deterministic transition temperatures are also shown. T_2 : the transition between beating and a burst of two spikes per cycle, and T_1 : the transition from beating to silence. Contrast this figure with the data shown in figure 3.2 (but note that in the figure above, temperature **increases** from left to right, while it **decreases** in figure 3.2).

To understand the origin of the staircase, re-interpret equation (3.13) as a gradient descent system in the limit of high friction

$$\frac{d\theta}{dt} = -\frac{dU}{d\theta} + \zeta(t) \quad (3.14)$$

and now view the model as a particle obeying a noisy dynamics in a time-dependent potential $U(\theta, t)$ of the form

$$U(\theta, t) = -\gamma(t) [\lambda(t)\theta + \sin(\theta)] \quad (3.15)$$

where

$$\gamma(t) = 1 + A \cos(\Omega t) \quad \text{and} \quad \lambda(t) = \frac{b - A \cos(\Omega t)}{1 + A \cos(\Omega t)} \quad (3.16)$$

which is equivalent to an *active rotator* [SK86] with periodic coefficients: the multiplicative term $\gamma(t)$ periodically re-scales the magnitude of U , while $\lambda(t)$ periodically sculpts the shape of U . The coefficients $\gamma(t)$ and $\lambda(t)$ are both periodic with period $2\pi/\Omega$, but are anti-phase.

3.4.1 The deterministic limit ($D \rightarrow 0$) – the Strutt map

At any time t , the bias $\lambda(t)$ characterizes the instantaneous deterministic dynamics. Three regimes occur:

- (i) $\lambda(t) < 1$: the oscillator has one stable ($\hat{\theta}_s$) and one unstable ($\hat{\theta}_u$) fixed point, each given by the solutions to $\hat{\theta} = \cos^{-1}(-\lambda)$. This is termed the *locked state* and the dynamics relaxes to the stable fixed point (see inset to figure 3.8a).
- (ii) $\lambda(t) = 1$: the stable and unstable fixed points coalesce via a saddle-node bifurcation to form a half-stable fixed point.
- (iii) $\lambda(t) > 1$: the potential U has no minima and the deterministic dynamics has no fixed points. The oscillator therefore rotates with the variable velocity

$$\dot{\theta}(t) = \gamma(t) (\lambda(t) + \cos(\theta)) \quad (3.17)$$

and each rotation corresponds to the firing of an action potential. Such a solution is termed a *running state* (see inset to figure 3.8b).

Thus the extremal values of $\lambda(t)$, say $\lambda_{max} = (b + A)/(1 - A)$ and $\lambda_{min} = (b - A)/(1 + A)$, define the global behaviour of the system.

- (i) $\lambda_{min} > 1$: the potential U never has a barrier. The neuron fires regularly, and the system is *always-unstable*.
- (ii) $\lambda_{max} < 1$: the potential always has a finite barrier. The neuron is quiescent, and the system is *always-stable*.
- (iii) $\lambda_{min} < 1$ and $\lambda_{max} > 1$: a potential barrier exists for part of the cycle, and the system is *partially-stable*.

An *always-unstable* neuron spikes epileptically³, with no useful temporal structure, and thus has no relevance to this study. Therefore choose A_0 and A_T such that at low temperatures the system is *partially-stable*, and at high temperatures the system is *always-stable*. Denote the critical temperature for which $\lambda_{max} = 1$ by T_c , which is defined by

$$b(T_c) + A(T_c) = 1 - A(T_c) \quad (3.18)$$

and so, for the linear system (3.11)

$$T_c = \frac{1 - b_0 - 2A_0}{2A_T - b_T} \quad (3.19)$$

(for the coefficients shown in figures 3.6 and 3.7 $T_c = 55^0C$). Thus, the n^{th} burst plateau corresponds to a partially-stable system for which the time when the barrier is absent is commensurate with the time to wind n times round the torus.

Perhaps surprisingly it is found that $T_1 < T_c$ (recall that T_1 is the temperature beyond which the deterministic neuron ceases ever to fire). In fact there is a finite temperature range between T_1 and T_c for which one would expect the running mode to persist over a

³*i.e.* continually and at its maximum frequency

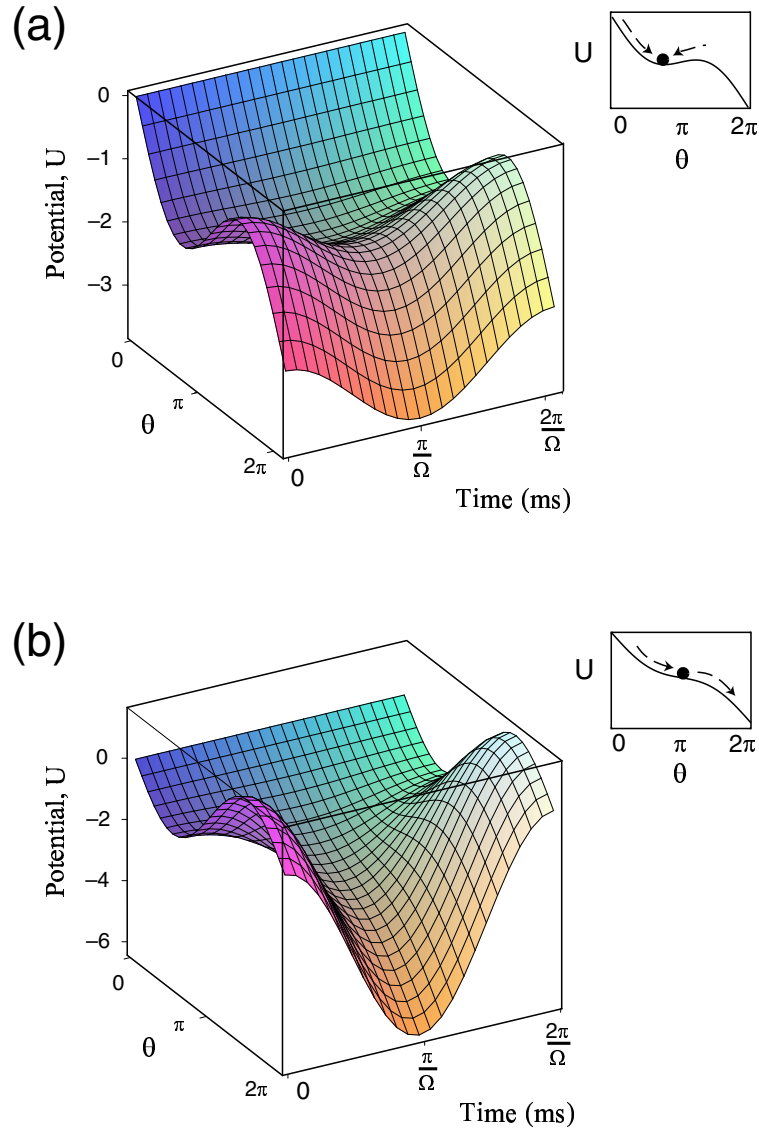


Figure 3.8: *The potential $U(\theta, t)$ for one cycle of the slow wave. (a) $\lambda_{max} < 1$, the always-stable potential. For low noise levels the oscillator tends to remain close to the minima of the potential. (b) $\lambda_{max} > 1$, $\lambda_{min} < 1$, the partially-stable potential. When the barrier is absent the oscillator may escape beyond 2π , generating an action potential. The particle is then re-injected at $\theta = 0$. The inset figures caricature the respective potentials at times $t = (2n + 1)\pi/\Omega$, $n \in \mathbb{Z}$.*

significant part of the oscillation period even though, in the limit $D \rightarrow 0$, no spikes are generated. This is a consequence of critical slowing down close to the bifurcation. If λ_{max} is only marginally greater than unity then a ‘ghost’ [Str94] of the half-stable fixed point causes the relaxation time τ_0 to become comparable to the slow wave oscillation period. The system is then unable to escape beyond this laminar region before λ decreases again below unity and the system undergoes a second saddle-node bifurcation.

A condition for beating to occur may in fact be derived. For at least one action potential to be generated per oscillation, θ must pass through π within the first half of the cycle, *i.e.* within $\tau_0 < \pi/\Omega$. If θ passes through π after one cycle then it moves so slowly that it is unable to escape before the bifurcation recurs and it becomes trapped by the barrier. Thus, if the oscillator is found at the stable state, $\hat{\theta}_s = \cos^{-1}(-\lambda_{min})$, at $t = 0$, this imposes the condition:

$$\int_0^{\pi/\Omega} \dot{\theta} dt \geq \pi - \hat{\theta}_s \quad (3.20)$$

The envelope function (3.10) is a heuristic that loosely predicts how the deterministic pattern varies with temperature. However, for this deterministic case, it is possible to predict exactly how many action potentials are actually generated during one cycle. Following Ermentrout and Kopell [EK86] the zero-noise limit of (3.13) may be recast as a Mathieu equation. Use the transformation

$$\frac{1}{V} \frac{d}{dt} V = \frac{1+b}{2} \cot\left(\frac{\theta}{2}\right) \quad (3.21)$$

and the identity

$$\cos(\theta) = \frac{\cot^2(\frac{\theta}{2}) - 1}{\cot^2(\frac{\theta}{2}) + 1} \quad (3.22)$$

to obtain

$$\frac{d^2}{ds^2} V + [a - 2q \cos(2s)] V = 0 \quad (3.23)$$

where time has been rescaled so that $2s = \Omega t$ and I have introduced, to accord with convention [McL47], the coefficients a and q

$$a = \frac{b^2 - 1}{\Omega^2} \quad q = \frac{A(b + 1)}{\Omega^2} \quad (3.24)$$

The Mathieu equation (3.23), is a linear equation with periodic coefficients [McL47], and hence, according to Floquet's theorem (see appendix A.1), has a general solution of the form

$$V(s) = c_1 \exp(\rho_1 s) p_1(s) + c_2 \exp(\rho_2 s) p_2(s) \quad (3.25)$$

where c_1 and c_2 are constants, ρ_1 and ρ_2 are termed characteristic exponents, and the $p_i(s)$ are periodic functions with the same minimal period as the periodic coefficient of the original equation (3.23). Four solution classes occur [JS87]:

- (i) $\rho_1, \rho_2 \in \mathbb{C}$ with $\rho_1 = \beta i$, $\rho_2 = \rho_1^*$, and $\beta \in \mathbb{R}$, and the general solution is

$$V(s) = c_1 \exp(i\beta s) p_1(s) + c_2 \exp(-i\beta s) p_2(s) \quad (3.26)$$

All solutions are therefore bounded and oscillatory but generally quasi-periodic since two frequencies, β and 2 (*i.e.* the forcing frequency of (3.23)), are present.

- (ii) $\rho_1, \rho_2 \in \mathbb{R}$ with $\rho_1 = \alpha > 0$, $\rho_2 = -\rho_1$, and the general solution is

$$V(s) = c_1 \exp(\alpha s) p_1(s) + c_2 \exp(-\alpha s) p_2(s) \quad (3.27)$$

All solutions are therefore unbounded.

- (iii) $\rho_1, \rho_2 = 0$, there is one solution of period 2π (and one unbounded solution).

- (iv) $\rho_1, \rho_2 = \frac{1}{2}i$, there is one solution of period 4π (and one unbounded solution).

The (a, q) plane is divided into a countable set of simply connected regions for which either all solutions fall into class (i) – the *stable* regions, or they belong to class (ii) – the *unstable*

regions. This situation is depicted in the Strutt stability map (figure 3.9). The boundaries between the stable (shaded) and unstable (un-shaded) regions are given by curves containing solutions of either class (iii) or class (iv) (bold and dashed lines respectively).

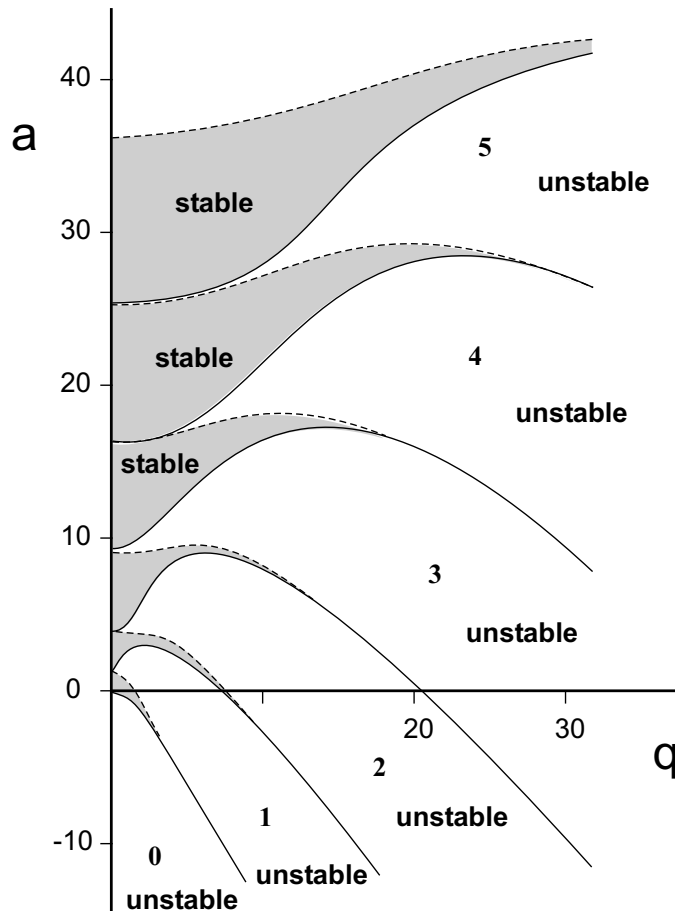


Figure 3.9: *The Strutt map: stability and instability regimes for the Mathieu equation. The graph is symmetric about the ordinate.*

The labelled ‘tongues’ in the Strutt map are instability regimes and contain unbounded solutions. Let I_j denote the j^{th} instability tongue, corresponding to general solutions of the form (3.27). Unbounded solutions generally fall into two qualitative types [NM95]: either oscillatory but with an amplitude that increases exponentially with time, or non-oscillatory but exponentially increasing; my interest is with the former. According to the Sturm

oscillation theorem [CL55], each of the periodic functions, $p_1(s)$ and $p_2(s)$ of a solution in the j^{th} instability region has exactly j zeros per oscillation period of the slow wave.

Returning to the original variable

$$\theta(s) = 2 \cot^{-1} \left[\frac{2(c_1(\alpha p_1(s) + p_1'(s)) + c_2 \exp[-2\alpha s](-\alpha p_2(s) + p_2'(s)))}{(1+b)(c_1 p_1(s) + c_2 \exp[-2\alpha s] p_2(s))} \right] \quad (3.28)$$

since $\alpha > 0$, then if $c_1 \neq 0$, $\theta(s)$ exponentially approaches the stable periodic solution

$$\theta_s(s) = 2 \cot^{-1} \left[\frac{2(\alpha p_1(s) + p_1'(s))}{p_1(s)(1+b)} \right] \quad (3.29)$$

Since $p_1(s)$ has j zeros over the period of the slow wave oscillation, the argument to $\cot^{-1}(\dots)$ ‘blows up’ j times over this period. Consequently θ passes through zero j times within a period. Furthermore, by use of (3.7) and (3.9) it is simple to verify that each time θ passes through zero, it does so with a positive velocity, $\dot{\theta}$. Thus, θ wraps around the torus j times per slow wave cycle. This then corresponds to a burst containing j spikes.

The coefficients of the Mathieu equation (3.23) are parameterized by the temperature, and so as T varies it carves a trajectory across the (a, q) plane. As the trajectory passes through the k^{th} instability region the neuron has a burst length of k spikes, generating the plateaus previously seen in figure 3.7.

3.4.2 Stochastic dynamics of bursting and beating – smoothing the Mathieu staircase

To clarify how the transitions between plateaus become ‘smoothed’ as noise is introduced, I will examine the transition from beating to quiescence, occurring at $T = T_1$, however my conclusions will extrapolate to each transition between the n^{th} and $(n-1)^{\text{th}}$ plateaus.

Now introduce a small amount of noise into the dynamics, $D \neq 0$. For T marginally greater than T_1 the neuron now emits a succession of single spikes which are entrained to the underlying slow wave, but occasionally cycles are skipped. As the temperature increases

beyond T_1 , periods are skipped more frequently until the neuron becomes silent. At any temperature the skipping rate depends on the noise level. Rappel and Strogatz [RS94a] and Gang *et al.* [GDNH93] have argued that (depending upon whether the system is above or below the saddle–node bifurcation) noise can propel the neuron either through the laminar bottleneck ($T < T_c$), or over the incipient barrier ($T > T_c$), and thus aid it to fire. The spectral signatures of such noise–induced crossings of a critical point, with an attendant rotation, have been termed *noisy precursors* by [Wie85, NSS97].

Conversely, for temperatures slightly below T_1 the noisy neuron is seen to occasionally misfire and thus skip a period of the slow wave oscillation. In this regime, although the deterministic neuron is able to fire, the noise can trap the system above the ghost bottleneck and postpone its firing. To understand this, note that critical slowing down in the laminar bottleneck means that the noisy dynamics has negligible drift in this region and so approximates a one–dimensional Wiener process. Thus, the neuron is equally likely to diffuse in either direction. If the diffusion acts to diminish $\dot{\theta}$, the firing condition (3.20) may be violated and firing retarded. Qualitatively similar retardation and trapping due to noise has been noted by Apostolico *et al.* [AGMS94] as a failure mechanism in bi–stable switches and by Mantegna *et al.* [MS96b] in the variations of the voltage across a periodically driven tunnel diode when coupled to an RC circuit and a source of noise.

These two skipping modes have a natural interpretation in terms of the Strutt map. Neural dynamics close to a transition temperature correspond to a region in parameter space that is close to a tongue boundary. The inclusion of noise allows the neuron to execute a random walk through the map, and so to explore adjacent regions of the parameter space. Thus, if the neuron is in the j^{th} tongue but lies close to the $(j + 1)^{\text{th}}$, then the noise can carry the neuron over the boundary, and thus augment the burst. Conversely, if the neuron lies closer to the boundary with the $(j - 1)^{\text{th}}$ tongue, the noise can delete a spike from the burst.

The skipping rate

I have shown that (equation 3.20) for the deterministic neuron, a spike is only generated if θ passes through π within the first half of the cycle. Numerical investigations of equation (3.14) show that the condition (3.20) generalizes to the case of weak noise, however now the *probability* that θ is greater than π after half a driving period must be considered instead. Introduce the conditional probability density $p(\theta, t|\theta_0, t_0)$ subject to the initial condition

$$p(\theta, 0|\hat{\theta}_s, 0) = \delta(\theta - \hat{\theta}_s) \quad (3.30)$$

Therefore the probability $P(\theta > \pi, t|\hat{\theta}_s, 0)$ that at a time t , θ is greater than π is given by

$$P(\theta > \pi, t|\hat{\theta}_s, 0) = \int_{\pi}^{2\pi} p(\theta, t|\hat{\theta}_s, 0) d\theta \quad (3.31)$$

which is equal to the probability of generating an action potential. By performing an ensemble average, this quantity may be equated with the mean firing, or skipping, rate (when measured in spikes per slow wave cycle).

The conditional probability density obeys a Smoluchowski equation (section 1.3 and [Ris89])

$$\frac{\partial}{\partial t} p(\theta, t|\hat{\theta}_s, 0) = \frac{\partial}{\partial \theta} \left[U'(\theta, t) + \frac{D}{2} \frac{\partial}{\partial \theta} \right] p(\theta, t|\hat{\theta}_s, 0) \quad (3.32)$$

where $U'(\theta, t)$ represents the spatial derivative of the potential. The time-dependence of the potential forbids a general closed solution to (3.32), and furthermore makes a numerical solution difficult to obtain. However, an approximation to the probability density, $p(\theta, t|\hat{\theta}_s, 0)$ may be ascertained. First, numerically iterate an ensemble of \mathcal{N} receptors $\theta_i(t)$, $i = 1 \dots \mathcal{N}$, for half a slow wave period, subject to the initial condition $\theta_i(t = 0) = \hat{\theta}_s \forall i \in \mathcal{N}$. An approximation to $p(\theta, t|\hat{\theta}_s, 0)$ will be given by a normalized histogram of the ensemble of $\theta_i(t = \pi/\Omega)$ and so an estimation of the firing rate may be found from equation (3.31) (see figure 3.10).

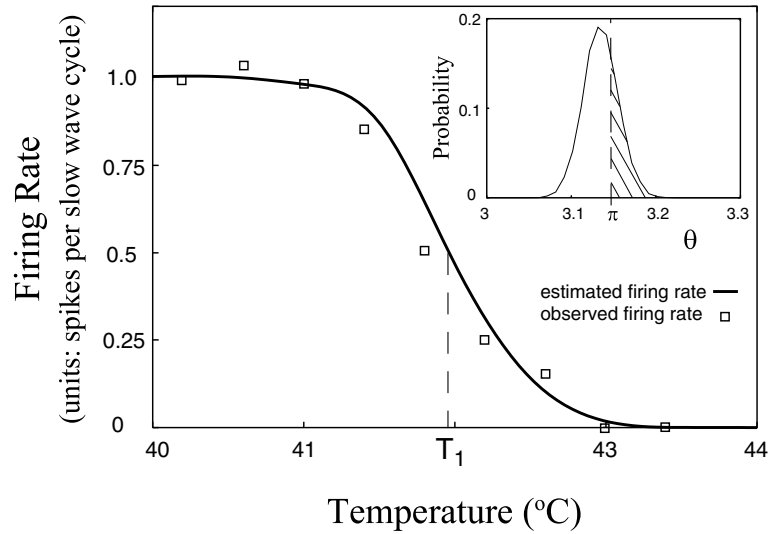


Figure 3.10: An estimation of the firing rate close to the transition temperature T_1 . The squares show numerically observed firing rates (measured in spikes per slow wave cycle) while the bold line depicts the rate as estimated by the method of section 3.4.2. Parameters are: $A_0 = 0.3$, $A_T = 0.001$, $b_0 = 0.675$, $b_T = 0.007$, $\Omega_0 = -\pi/150$, $\Omega_T = \pi/1500$, and $D = 10^{-4}$. The inset figure shows a histogram approximation to the probability density $p(\theta, t = \pi/\Omega|\hat{\theta}_s, 0)$ at $T = 42^\circ\text{C}$.

3.5 Analysis of the near-threshold regime – noise enhanced stability and resonance

In this section I wish to shift the focus of attention to how the firing patterns depend upon noise intensity rather than upon the temperature. Understanding the influence of noise on the phase model (3.7) can provide insight into its effect on temporal coding in this and other systems. I have established that noise can increase the dynamic range of a bursting neuron, and so now ask how this enhancement depends upon the noise strength.

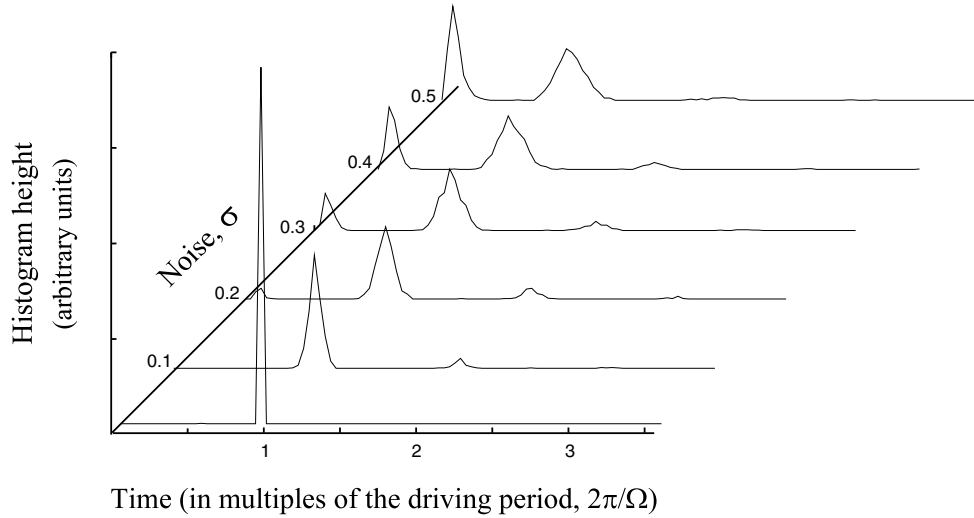


Figure 3.11: *Inter-spike interval histograms for $T < T_1$. Parameters are: $A_0 = 0.3$, $A_T = 0.001$, $b_0 = 0.675$, $b_T = 0.007$, $\Omega_0 = -\pi/150$, $\Omega_T = \pi/1500$, and $T = 38^\circ\text{C}$. Several values of the noise standard deviation σ are shown.*

3.5.1 Stability and trapping for $T < T_1$

$\bar{N}(T)$ is too coarse a measure of the neuronal dynamics when considering the influence of noise since it neglects much of the fine detail of the distribution of firing times. A more informative measure is the inter-spike interval histogram (ISIH). First consider the neuronal spike train generated when $T < T_1$ (figure 3.11). To compute the ISIH, the time intervals between 2×10^4 consecutive spikes are measured, normalized, binned and histogrammed. The resulting histogram for $D = \sigma^2 = 0$ has a single narrow peak at $2\pi/\Omega$, corresponding to one spike per cycle with infrequent skipping. The width of the peak indicates that each spike is tightly synchronized to the slow wave. For increasing D the ISIH begins to show a multi-peaked structure with peaks located at sub-harmonics of the slow-current, and with heights that decay exponentially. Furthermore, as D increases, the peaks begin to splay showing that synchronization to the slow-wave becomes less exact.

There is a critical noise level, D_c , which is strongly temperature-dependent and for which

the multi-peaked structure is most pronounced. For $D > D_c$ the higher sub-harmonics subside and a new peak close to the origin begins to dominate the histogram. Examination of the spike trains for $D \gg D_c$ shows that the high noise causes the generation of several spikes in one period, $2\pi/\Omega$, indicating that the new peak in the ISIH corresponds to a noise-induced intra-burst period. However, such phenomena are rare in the experimental data [BBH80] and so it is clear that these noise levels are unphysical. The major result of

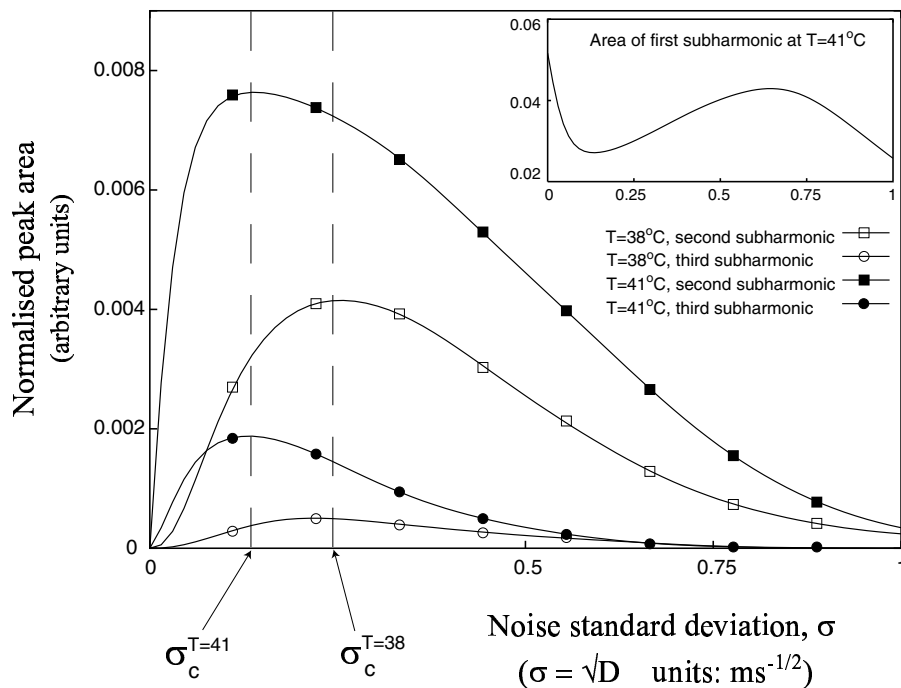


Figure 3.12: *Residual SR: the variation with noise of the area under the 2nd and 3rd sub-harmonic peaks, (\mathcal{P}_2 & \mathcal{P}_3) for $T < T_1$, ($T = 38$ and $T = 41$). The standard deviation of the noise, σ , is shown rather than the variance D since the maxima are better defined on this axis. For clarity the curves drawn are interpolations through the data, the symbols are merely meant to guide the eye.*

both [AGMS94] and [MS96b] was that the mean escape time for a periodically modulated particle moving in a partially-stable potential depends strongly, and non-monotonically, on the noise strength. In this formalism, an escape event corresponds to the firing of an

action potential. For vanishingly small noise levels, firing is entrained to the slow wave and thus the mean firing time is close to one period of oscillation, $2\pi/\Omega$. For high levels of noise, escape events are noise driven and interval times are randomly distributed with a mean that is much less than $2\pi/\Omega$. However, intermediate noise levels can trap the particle, causing it to skip cycles of the slow oscillation and thus prolonging the mean escape time (a related phenomenon arises in the thermally-dependent Plant model [LH96]). In this intermediate noise regime the distribution of firing times shows the multi-modal structure [CM94] previously observed. A resonance effect was noted [AGMS94], termed *residual stochastic resonance*: as the noise increases, the area under each peak except the first increases to a maximum, and then decreases. As we have seen, all sub-harmonics reach their maximum simultaneously, and thus the mean escape time is maximized. This maximal condition signifies a resonance, which further implies that two (or more) of the system's time-scales must match. In fact, resonance is attained when the trapping time due to noise is close to half of the driving period [AGMS94].

To measure D_c at a particular temperature, we follow [GMS95] and compute the strength of the n^{th} peak according to (1.48).

A plot of \mathcal{P}_n , ($n \neq 1$) versus noise, now gives the uni-modal graph shown in figure 3.12. Furthermore, it is clear that D_c is a function of the temperature: as T increases, D_c decreases. This may be readily explained by considering that since the oscillation frequency $\Omega(T)$ is a function of temperature, so too is the resonance condition.

Residual SR should be contrasted with the complimentary effect for sub-threshold forcing [GMS95] in which resonance is attained when the **first**, or harmonic, peak is maximal (see section 1.5 and below).

3.5.2 Resonance for $T > T_1$

The dogfish data of [BWSH94] indicates that noise is an important determinant of the neuronal discharge pattern. Furthermore, the experiments reported in section 1.5.3 indicate that noise might also aid the transduction of small sub-threshold signals by various sensory

neurons. Autonomous SR (ASR) [GDNH93] (also termed “coherence SR” [NSS97]) is noise-induced coherent motion in systems that are not subject to an external forcing. Longtin [Lon97] has shown that autonomous stochastic resonance can occur in other models of neuronal bursting: the Plant model and also the Hindmarsh–Rose model (a spike-driven bursting model) [HR84]. The slow wave is an endogenous excitation, coupling multiplicatively to the dynamics, and consequently this model is a likely candidate to exhibit autonomous SR.

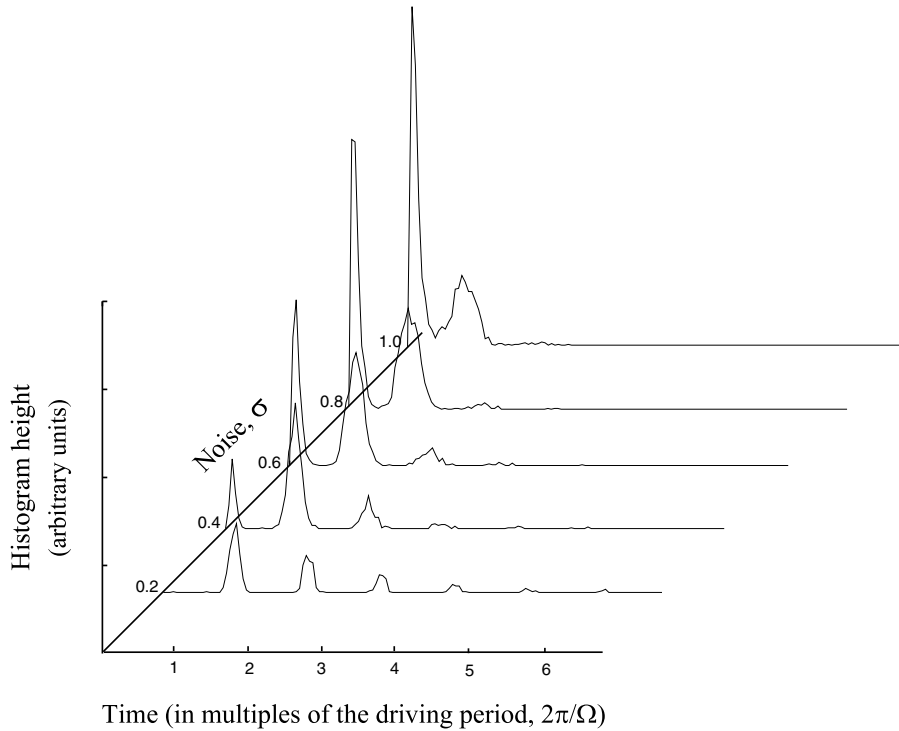


Figure 3.13: *Inter-spike interval histograms for $T > T_1$. Parameters are: $A_0 = 0.3$, $A_T = 0.001$, $b_0 = 0.675$, $b_T = 0.007$, $\Omega_0 = -\pi/150$, $\Omega_T = \pi/1500$, and $T = 44^\circ C$. Several values of the noise standard deviation σ are shown.*

At first glance, the discharge patterns for $T > T_1$ are indistinguishable from those for $T < T_1$, since the spike trains for both regimes comprise single spikes with skipping. However, computation of histograms of firing intervals at various noise levels (figure 3.13), now shows that the histogram for $D \rightarrow 0$ is multi-peaked, with peaks located at sub-harmonics

of the driving force, and with an exponential fall off. With increasing noise the height of each harmonic first rises and then decreases, reaching a maximum at a critical noise strength. For high noise levels a new peak close to the origin occurs again, representing noise induced bursts of spikes. In contrast to residual SR the peaks do not reach their maximum simultaneously, instead each peak has a unique critical noise (figure 3.14) and so this model also exhibits ASR.

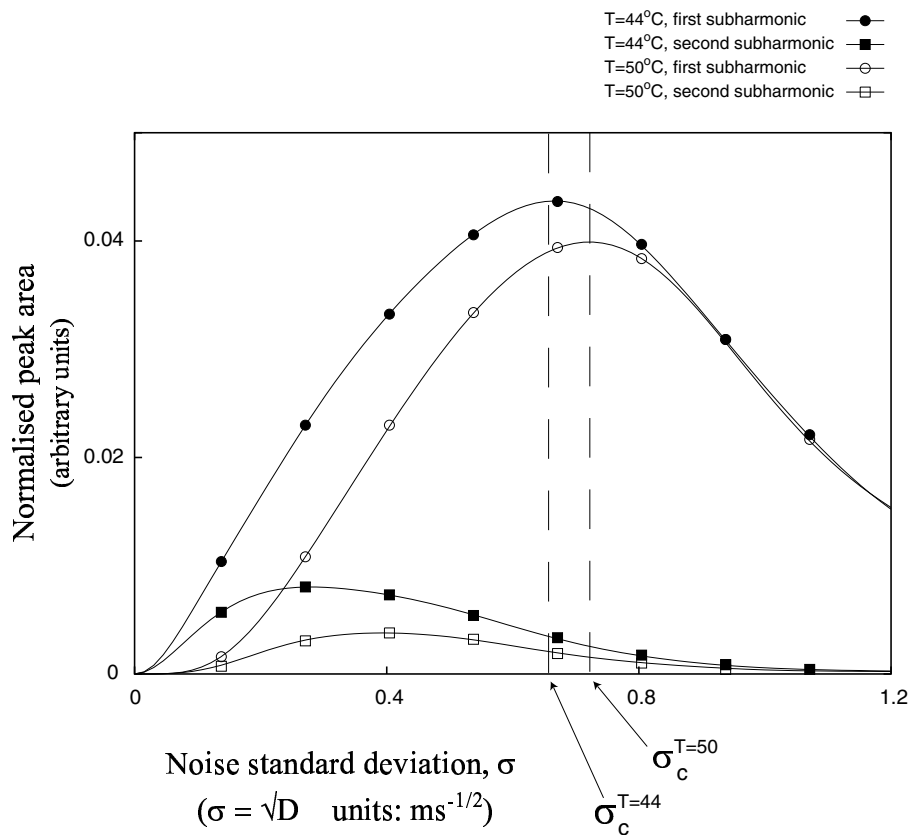


Figure 3.14: Stochastic Resonance: the variation with noise of the area under the first three harmonic peaks (\mathcal{P}_1 , \mathcal{P}_2 & \mathcal{P}_3) for $T > T_C$, ($T = 38$ and $T = 41$). The standard deviation of the noise, σ , is shown rather than the variance D since the maxima are better defined on this axis. For clarity the curves drawn are interpolations through the data, the symbols are merely meant to guide the eye.

3.6 Discussion

3.6.1 Paths for other receptors

There are many different thermally responsive bursting cells [BSWH84], for example: the feline lingual and infra-orbital nerves, the Boa constrictor warm fibre, and the dogfish ampullae of Lorenzini. The discharge patterns of all of these cell types exhibit many similar qualitative features, but quantitatively they differ, *e.g.* differing burst lengths at a given temperature. In addition, there can also be considerable variation within a single cell type (recall section 3.2). Therefore, this paradigm of a temperature-dependent noisy trajectory through the Strutt map allows a universal model that may explain the discharge patterns of all of these cells.

3.6.2 Chaos

The existence of chaos in thermo-responsive neuronal spike-trains has been recently studied in both real, [BSV⁺97] and model, [LH96] neurons. However, the phase model reported here does not support chaos, instead its spike-train irregularities have a stochastic origin. Is this important? For this class of neurons at least, the answer is “probably not”, since it is more likely that the bursting pattern itself is the fundamental carrier of information rather than the timing of individual spikes within a burst. Such patterns are more reliably detected by higher neurons due to synaptic facilitation, and furthermore even a single burst cause long-term synaptic modification [Lis97].

3.6.3 Noise distributions

I have chosen to describe thermal and pump noise by a simple, additive, white noise term. Recall that the discharge pattern derives from a random walk through the Strutt map, and that spike augmentation and deletion arise when the random walk crosses a tongue boundary. In consequence, note that other additive noise distributions will produce quali-

tatively similar burst patterns, and so the actual noise distribution is not pertinent to an understanding of the general model. However, the noise distribution is extremely important when describing a specific burst pattern.

3.6.4 Asymmetric burst patterns

In contrast to this phase model, discharge patterns from real cold-receptors do not exhibit symmetric burst patterns. Typical [BBH80] burst profiles comprise a rapid increase followed by a slower decrease in spike frequency, resulting in a ‘sawtooth’ profile. Such a saw tooth could be generated by a fast-activating and slowly in-activating calcium dynamics, *e.g.* calcium-induced-calcium release from internal stores. Within the phase model paradigm, the spike distribution within a burst may therefore be changed by a selecting a different functional form of the slow oscillation. However, as a consequence of the lack of intracellular recordings, there is no experimental evidence to guide this choice, and so as a first approximation I have chosen a cosine for its tractability.

3.7 Conclusions

I have presented a tractable phase-model for cold-receptor function. This canonical phase-model can be related to more complex, bio-physical, models of neuronal operation. I have investigated the phase-model (both numerically and analytically) in the deterministic regime and also when subject to a finite amount of thermal noise. Numerically obtained spike trains and inter-spike interval histograms from the phase model agree well with the experimental data. My investigations indicate that skipping might be caused by noise. I have further shown that both the number of spikes in a burst, and also the skipping rate at any given temperature may be predicted. I have studied how altering the noise level affects the dynamics and I have seen the skipping regime may be sub-divided: the first part of skipping is caused by noise-induced trapping and the second part is due to noise-induced spiking. Finally, I have demonstrated that the phase-model displays a non-monotonic dependence on noise strength, and in fact exhibits both resonant trapping and autonomous stochastic resonance. The main results of this chapter are to appear in [RBL98].

Chapter 4

The perception of ambiguous images

4.1 Introduction

The perception of an ambiguous figure is a multi-stable process [Att71]. An ambiguous figure is one that has two (or more) perceptual alternatives, and classic examples are the Necker cube [Nec32] (figure 4.1 (a)) and Fisher's man/girl figure [Fis67] (figure 4.1 (b)). When one looks steadily at such a figure, the information impinging upon the retina remains constant. In spite of this, the perception of the figure is found to flip continually and randomly between the possible interpretations, although both are never seen simultaneously. This reversal of perception can be influenced by will and practice, but cannot be prevented. The perceived pattern is stable between flips, but if a subject looks at an image for several minutes the stability periods initially habituate for 1–3 minutes during which time the flipping rate increases. After this initial time a stable average period is observed, and this average stability period of an interpretation is approximately constant if all other factors are held fixed. However, mean stability times differ significantly between people and between patterns. A probability distribution of switch times may be generated by taking an histogram of the switching time series, and the resulting distribution has been fitted to

a gamma distribution¹ [BDA⁺72].

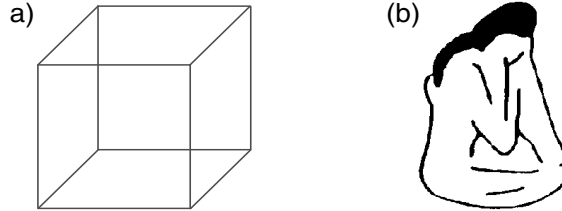


Figure 4.1: *Ambiguous figures: (a) the Necker cube and (b) Fisher's man/girl figure (reproduced from [CA93]).*

An instructive demonstration of how stable an interpretation can be is to fold a piece of card along its longitudinal axis and place it on a flat surface. When the card is viewed from above at a 45° angle for several seconds with only one eye, it is seen to reverse and appears to stand up on end like an open book. If one's head is now moved from side to side while the card is reversed, the brain attempts to make sense of the resulting change in perspective. The only way it can do this is by attributing motion to the card and so it appears to twist backwards and forwards.

One can clearly observe 'locking in', or stabilization, of a perceptual alternative while viewing the Leeper–Boring figure (frontispiece). For example, if the nose/chin line is tentatively identified as a nose, then the line below is assumed to be a mouth and the shapes above to be eyes. These partial identifications mutually support each other to form the stable perception of an old woman. If however the line is seen as a chin then a similar process provides the perception of a young woman. Which facet is perceived first depends not only on accidental factors, such as which part of the figure is seen first, but also on the subject's pre-conceptions. For example, initial interpretations of the Leeper–Boring figure

¹The gamma distribution of integer order $a > 0$ is the waiting time to the a^{th} event in a Poisson process. A gamma deviate has the probability density

$$p_a(x) = \frac{x^{a-1} \exp(-x)}{\Gamma(a)} \quad (4.1)$$

where $\Gamma()$ is the gamma function. When $a = 1$ it reduces to the exponential distribution.

are distributed among the general population according to 40% perceiving the old and 60% perceiving the young woman. If a group is first exposed to a strongly biased version of the figure (figure 4.2) and is then shown the unbiased one, close to 100% perceive the old woman first. Furthermore, spontaneous reversals are inhibited until the other aspect of the figure is pointed out to the subject.



Figure 4.2: *The biased Leeper–Boring figure (compare with frontispiece). If a group of subjects is first exposed to this figure and then shown the unbiased one, close to 100% will perceive the old woman first (see text). (Reproduced from [Hak91]).*

This notion of the brain dynamics locking in to an attractor is a metaphor that has proved invaluable to the understanding of associative memory [Hop82] and olfactory recognition [Fre91]. Furthermore, such a paradigm relates well to Shepherd’s thesis [She87] of a *metric of similarity*: the brain represents objects as points in some psychological space in such a way that ‘similar’ objects inhabit proximal regions. The putative neural mechanism for recognition is [Att71, SH95] that each interpretation is represented by a distinct attractor, and the dynamics relaxes to whichever attractor has the greatest overlap with the retinal input. Reversal was originally thought to be due to habituation: active neurons would become satiated and fire less frequently, de-emphasizing the attractor. However, habituation is a largely deterministic process, and analysis of the return map of the switching times [SH95] reveals that the switching dynamics is stochastic with no causal component. Reversal is therefore a noise-induced transition between two attractors, and is due to fluctuations in the perceptual process. It has little dependence on habituation. Since switching can still

occur without changing one's focus of attention, these fluctuations are presumed to have a neural origin (chapter 2).

With the exception of the Necker cube, the two perceptual alternatives are rarely of equal strength and typically one interpretation is preferred. Reversion still occurs if this bias is weak, but the reversion times of each individual component differ and the stronger the bias, the longer the reversion time. To invoke the attractor metaphor, such a preferred interpretation would be an attractor with a deeper minima than the other.

Perceptual ambiguity is not confined to humans, since other animals appear to exhibit similar responses to these figures. If hens are exposed to figure 4.3 moving to the left a fear response is elicited since it resembles the motion of a bird of prey. However, if it is shown moving to the right it appears to be a goose in flight and so is ignored [SK95].

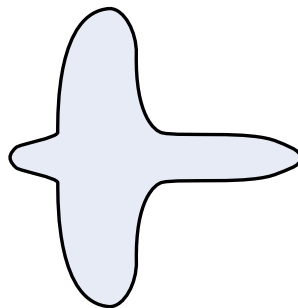


Figure 4.3: *If the figure moves to the left it appears as a bird of prey and so generates a fear response in hens, but moving to the right it resembles a goose and is ignored.*

4.2 Stochastic resonance in cognition

Recent experiments imply that perceptual fluctuations can interact with a periodic bias in a manner that is consistent with stochastic resonance.

4.2.1 Riani and Simonotto's experiment

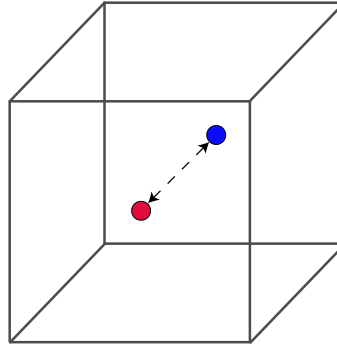


Figure 4.4: *The biased Necker cube: fixation on the red dot skews one's perception toward the lower left corner appearing in the foreground, while fixation on the blue emphasizes the upper right as foreground (see text).*

There is a weak correlation between one's fixation point on a figure and one's interpretation of that figure [ES78]. This is readily seen by fixing on one of the dots in figure 4.4: fixation on the red dot skews one's perception toward the lower left corner appearing in the foreground, while fixation on the blue emphasizes the upper right as foreground. Riani *et al.* [RS95] have exploited this fact to bias periodically a Necker cube. They superimposed a moving coloured spot which travelled along a line contained within the middle of the figure and inclined at 60° to the horizontal. The amplitude of the trajectory was smaller than the dimensions of the cube, and its motion was sinusoidal with a period of 10 seconds. For the unbiased Necker cube, reversal times are symmetric, and they are gamma distributed. The mean and the standard deviation of the gamma distribution depend upon the size and aspect ratio of the cube [BCR⁺82], increasing for larger cubes. The dimensions of the cube therefore parameterizes the effect of perceptual fluctuations on the recognition process. Thus we have a bi-stable system with a deterministic time-scale and a variable source of noise.

Cubes of varying size were presented to test subjects and a time series of reversal periods taken. The power spectra of the time series clearly show the effect of periodic modulation.

Pronounced peaks appear at the signal frequency and at its higher harmonics, which are absent when there is no external modulation. Such peaks indicate that reversal times are partially entrained to the periodic bias, and are clear evidence of stochastic resonance.

4.2.2 Chialvo and Apkarian's experiment

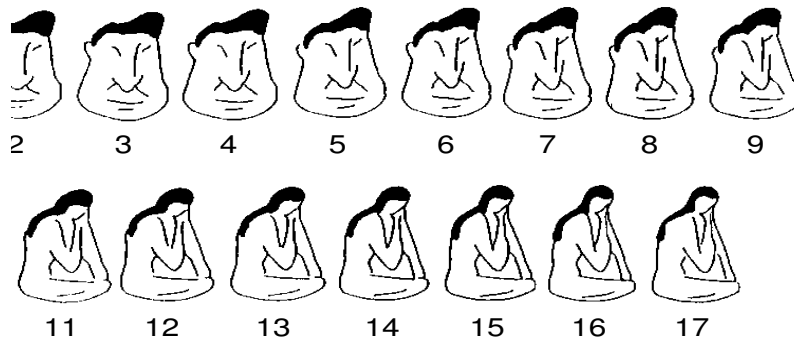


Figure 4.5: *Interpolations between the two extremes (figures 1 and 17) of Fisher's man/girl figure. (Reproduced from [CA93].*

Two biased versions of Fisher's man/girl figures were drawn [CA93], representing each of the two possible interpretations. A series of 17 images interpolating between them was generated, as shown in figure 4.5. Images from this series were selected at random and presented to each of a group of subjects, and the subject was asked to rank each image as to its position in the series. As the histogram in figure 4.6 clearly shows, the subjects wrongly identified most of the images. They tended to classify them to the two extremes – the man's face and the young girl, and rarely identified them as transitional images, showing that each person's perception can be reduced to a bi-stable map.

Therefore, in analogy with other work on noisy bi-stable systems, image perception was studied iteratively. An initial image was presented and categorized from 1 to 17 by the subject. A random number and a sinusoidal modulation were added to the number corresponding to the identified image, and the resulting number determined the next figure to present. This new figure was then categorized and the process repeated, and so on.

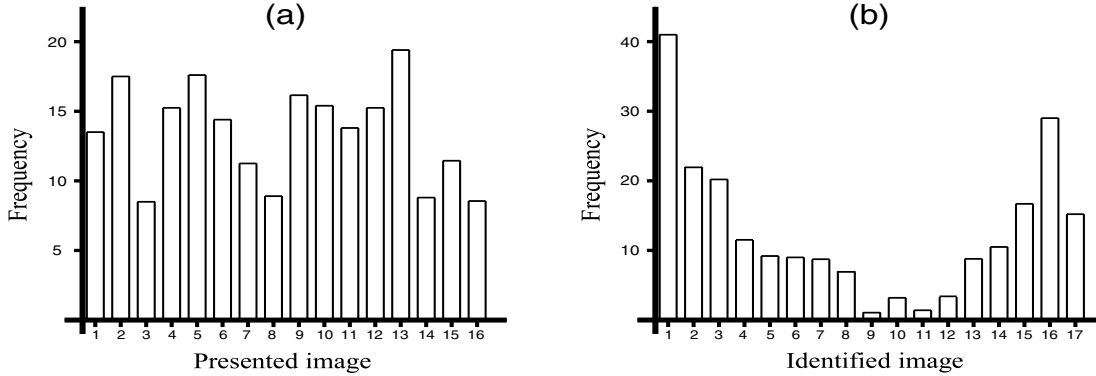


Figure 4.6: *Perception as a bi-stable map.* (a) Images were drawn at random from the interpolated sequence (figure 4.5) and then presented to a subject. The graph shows how frequently a particular image was presented during the experiment. (b) The images were classified by the subject. The graph shows how frequently a classification was made. (After [CA93].)

To continue with the analogy to a bi-stable system, the authors define a ‘residence time’ as the number of images presented before perception switches from one extreme interpretation to the other. Both the statistics of residence times, and the signal to noise ratio of the switching time series clearly show a degree of coherence between the reversal times and the (masked) periodic modulation, again suggesting stochastic resonance at the cognitive level.

4.3 A cognitive model of the perceptual process

Rumelhart *et al.* have used the framework of Parallel Distributed Processing (PDP) [RSMH86] to describe the perception of ambiguous figures, and have devised a constraint satisfaction network capable of interpreting the Necker cube. Such networks are equivalent to a suitably configured Hopfield network [Hop82], where each node corresponds to a hypothesis about the image, and each connection represents constraints between hypotheses. Connections, ω_{ij} , between nodes are either excitatory (hypotheses i and j are complementary), or inhibitory (they are conflicting). If the activation of the i^{th} node is $a_i \in \{0, 1\}$

then each node evolves according to

$$\begin{aligned} a_i &\rightarrow 1 && \text{if } \sum_{j \neq i} \omega_{ij} a_j > 0 \\ a_i &\rightarrow 0 && \text{otherwise} \end{aligned} \quad (4.2)$$

and the network is updated asynchronously. It can be shown [Hop82] that the energy

$$E = -\frac{1}{2} \sum_{i=1}^N \sum_{j=1}^N \omega_{ij} a_i a_j \quad (4.3)$$

is a Lyapunov function for the dynamics. The connections, ω_{ij} , are chosen so that the energy landscape of the network has two global minima, and each minimum corresponds to one interpretation of the cube.

The analysis of [RSMH86] extends only to recognition, and switching does not occur in their model. An obvious extension is to model perceptual fluctuations by the inclusion of a random component in either the energy function, or each nodal activation. If enough noise is present, transitions between minima will occur. With this in mind, Riani and Simonotto [RS94b] have extended the PDP model to account for stochastic resonance. The network is again updated asynchronously, and noise is added at each update by randomly selecting a single neuron and flipping it (*i.e.* $0 \rightarrow 1$ or $1 \rightarrow 0$) and evolving the network according to the Metropolis algorithm [HKP91]: the new network state has an acceptance probability of $P(\delta E)$ depending on the energy change $\delta E \leq 0$, with

$$\begin{aligned} P(\delta E) &= 1 && \text{if } \delta E \leq 0 \\ P(\delta E) &= \exp\left(-\frac{\delta E}{k_B T}\right) && \text{otherwise} \end{aligned} \quad (4.4)$$

where k_B is Boltzman's constant, and the parameter T now introduces a 'temperature' into the dynamics. Thus, the network state can now switch between minima with a mean rate that has an Arrhenius dependence on T . When a weak periodic driving term (of amplitude

A and frequency Ω) is added to the energy function, such that

$$E = -\frac{1}{2} \sum_{i=1}^N \sum_{j=1}^N \omega_{ij} a_i a_j + A \sin(\Omega t) \left[\sum_{i \in \mathcal{A}} a_i - \sum_{i \in \mathcal{B}} a_i \right] \quad (4.5)$$

(where $\{\mathcal{A}\}$ is the set of active nodes, and $\{\mathcal{B}\}$ the set of inactive ones) then transitions between minima become partially entrained to the forcing and the network displays stochastic resonance.

4.4 Haken's competitive network

A second model of the perceptual process is due to Haken [Hak87, Hak91]. Haken's network obeys a competitive gradient dynamics in a potential which has strictly-localized ground states: a single node is active and all others silent. To model the interpretation of ambiguous figures: the recognition process is identified with the network's relaxation to a ground state, and each such state is ascribed to one of the possible interpretations of the figure.

The remainder of this chapter will analyse the dynamics of Haken's network and further show how it may be extended to model reversal and stochastic resonance.

4.4.1 Network dynamics

Haken's original model comprises a single-layer network of N nodes, where the state of the i^{th} node is $q_i \in \mathbb{R}$ with $i = 1 \dots N$. Each activation q_i is interpreted as the overlap between a presented pattern and some stored prototype. A network of N nodes can therefore store and recognize N percepts. Each prototype is first encoded as a vector $\hat{\mathbf{v}}_{\mathbf{k}}$ with $k = 1 \dots N$, for example its components could be pixel values of the image. The image to be recognized is then pre-processed and similarly encoded to give a vector \mathbf{v} . This vector is then presented to the network, and the overlap

$$q_i = \hat{\mathbf{v}}_{\mathbf{i}} \cdot \mathbf{v} \quad (4.6)$$

with each prototype computed. The network then evolves according to the gradient dynamics [Hak91]

$$\dot{q}_i = -\frac{\partial U(\mathbf{q})}{\partial q_i} = (1 - 2\mathcal{Z}(\mathbf{q}) + q_i^2)q_i \quad (4.7)$$

with

$$U(\mathbf{q}) = -\frac{1}{2}\mathcal{Z}(\mathbf{q}) + \frac{1}{2}\mathcal{Z}(\mathbf{q})^2 - \frac{1}{4}\sum_i q_i^4 \quad (4.8)$$

and

$$\mathcal{Z}(\mathbf{q}) = \sum_i q_i^2 \quad (4.9)$$

represents a form of global coupling. Note that the lack of local interactions implies that there is no natural network topology. Figure 4.7 shows a plot of the potential $U(\mathbf{q})$ for a network of two neurons, q_1 and q_2 .

Equation (4.7) is invariant under the transformation $\mathbf{q} \rightarrow -\mathbf{q}$. Moreover, $q_i(t) \geq 0$ for all $t > 0$ and i if $q_i(0) \geq 0$ for all i . For suppose that $q_i(t) = 0$ and $q_j(t) \geq 0$ for all $j \neq i$. Setting $q_i = 0$ on the right-hand side of equation (4.7) shows that $\dot{q}_i(t) \geq 0$. That is, q_i cannot cross over to the negative real axis. The network converges to one of the stationary states of the potential U , that is,

$$-\frac{\partial U}{\partial q_i} = q_i^3 + (1 - 2\mathcal{Z})q_i = 0 \quad (4.10)$$

for all i . Thus the equilibria of equation (4.7), denoted by $\bar{\mathbf{q}}$, satisfy

$$\bar{q}_i = 0 \quad \text{or} \quad \bar{q}_i = \sqrt{2\mathcal{Z} - 1} \quad (4.11)$$

with \mathcal{Z} determined self-consistently. Hence the set of stationary states can be divided into $N + 1$ classes, each of which is determined by the number m of excited sites. For a given

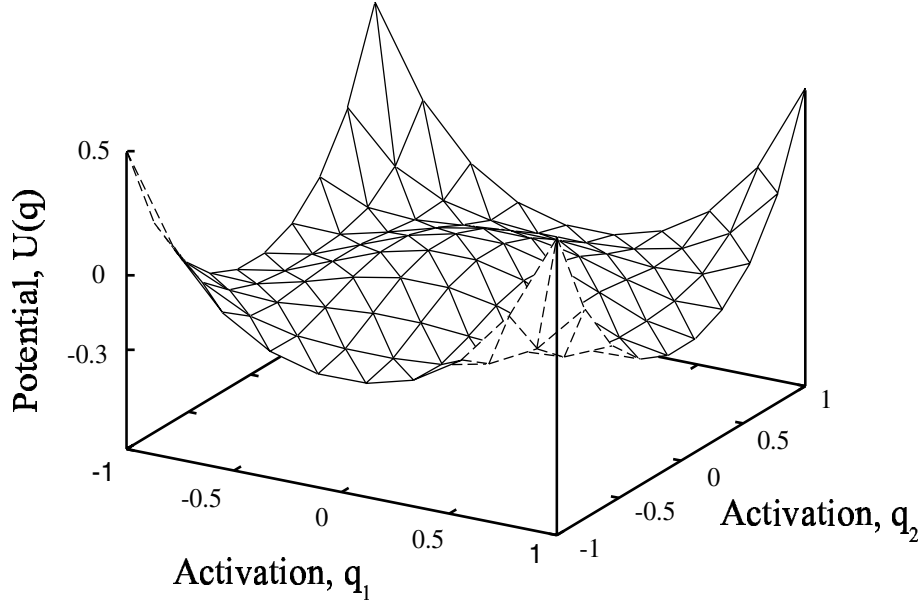


Figure 4.7: Plot of the potential for a two-neuron network. Minima are shown at $(1,0)$, $(0,1)$, $(-1,0)$, $(0,-1)$ and a maximum at $(0,0)$.

m ,

$$\mathcal{Z} = \frac{m}{(2m-1)} \quad (4.12)$$

and the corresponding potential at a stationary state is

$$U^{(m)} = -\frac{m}{(8m-4)} \quad (4.13)$$

Linear stability analysis [Hak91, Bre97] establishes that only the stationary states $m = 1$ are stable, whereas all other stationary states are either unstable ($m = 0$) or saddle points ($m > 1$). For each state in the class $m = 1$, there exists a single excited site, i_0 say, such that $\bar{q}_i = \delta_{i_0,i}$. Moreover $\mathcal{Z} = 1$ and $U^{(1)} = -\frac{1}{4}$. These are the N strictly localized ground states of the network. There are two homogeneous stationary states given by the *vacuum*

state $m = 0$ and the *dissipative* state $m = N$. The former satisfies $q_i = 0$ for all i and $U^{(0)} = 0$ and the latter has

$$\bar{q}_i = \frac{1}{\sqrt{2N-1}} \quad \forall i \quad (4.14)$$

and

$$U^{(N)} = -\frac{N}{(8N-4)} \quad (4.15)$$

In conclusion, the ground states of the system consist of strictly localized states in which a single site is excited and the remainder are silent; the particular ground state selected depends on the initial data and/or additional applied inputs. If there are no external inputs, then the excited node is the one with the highest initial activity (see figure 4.8). The network therefore assigns the pattern to the prototype with which it had the largest initial overlap. In other words it dynamically realizes a *winner-takes-all* strategy, and such networks are also known as *competitive* networks. Competitive networks signify their outputs by the firing of a single node, or a small proximal group of nodes. They thus classify data by the firing of the same node(s) for all inputs that belong to a single category. The network can therefore recognize only one pattern at a time, and thus dis-ambiguates its input in a way that is consistent with the perception of ambiguous figures. It can also be shown that these winner-takes-all networks are equivalent to associative memories [Koh84], and Haken has demonstrated that this particular network can perform associative recall of digitized photographs [Hak91].

One obvious drawback to this model is its inability to learn. Output states are 'hard wired' into the dynamics, and all have the same size basins of attraction. For a truly biological system one would want the facility to learn new categories, and also to emphasize or de-emphasize others (for example the biasing of the Leeper-Boring of figure 4.2). In fact, Haken's original formulation included variable synaptic strengths but for simplicity I have set them to be equal to unity and thus have neglected their effect.

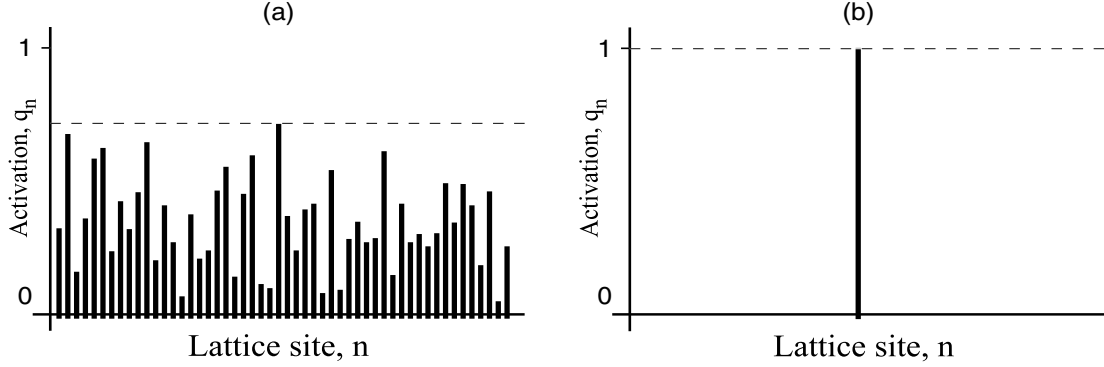


Figure 4.8: *Evolution of Haken's network. Given the initial set of activations (overlaps) shown in (a), the network evolves to a stationary state (b) such that the node with the highest initial activation also has the highest final activity ($q = 1$), while all others are silent ($q = 0$).*

4.4.2 Stochastic dynamics of the Haken model

Since Haken's network is a tenable model for the perception of ambiguous figures, it is illuminating to push the analogy further. Ditzinger and Haken [DH89] reformulate the model to include habituation-induced reversal. Specifically, they describe a network of two nodes ($n = 1, 2$) which satisfy

$$\dot{q}_i = (\Lambda_i(t) - 2\mathcal{Z}(\mathbf{q}) + q_i^2) q_i \quad (4.16)$$

where the $\Lambda_n(t)$ are termed *attention parameters*, and evolve according to

$$\dot{\Lambda}_i(t) = a - b \Lambda_i(t) - c q_i + \zeta_i(t) \quad (4.17)$$

where $\zeta_i(t)$ is a zero-mean white-noise source. In the absence of noise, the coupled equations (4.16) and (4.17) naturally oscillate; and so the inclusion of noise simply causes fluctuations about a mean oscillation period. This model can therefore reproduce experimentally ob-

tained reversal–time distributions. The underlying switching dynamics of Ditzinger's model are periodic (albeit with a stochastic component which 'randomizes' the switching times), however the return–map analysis of Schöner *et al.* [SH95] has shown that reversal is a purely stochastic process and has no periodic component, and this weakens the plausibility of Ditzinger's model.

Instead, model the reversal phenomena by introducing a simple, local, additive–Gaussian noise to the dynamical equation of each neuron (equation (4.7)). This could correspond, say, to the inclusion of internal neuronal noise (chapter 2). Transitions between states (each of which is a reversal) will now be dictated by the Arrhenius–type escape rate discussed in section 1.4 and so will be exponentially distributed.

Furthermore, to explore the possibility of stochastic resonance, select two neurons $i = 1, 2$, say, and drive the network with the weak periodic bias

$$I_i(t) = A(\delta_{i,1} \cos^2(\Omega t) + \delta_{i,2} \sin^2(\Omega t)) \quad (4.18)$$

(such a bias could correspond to the moving coloured dot in figure 4.4). Further impose that the forcing be weak (A is small), so that the bias itself is unable to cause transitions between states, *i.e.* a sub–threshold forcing. Equation (4.7) then becomes

$$\dot{q}_i(t) = -\frac{\partial U(\mathbf{q})}{\partial q_i} + \zeta_i(t) + I_i(t) \quad (4.19)$$

where $\zeta_i(t)$ is a zero–mean Gaussian white noise process with

$$\langle \zeta_i(t) \rangle = 0 \quad \text{and} \quad \langle \zeta_i(t_1) \zeta_j(t_2) \rangle = \sigma^2 \langle \xi_i(t_1) \xi_j(t_2) \rangle = \sigma^2 \delta_{i,j} \delta(t_1 - t_2) \quad (4.20)$$

Thus the noise is un–correlated between neurons, and has variance $D = \sigma^2$.

Numerical simulations show that at low noise levels the network tends to remain in one of two possible output states, and that switching events between these two states occur

exceedingly rarely. In the limit of zero noise these states correspond to $q_i = \delta_{i,1}$ and $q_i = \delta_{i,2}$, and the occupied one depends on initial conditions. As the noise is gradually increased the network begins to jump between output states with a transition rate that is partly entrained with the driving force. For high noise levels the network randomly flips between output states and there is no synchrony with the driving signal. Simulations also show that in the entrained regime there is a clear separation of time-scales for the system, the two scales are: the time to relax to an output state t_{relax} , and the mean residence time of an output state, t_{res} , with $t_{res} \gg t_{relax}$. Therefore make the adiabatic assumption and neglect the relaxation time.

To quantify the behaviour of the network, tabulate and histogram the residence times of an output state (recall section 1.5). The resulting distribution typically displays peaks centred at

$$\mathcal{T}_p = \left(p - \frac{1}{2}\right) \mathcal{T}, \quad p \in \mathbb{Z} \quad (4.21)$$

where $\mathcal{T} = \pi/\Omega$ is the driving period. These peaks are superimposed on an exponentially decaying background (see inset to figure 4.9). Denote the strength of the k th peak by \mathcal{P}_k , computed according to (1.48). Recall that each \mathcal{P}_k passes through a maximum as a function of both noise strength and also of the forcing period [GMS95], and further that for a particular driving frequency $\nu = \mathcal{T}^{-1}$, stochastic resonance is attained at the particular noise strength σ for which the strength of the first harmonic, \mathcal{P}_1 , is maximal. Figure 4.9 shows how \mathcal{P}_1 for the Haken network varies with noise strength σ . Several values of the driving frequency are shown. It is seen that the maximal value of \mathcal{P}_1 occurs at a non-zero value of ν , and that as ν increases, this maximum is shifted to higher noise levels.

To analyse the dynamics of this system, its effective dimensionality must be reduced and it is not *a priori* obvious how to do this. However, note that for low noise levels $q_n(t) \approx 0 \forall n \neq 1, 2$, and thus to a good approximation equation (4.19) reduces to a two-dimensional system ($n = 1, 2$) with U given by equation (4.7) for $N = 2$. In the positive quadrant the potential $U(q_1, q_2)$ has two minima \mathbf{q}_a at $(1, 0)$ and $(0, 1)$, and a saddle at $\mathbf{q}_s = (\frac{1}{\sqrt{3}}, \frac{1}{\sqrt{3}})$

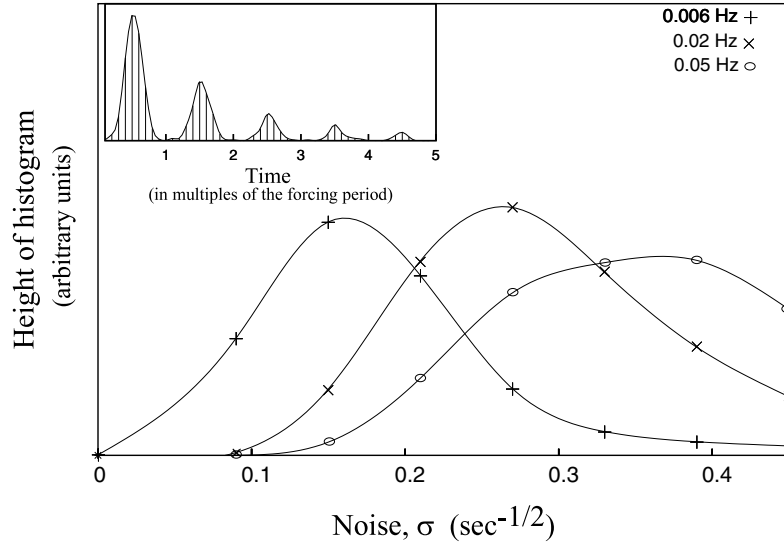


Figure 4.9: Variation of \mathcal{P}_1 with noise strength σ for the non-diffusive network. Three different values of the driving frequency ν are shown, and as ν increases σ_{opt} increases. The inset shows a typical exponentially decreasing histogram of residence times: time is in multiples of \mathcal{T}_0 (see text).

with $U(\mathbf{q}_s) = -\frac{1}{6}$, see figure 4.7. Since the periodic forcing is chosen to be positive-valued the system is retained in the positive quadrant and thus the effects of the minima at $(-1, 0)$ and $(0, -1)$ may be neglected. Recall that the system remains in the positive quadrant in the absence of any noise or external forcing. U may therefore be reduced to a two-dimensional bi-stable potential, provided that the driving amplitude, A , is not too small and the noise, σ , is not too large.

To qualify as resonance, the time-scale matching relation (1.46) must be satisfied. Recall that this occurs when \mathcal{P}_1 is maximal (see chapter 1). Assume that all transition events occur at the saddle point, since transitions at all other points are exponentially less likely. Recall that the mean escape-rate from a given minimum in an unperturbed multi-dimensional

multi-stable potential is given by the generalized Kramers' rate formula (equation (1.41))

$$r(\sigma) = \frac{\lambda}{2\pi} \sqrt{\frac{\det \mathbf{H}(\mathbf{q}_a)}{|\det \mathbf{H}(\mathbf{q}_s)|}} \exp\left(-\frac{2\delta U}{\sigma^2}\right) \quad (4.22)$$

The Hessian \mathbf{H} of the potential has components

$$H_{mn} = \frac{\partial^2 U}{\partial q_m \partial q_n} \quad (4.23)$$

and is evaluated at the minima, \mathbf{q}_a , and the saddle, \mathbf{q}_s . λ is the positive eigenvalue of the Hessian of the potential at the saddle, and $\delta U = U_s - U_a = \frac{1}{12}$ is the height of the potential barrier at the saddle. For this system the pre-factor in equation (4.22) has the value 0.39.

Resonance occurs when the time for the system's mean residence in one minimum is close to half the driving period [GMS95], thus $r = 2\nu$. Therefore, for a particular driving frequency ν , the optimal noise level, σ_{opt} , for resonance may be experimentally determined. Using (4.22), σ_{opt} determines r_{opt} , the corresponding theoretical escape rate. Thus r_{opt} may be compared with the original driving frequency ν . Figure 4.10 shows plots of $r(\sigma)$ versus noise strength σ , and 2ν versus optimal noise strength σ_{opt} . It is seen that the optimal noise level matches well that predicted by the theory.

Note that in the absence of any periodic forcing the histogram of residence times is essentially a decaying exponential as predicted from Kramers' theory and as observed in Borsellino's reversal data [BDA⁺72].

4.5 The diffusive Haken model

Connectionist models such as Rumelhart's describe psychological phenomena in terms of the interactions between such cognitive processes as ideas and schemata. They are therefore *high level* explanations of how ambiguous figures are perceived. The question therefore arises as to the *low level* neural substrate underlying this effect.

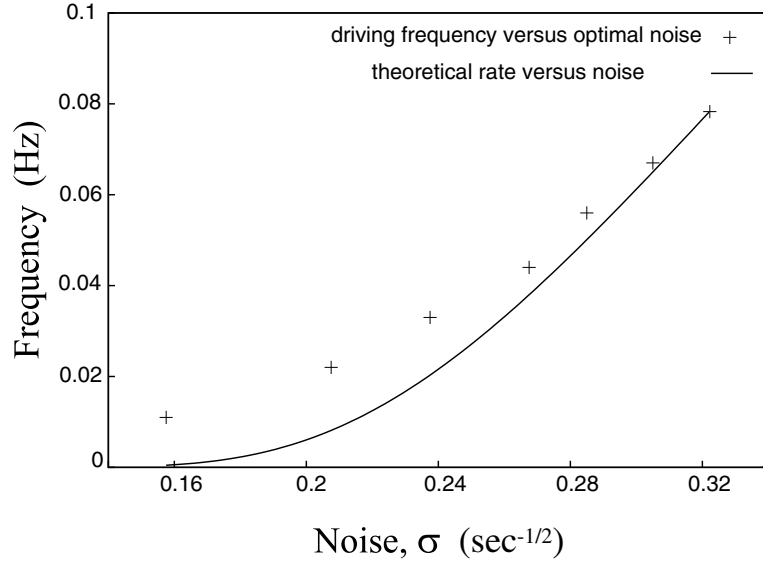


Figure 4.10: *Stochastic resonance: the matching of the theoretical escape rate r with twice the driving frequency ν .*

Electro-physiological recordings from single cortical cells indicate that in the brain the representation of sensory information is not encoded by the global activity of the entire cortex, but rather by the firing patterns of small groups of neurons (see [FY95] and references therein). Furthermore, neurobiologists have noted that in many regions of the cortex, groups of adjacent neurons appear to form higher functional units that serve to analyse some particular stimulus feature such as the orientation of an edge of an image [Swi96], or the position of a sensory stimulus on the skin [KNS⁺79]. If each node in a competitive network is interpreted as a neuron, then such networks can provide rudimentary models of how perception and categorization may occur in real brains [vdM73]. However, it is clear that a competitive network with a single output neuron is not robust to degradation: if a single cell is destroyed then the entire corresponding category is lost. Neural network models of the formation and behaviour of these coherent structures in brain activity therefore generally involve two aspects: (i) a selection mechanism that determines the centre of a localized excitation in response to an input, and (ii) an interaction mechanism that serves to spread the response over a neighbouring region of the network, leading to a *distributed*

response. Haken's network dynamically implements a selection mechanism, and recent work [SB92, Bre95, Bre97] has extended the model to take into account a simple interaction mechanism, resulting in a distributed representation.

This interaction mechanism comprises the inclusion of a diffusive coupling term in the potential of the original Haken model. For certain values of the coupling strength there can exist a balance between the effects of this diffusion and of the localizing potential, yielding new states that are localized excitations (or *bubbles*) distributed over many neurons. These bubbles represent a very robust coding of information since neighbouring cells aid the reconstruction of lost information following the 'death' of a single cell. Furthermore, Kohonen [Koh82] has shown that such bubbles can enable the construction of *topographic maps*.

First impose a d -dimensional square lattice topology upon the network; the diffusive Haken model has a potential [SB92]

$$\hat{U}(\mathbf{q}) = \frac{\mu}{2} \sum_{\langle i,j \rangle} (q_i - q_j)^2 + U(\mathbf{q}) \quad (4.24)$$

where $\langle i, j \rangle$ denotes summation over nearest neighbour pairs. The first term on the right-hand side of equation (4.24) represents a diffusive interaction with coupling strength μ . Using the idea of an *anti-continuum limit* [Aub95] a uniform continuation from the zero diffusive coupling ($\mu = 0$) case can be performed (see appendix A.2) to show that delocalizations of the original ground states occur (see figure 4.11), and that these continued solutions can persist for some finite coupling (*i.e.* for $\mu < \mu_c$).

Furthermore one can show that to a first approximation each state has a potential

$$\hat{U}_{min}(\mu) \approx U_{min} + d\mu \quad (4.25)$$

where d is the dimensionality of the network. It may be shown that such states persist for all values of μ in one-dimension [SB92], whereas for $d > 1$ there exists a critical coupling $\mu_c(d)$

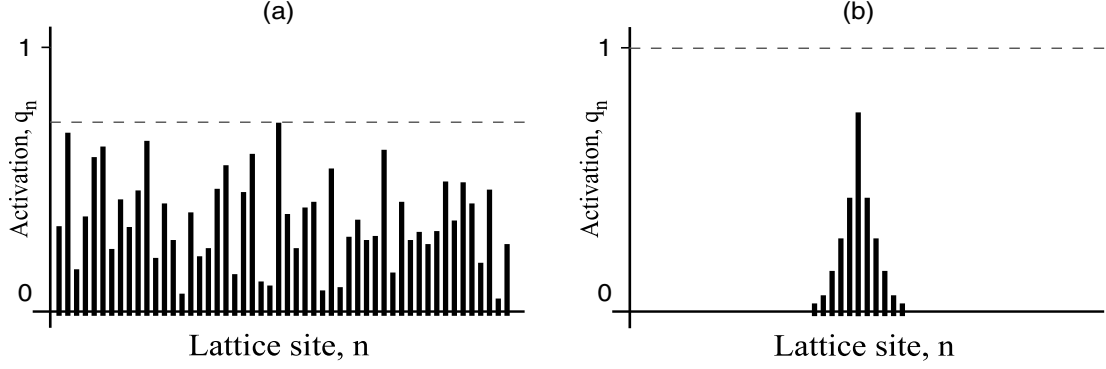


Figure 4.11: *Evolution of the diffusive Haken network. Given the initial set of activations shown in (a), the network evolves to a stationary state (b) such that the node with the highest initial activation also has the largest final activity (say q' , with $q' \leq 1$). However, now adjacent neurons are also excited, and the original ground state is de-localized (compare with figure 4.8).*

beyond which localized ground states cease to exist and the effects of diffusion dominate [Bre95]. The critical coupling can also be computed and is found to be

$$\mu_c(d) = \frac{1}{10d} \quad (4.26)$$

In fact, the analysis of [Bre95] shows that these continued solutions occur for more general forms of coupling than the simple diffusive one considered here. The only criterion being that the interaction function be C^1 [MS95] and that coupling strength decays exponentially with distance [Bre95] (where the distance between two points on the lattice is measured as being the number of lattice sites separating them).

4.5.1 Stochastic dynamics of the driven diffusive model

For concreteness, consider a one-dimensional lattice and select two neurons separated by X lattice sites with X sufficiently large such that the ground states centred at the two sites

have very little overlap. As in the non-diffusive case, introduce local additive noise together with a periodic stimulation of the two selected neurons given by $A \cos^2(\Omega t)$ and $A \sin^2(\Omega t)$ respectively. The equations of motion are thus of the form

$$\dot{q}_i(t) = -\frac{\partial \hat{U}(\mathbf{q})}{\partial q_i} + \sigma \xi_i(t) + I_i(t) \quad (4.27)$$

with $\hat{U}(\mathbf{q})$ given by (4.24). A resonant effect is again observed with the system switching between the states localized about the two centres (see figure 4.12).

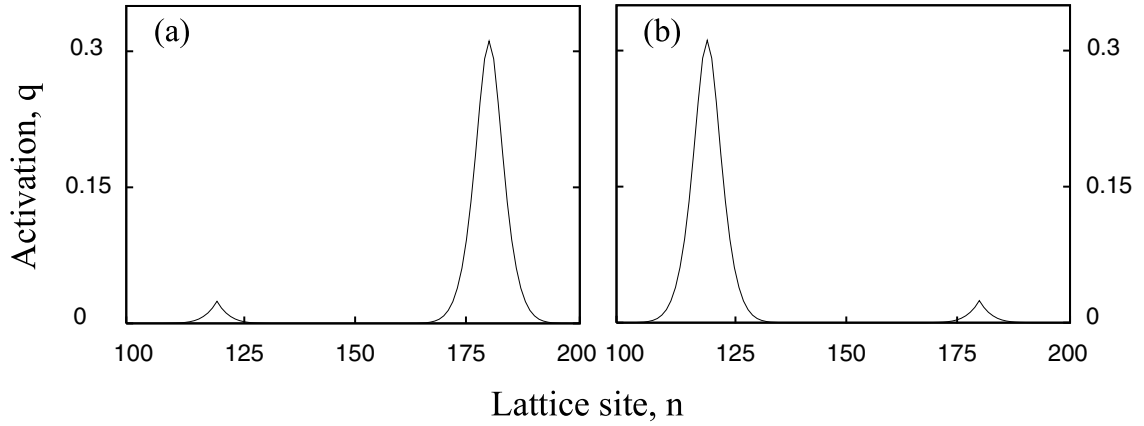


Figure 4.12: *Two snapshots of the evolution of the network with diffusive coupling $\mu = 0.5$: (a) before and (b) after the network has flipped between states. For clarity the low noise case is shown.*

Plots of \mathcal{P}_1 versus σ are shown in figure 4.13 for various coupling strengths. Observe that as μ is increased, the maxima of \mathcal{P}_1 , corresponding to resonance, is shifted to lower noise levels. This may be explained by noting that increasing μ causes a decrease in the barrier height $\delta \hat{U}(\mu)$ and thus an increase in the unperturbed transition rate (4.22). A method for calculating $\delta \hat{U}(\mu)$ is shown below.

When μ is sufficiently large, the localized solutions of the one-dimensional diffusive Haken model (in the absence of noise and external forcing) are distributed over many lattice sites suggesting that they can be approximated by a continuum version of the model. Following

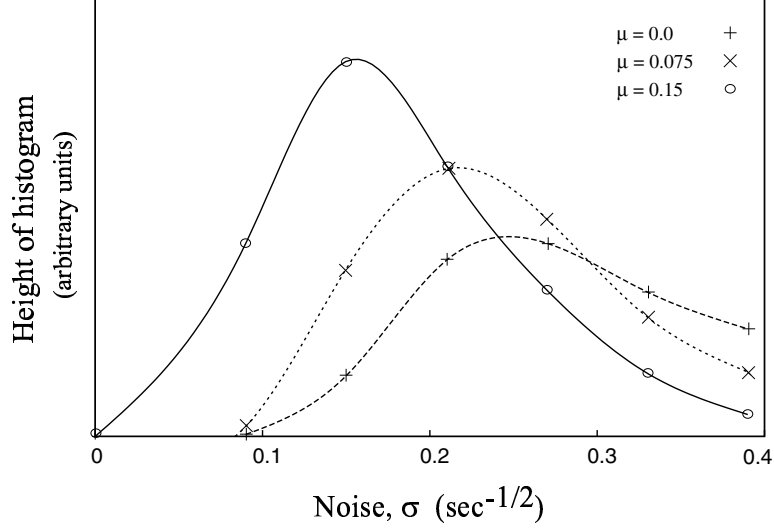


Figure 4.13: Variation of \mathcal{P}_1 with noise strength σ for the diffusive network. Three different values of the coupling strength μ are shown, and as μ increases σ_{opt} decreases. The driving frequency ν is held constant.

[SB92, Bre97], the potential governing the gradient dynamics of the continuum model takes the form

$$\hat{U}[q, \mu] = \int_{-\infty}^{\infty} dx \left[\frac{\mu}{2} \left(\frac{\partial q(x)}{\partial x} \right)^2 - \frac{q(x)^4}{4} \right] - \frac{1}{2} \mathcal{Z} + \frac{1}{2} \mathcal{Z}^2 \quad (4.28)$$

with

$$\mathcal{Z}[\mathbf{q}] = \int_{\mathbb{R}} dx q(x)^2 \quad (4.29)$$

and μ a renormalized diffusion constant. By means of the Euler–Lagrange equation, stationary solutions of the dynamics satisfy

$$\mu \frac{d^2 q}{dx^2} = (2\mathcal{Z}[\mathbf{q}] - 1) q(x) - q(x)^3 \quad (4.30)$$

Localized states can now be interpreted as finite energy configurations, or instantons, of the continuum model. Using phase-plane analysis it can be shown that for fixed \mathcal{Z} , an instanton centred at $x = 0$ is described by [SB92, Bre97]:

$$q(x) = q_0 \left[\cosh \left(\frac{q_0 x}{\sqrt{2\mu}} \right) \right]^{-1} \quad (4.31)$$

where the instanton amplitude is

$$q_0 = \sqrt{(2\mathcal{Z} - 1)2} \quad (4.32)$$

This leads to a self-consistency condition for \mathcal{Z} of the form

$$\mathcal{Z} = 4\sqrt{\mu(2\mathcal{Z} - 1)} \quad (4.33)$$

which has real solutions provided that

$$\mu \geq \bar{\mu} = \frac{1}{16} \quad (4.34)$$

Keeping only the lower energy solution, the amplitude of the instanton as a function of the coupling μ is

$$q_0(\mu) = \sqrt{2\frac{\mu}{\bar{\mu}}} \left(1 - \sqrt{1 - \frac{\bar{\mu}}{\mu}} \right) \quad (4.35)$$

It follows that the energy of the instanton is (note that equation (4.25) is only valid in the limit $\mu \rightarrow 0$)

$$\hat{U}_{\min}(\mu) = F(q_0(\mu), \mu) \equiv -\sqrt{2\mu}q_0 + 4\mu q_0^2 - \sqrt{2\mu}\frac{q_0^3}{6} \quad (4.36)$$

The barrier height for transitions between two single-instanton states can now be computed. Suppose that the instantons are centred at x_1 and x_2 respectively (cf. figure 4.12), and

further that x_1, x_2 are well separated on the lattice. The most probable path of escape is therefore via a saddle consisting of an instanton doublet centred about the two selected sites. By solving the self-consistency condition for \mathcal{Z} , the height of each instanton in the doublet is found to be

$$q'_0(\mu) = \sqrt{2\frac{\mu}{\bar{\mu}}} \left(2 - \sqrt{4 - \frac{\bar{\mu}}{\mu}} \right) \quad \text{with } q'_0 < q_0 \quad (4.37)$$

Figure 4.14 shows how the amplitudes of the single instanton, and a member of the doublet, vary with the coupling strength μ . As expected, the continuum limit breaks down for small μ .

The energy of the doublet (assuming that the local interaction energy of the two instantons can be neglected) is

$$\hat{U}_d(\mu) = 2F(q'_0(\mu), \mu) + 8\mu q'_0(\mu)^2 \quad (4.38)$$

and the required barrier height is

$$\delta\hat{U}(\mu) = \hat{U}_d(\mu) - \hat{U}_{\min}(\mu) \quad (4.39)$$

The inset to figure 4.14 demonstrates that the barrier height rapidly decreases with increasing coupling strength, as expected. One consequence of this is that there appears to be a trade-off between the strength of the local coupling, μ , and hence the network's ability to withstand damage, and its robustness to noise. Strong coupling ($\mu > 0.2$) means that information about an output state is dispersed over many neurons, making a resilient system. However this also means that the barrier height between output states becomes so small that noise induced transitions become important, even for low noise levels. Thus the network is unable to function as a classifier.

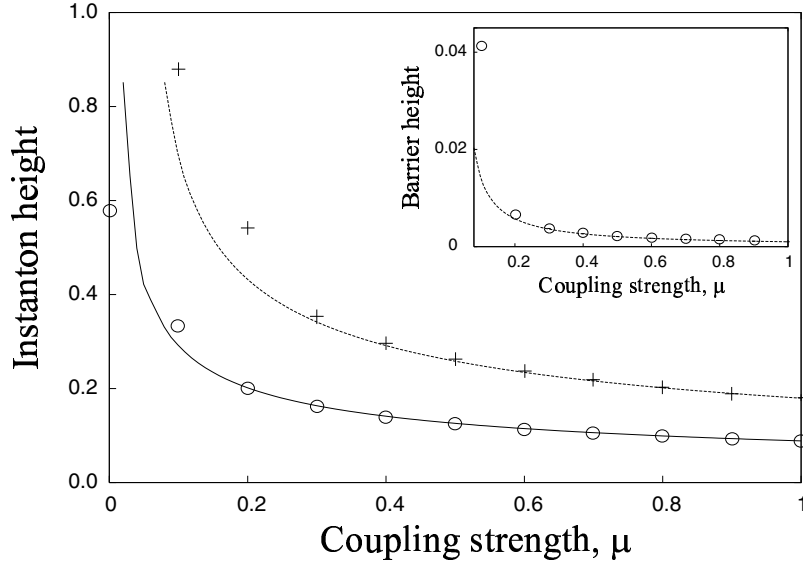


Figure 4.14: *The variation of the instanton amplitudes, q_o and q'_0 , with coupling strength μ . The dashed curve shows the singlet amplitude, (equation (4.35)), the bold one shows the doublet amplitude (equation (4.37)). Simulation results are also shown: results for the singlet state are represented by a plus sign, and for the doublet state by a circle. Inset: The variation of the barrier height with coupling strength μ is shown both analytically (solid line) and numerically (circles).*

4.6 Discussion

This chapter has been concerned with the role of noise in the perception of ambiguous figures. To motivate my study I first reviewed the psycho-physics of this phenomenon, and I then introduced Haken's network, a possible model for this perceptual process. I believe that Haken's model provides a useful toy model for mental categorization tasks in the same way that the Hopfield model, though biologically implausible, is a viable metaphor for associative memory.

Two sets of experiments show that stochastic resonance can be present even at this cognitive level. By the incorporation of weak noise and a sub-threshold driving signal I have extended

Haken's treatment first to account for SR, and then incidentally to explain the distribution of spontaneous reversals.

In common with many mathematical models, Haken's network admits more than one interpretation. When a diffusive coupling is included in the dynamics, the ground states become de-localized and the network becomes more robust. Related competitive networks have previously been used as models of cortical function, and so I have proposed that Haken's network might also function as a *low level* model for recognition. Stochastic resonance persists even in the presence of this diffusive coupling, and I therefore suggest that perceptual SR might originate from the dynamics of either single neurons, or small groups of neurons.

Despite superficial similarities, the behaviour of Haken's model must be distinguished from *array enhanced stochastic resonance* [LMD⁺95] which is a noise induced phase locking phenomenon. My analysis has shown that for small diffusive coupling the stochastic Haken model can be approximated by a bi-stable system and thus has more in common with traditional SR models.

The main results of this chapter were published in [BR98].

Neuronal dynamics with intrinsic noise

5.1 A deterministic leaky–integrate–and–fire neuron

The neuronal spike train is largely determined by the membrane potential, $V(t)$, at the trigger zone (recall section 2.1.5). Recall: afferent excitatory and inhibitory PSPs are summed in the soma, and a spike is fired if the total charge at the trigger zone exceeds a threshold. Following excitation, the membrane slowly resets to its resting value, say V_0 , and there is a refractory period during which the cell may receive input, but cannot fire. If instead the PSP summation is sub–threshold, $V(t)$ relaxes towards V_0 without spiking.

5.1.1 Continuous time formalism

A simple model of the time course of $V(t)$ is due to Lapicque [Lap07, Tuc88]. If the membrane of cell i has a constant resistance R_i and a capacitance C_i , the Ohmic current through it will be V_i/R_i and the current through the capacitance will be $C_i dV_i/dt$. Therefore, by conservation of current:

$$C_i \frac{dV_i}{dt} = -\frac{V_i}{R_i} + I_i(t) \tag{5.1}$$

(compare with the full Hodgkin–Huxley model, section 2.1.5) where $I_i(t)$ represents all extra-cellular input currents. For convenience let $\kappa = (RC)^{-1}$ and $I'_i(t) = I_i(t)/C_i$. $I'_i(t)$ has three contributions: any time-independent inputs or biases I_0 ; external time-dependent input $I_E(t)$ such as a physical stimuli; and time-dependent inputs from the other N neurons of the network, $I_N(t) = \sum A_{ij}(t)$, so that

$$\frac{dV_i}{dt} = -\kappa V_i + I_0 + I_E(t) + \sum_{j=1}^N A_{ij}(t) \quad (5.2)$$

where $A_{ij}(t)$ is the input signal from the j^{th} to the i^{th} neuron. For the present assume that there is no external input, and so $I_E(t) = 0$. In the absence of other neuronal input ($I_N(t) = 0$), the neuron has a stable state corresponding to a resting potential at $V_0 = I_0/\kappa$.

There is no natural threshold for this model, and one must be imposed. A simple choice is a variable threshold $h_i(t)$ that remains constant, $h_i(t) = h_i$, until $V_i(t) > h_i$, at which time a spike is fired. The effect of a refractory period is then included by setting $h_i(t)$ to be infinite for a time t_R after firing, after which it returns to its original value. A further natural time-scale for the neuron is the synaptic delay t_d , which accounts for the finite time between the arrival of a PSP and the resulting change in the membrane potential at the trigger zone. Spikes have no structure in this model, but could be represented by any suitable function, *e.g.* the alpha-function of [JNT75].

The output, $\hat{a}_j(t)$, of the j^{th} neuron at a time t is therefore some function of the its membrane potential, $V_j(t)$ and its threshold $h_j(t)$, so that

$$\hat{a}_j(t) = g(V_j(t) - h_j(t)) \quad (5.3)$$

For simplicity assume that a spike is well described by a delta function. Thus the time-course of $\hat{a}_j(t)$ becomes a set of delta functions, with one located at each firing time. This signal propagates via the axon and telodendria to a synapse on the i^{th} neuron. If the finer details (*e.g.* ion channel processes) of dendritic and synaptic processing are ignored, the resulting input signal, $A_{ij}(t)$, depends upon how this synapse modulates the impinging

action potential. It comprises two parts: the original spike, $\hat{a}_j(t)$, and a term ω_{ij} quantifying transmitter release

$$A_{ij}(t + t_d) = \omega_{ij}\hat{a}_j(t) \quad (5.4)$$

where a delay t_d has been included to describe the synaptic processing time.

In contrast with other leaky-integrator models, *e.g.* [GM64], the membrane potential is not artificially reset to zero following firing. Discontinuous reset is known [RL93] to cause the elimination desirable biological features such as positive correlations between inter-spike intervals. Instead, therefore, $V(t)$ decays exponentially during the refractory period.

5.1.2 Discrete time formalism

The i^{th} neuron spikes for the n^{th} time at \mathcal{T}_n^i , thus equation (5.4) may be written

$$A_{ij}(t + t_d) = \omega_{ij} \sum_{n=1}^{\infty} \delta(t - \mathcal{T}_n^j) \quad (5.5)$$

Subsequent neuronal firing times are determined by both the refractory period t_R and the synaptic delay t_d . Following the generation of an AP at \mathcal{T}_n^i , two possibilities may occur:

- the membrane potential remains above threshold after the refractory time and the neuron spikes again, irrespective of its input

$$V(\mathcal{T}_n^i + t_R) \geq h_i \quad \text{and} \quad \mathcal{T}_{n+1}^i = \mathcal{T}_n^i + t_R \quad (5.6)$$

- after the refractory time, the membrane potential is sub-threshold and so is unable to fire. The neuron therefore fires its next action potential at a time t_d after the arrival of an afferent spike from another (say the j^{th}) neuron at a time \mathcal{T}_l^j

$$V(\mathcal{T}_n^i + t_R) < h_i \quad \text{and} \quad \mathcal{T}_{n+1}^i = \mathcal{T}_l^j + t_d \quad (5.7)$$

note that $\mathcal{T}_i^j + t_d > \mathcal{T}_n^i + t_R$ since the neuron is unable to spike during a refractory period.

The \mathcal{T}_n^i are therefore determined by the iterative condition

$$\mathcal{T}_n^i = \inf\{t | V_i(t) \geq h_i; t \geq \mathcal{T}_{n-1}^i + t_R\} \quad (5.8)$$

and so

$$\mathcal{T}_n^i = \sum_{k=1}^N A_n^{ik} \mathcal{T}_1^k + B_n^i t_R + C_n^i t_d \quad \text{with } A_n^{ik}, B_n^i, C_n^i \in \mathbb{Z} \quad (5.9)$$

Thus, the firing times are distributed on a lattice spanned by t_R , t_d , and the set of first firing times, $\{\mathcal{T}_1^k\}$. For convenience, set

$$t_d = t_R = \eta \quad (5.10)$$

and further choose initial conditions such that the first firing times are all integer multiples of the delay, thus $\mathcal{T}_1^j = k\eta$, $\forall j$ and for $k \in \mathbb{Z}$. Thus, the discrete-time equation (corresponding to (5.3)) for the output $a_j()$ at the m^{th} time step is

$$a_i(m\eta) = \Theta [V_i(m\eta) - h_i] \quad (5.11)$$

where the step function $\Theta(x) = 1$ if $x \geq 0$ and $\Theta(x) = 0$ if $x < 0$, and so $a_i(m\eta) = 1$ if $\mathcal{T}_i^n = m\eta$ for some $n \geq 1$, and $a_i(m\eta) = 0$ otherwise. Therefore, the neuronal input (5.4) may now be written

$$A_{ij}(t + \eta) = \omega_{ij} \sum_{m=0}^{\infty} \delta(t - m\eta) a_j(m\eta) \quad (5.12)$$

Following [BT91], a discrete time approximation to this Lapique model may be constructed by first solving equation (5.2), subject to the initial condition, $V(0) = 0$ (assuming $I_E = 0$)

$$\begin{aligned} V_i(t) &= \int_0^t ds \left(\sum_{j=1}^N A_{ij}(s - \eta) + I_0 \right) \exp(-\kappa(s - t)) \\ &= \frac{I_0}{\kappa} (1 - \exp(-\kappa t)) + \int_0^t ds \sum_{j=1}^N A_{ij}(s - \eta) \exp(\kappa(s - t)) \end{aligned} \quad (5.13)$$

In the absence of any other input, the first term on the RHS of equation (5.13) imposes the exponential relaxation $V \rightarrow V_0$. However, substitution of equation (5.12) into (5.13) shows that the second term is completely specified by its solutions at the discrete times $t = m\eta$, $m \geq 0$. Thus, a natural discretization is to consider the evolution of (5.2) at integer multiples of η

$$V(n+1) - V(n) = \eta \left(-\kappa V(n) + \sum_{j=1}^N A_{ij}(n) + I_0 + I_E(n) \right) \quad n \in \mathbb{Z} \quad (5.14)$$

5.1.3 Single neuron dynamics

To illustrate the dynamics, consider the $N = 1$ case with no external input ($I_E = 0$)

$$V(n+1) - V(n) = \eta (-\kappa V(n) + \omega \Theta [V(n) - h] + I_0) \quad (5.15)$$

which describes a single neuron with a self-coupling¹, ω . Note that real neurons do not synapse directly to themselves in this manner, but instead any such feedback is mediated by one or more inter-neurons. For example, various sensory neurons are thought to receive some form of active feedback: *e.g.* the hair cells of the auditory system [NK86]. Two related single neuron approximations may be derived from the large network limit: Schieve *et al.* [SBD91] assume that all other neurons in the network relax on a faster time-scale

¹The bi-stable element represented by equation (5.15) has applicability outside the neural domain. It has, for example, been used to describe an A/D converter [WC94].

than does the i^{th} neuron, and so adiabatically eliminate them to derive a *single effective neuron*. In contrast, Ohira and Cowan [OC93] replace interactions from other neurons by a self-consistent mean field, and show that this is equivalent to self-coupling.

For the moment assume that ω is time-independent, and that $h = 0$. If the self-coupling is inhibitory (*i.e.* $\omega < 0$) and $I_0 > 0$ then the model (5.15) reduces to the Nagumo–Sato equation [NS72]. Neuronal dynamics are therefore generated by a circle map, and exhibit either periodic or quasi-periodic behaviour [ATT90, BS90]. If instead the self-coupling is excitatory, so that $\omega > 0$, and also $I_0 < 0$ with $\omega + I_0 > 0$ then the deterministic dynamics is trivial. Equation (5.15) has two stable fixed points

$$V_1 = \frac{I_0}{\kappa} \quad \text{and} \quad V_2 = \frac{I_0 + \omega}{\kappa} \quad (5.16)$$

with a basin boundary at $V = 0$. Consequently the neuron relaxes to one of two possible equilibria: at V_1 it is perpetually sub-threshold and never fires, while at V_2 it is always super-threshold and so fires at every time step.

5.2 Intrinsic noise

In the deterministic limit, a neuron with excitatory self-coupling displays trivial dynamics. However, the inclusion of noise induces a richer behaviour. Single neuron models with additive [OC95] and multiplicative [BBJ89] Gaussian noise have been previously been studied. Both of these models show qualitatively similar behaviour in their respective deterministic limits, both exhibiting two stable fixed points.

Ohira and Cowan’s model The *ad hoc* inclusion of additive Gaussian white noise to the model of Ohira and Cowan [OC95] induces a bi-modal stationary probability distribution. The distribution is symmetric about some mean activation, and the peak widths increase with noise strength.

The single effective neuron In contrast, two such noise sources are included by Bulsara *et al.* The self-coupling term includes multiplicative noise, and there is also an additive Langevin term. It is found that the multiplicative noise both suppresses the bi-stable nature of the underlying deterministic system, and also induces bi-stability in parameter regimes where such effects would not otherwise be expected.

The motivation for inclusion of noise in both of these models is to aid the analysis of an electronic model neuron due to Babcock and Westervelt [BW86, BW87]. Both the manner in which noise is included, and also the interpretation of its effects therefore have weak biological credentials. It is therefore interesting to consider what effect a more plausible noise source might have on neuronal behaviour.

The sources of neuronal noise with the strongest influence on the firing dynamics are threshold and synaptic (chapter 2):

5.2.1 Synaptic noise

Synaptic noise may be incorporated by taking the synaptic efficacy ω to be a random variable $\omega(n)$ drawn at each time-step according to some probability distribution and also according to the state of the neuron. The components of synaptic noise are (section 2.2.1) a Poisson distributed vesicular release probability, and a Gaussian distributed vesicle size. The probability of release due to an afferent AP is p , and in the absence of excitation it is p' , with $p' \ll p$.

For simplicity set $p' = 0$, and so neglect spontaneous fluctuations. Furthermore assume that all quanta have the same size, say ω_0 , and that the synapse is excitatory ($\omega_0 > 0$). A synapse from the mammalian CNS typically contains less than ten vesicles [KF87]. Therefore consider the *one-vesicle model* of [Bre92], and assume that an incident action potential can only cause the release of a single vesicle. Thus, if the neuron fires at the n^{th} time-step then $\omega(n) = \omega_0$ with probability p and $\omega(n) = 0$ with probability $1 - p$; if the neuron does not fire then $\omega(n) = 0$ with probability 1.

5.2.2 Threshold noise

Threshold noise is best modeled by making h a stochastic variable $h(n)$, generated at each time-step from a fixed probability density $p(h)$. For tractability, I will approximate Lecar and Nossal's distribution of firing probabilities, $P(V)$, for a given excitation, V , [LN71b] (recall section 2.2.3)

$$P(V) = \frac{1}{2} \left[1 + \operatorname{erf} \left(\frac{V}{\mathcal{S}} \right) \right] \quad (5.17)$$

by a similar (but more tractable) sigmoidal firing probability, and so choose the threshold at the n^{th} time-step, $h(n)$, to be drawn from the distribution

$$\rho(h) = \frac{d}{dh} \left(\frac{1}{1 + \exp(-\beta h)} \right) \quad (5.18)$$

(this density has been shown [BT90] to reproduce the update rule for the Little model [Lit74].) Therefore, the probability of firing for a given V is

$$P(V) = \int_{-\infty}^{\infty} \rho(h) \Theta(V - h) dh = \frac{1}{1 + \exp(-\beta V)} \quad (5.19)$$

where β parameterizes the spread of the distribution², and the mean threshold is $\langle h(n) \rangle = 0$.

5.3 Stochastic dynamics

With the inclusion of noise, equation (5.15) becomes a stochastic difference equation of the form

$$V(n+1) = V(n) + \eta F_{\alpha(n)}(V(n)) \quad (5.20)$$

²A Taylor expansion of both (5.17) and (5.19) shows that the two distributions agree to first order when $\beta = -4/(\mathcal{S}\sqrt{\pi})$

where the index $\alpha = 0, 1$ and $F_{\alpha(n)} = F_\alpha$ with probability $\Phi_\alpha(V(n))$, so that

$$F_0(V) = -\kappa V + I_0 \quad \text{and} \quad F_1(V) = -\kappa V + I_0 + \omega \quad (5.21)$$

with respective probabilities

$$\Phi_0(V) = 1 - pP(V) \quad \text{and} \quad \Phi_1(V) = pP(V) \quad (5.22)$$

Equation (5.20) implies that the time course of V is specified completely by the random symbol sequence $\{\alpha(n), n = 0, 1, \dots | \alpha(n) \in \{0, 1\}\}$ together with the initial value $V(0)$. Further note that the symbol sequence specifies the output spike train of the neuron. The interval $[V_1, V_2]$, with V_1 and V_2 given by equation (5.16), is an invariant domain of the dynamics. If $V(n) \in [V_1, V_2]$ then $V(m) \in [V_1, V_2] \forall m > n$, and so if V enters the interval it is confined there indefinitely.

The set $\{F_\alpha, \Phi_\alpha | \alpha \in \{0, 1\}\}$ defines a *random iterated function system* (random IFS) on the interval $[V_1, V_2]$ [Bar95], and has been used by Bressloff [Bre92] to show that the stochastic dynamics converge to a unique³ stationary probability density $u_\infty(V)$. An approximation to $u_\infty(V)$ may be obtained by sub-dividing the V -axis into small intervals and plotting an histogram of numerical iterates of equation (5.20).

5.3.1 Heuristic results

Assume for concreteness that $I_0 = -\frac{1}{2}p\omega_0$, which is half the mean transmitter release (this choice will be explained later). Equation (5.16) therefore gives $V_1 \leq 0$ and $V_2 > 0$. First consider zero-synaptic noise, *i.e.* $p = 1$, and so $V_1 = -V_2$. In the limit $\beta \rightarrow \infty$ the deterministic limit is recovered and the neuron has two stable states, V_1 and V_2 . As β is decreased, these two states become de-localized with a stationary probability distribution

³For the system considered here, convergence to a unique $u_\infty(V)$ is guaranteed since it is Markovian and so can be described by a master equation (see later). Such convergence may be proved by constructing the entropy, which is a Lyapunov function for the dynamics [Rei98].

that is bi-modal and symmetric about the origin. The peaks of the distribution are located close to V_1 and V_2 and their widths depend on β (figure 5.1(a)).

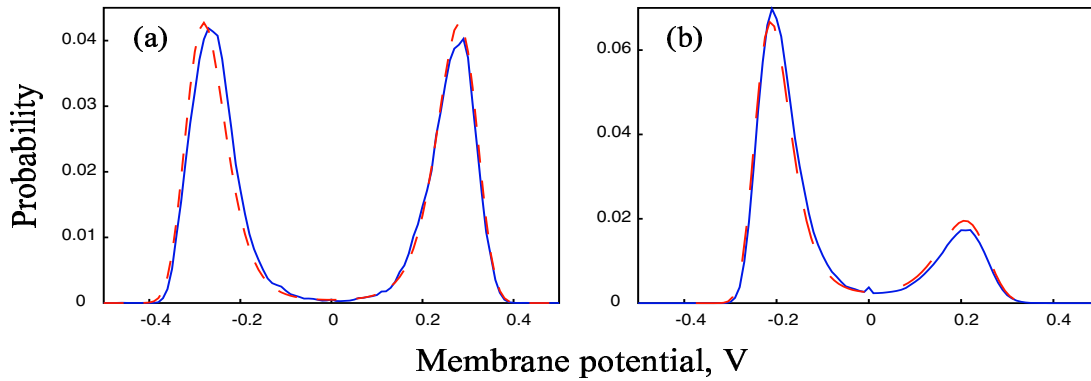


Figure 5.1: Approximations to the stationary probability distribution function $u_\infty(V)$ (bold lines) obtained from numerical iterates of equation (5.20). β large: (a) zero synaptic noise ($p = 1$), (b) non-zero synaptic noise ($p = 0.8$). The dashed lines show the corresponding probability densities obtained from the Fokker-Planck analysis (section 5.3.2). Parameters are: $\kappa = 1$ and $\omega = 1$

Such a bi-modal distribution has a simple physical interpretation. Recall that the mean threshold probability is $\langle h \rangle = 0$. The negative maximum therefore represents a quiescent state: the neuron remains close to its membrane resting potential and fires only rarely. The mean firing rate is $r = 1/\langle P \rangle \approx 1/\psi(V_1)$, where $\langle P \rangle$ is the mean firing probability. On the other hand, the positive maximum corresponds to a de-polarized state. Here the neuron has a high probability of firing, and if the neuron remains in this state for several time steps it will fire regularly and thus exhibit bursting. Transitions from the negative to the positive state are due to the neuron firing at least once whilst in the quiescent phase, and this in turn is caused by the selection of a low threshold. The converse transition is caused by the neuron failing to fire even though it is excited: the consequence of an high threshold. The neuron spends little time in the transition region.

If the synaptic noise is now switched on, by decreasing p , the bi-modal probability density

becomes asymmetric with a negative maximum that has a greater area than the positive one (figure 5.1(b)). This asymmetry is caused by there now being two ways in which the neuron can fail to receive excitatory input: either the imposition of a high threshold at the previous time-step, or vesicle release failure. In this regime the neuron will therefore spend most of its time in the silent state until a ‘rare’ event causes it to cross over to the bursting phase.

However, in the limit $\beta \rightarrow 0$ and $p = 1$ the firing probability is uniform at each time step, with $P(V) = 0.5 \forall V \in [V_1, V_2]$. Therefore

$$F_0(V) = -\kappa V - \frac{\omega_0}{2} \quad \text{and} \quad F_1(V) = -\kappa V + \frac{\omega_0}{2} \quad (5.23)$$

with $\Phi_0(V) = \Phi_1(V) = 0.5$. Equation (5.20) therefore has two components: an exponential drift term by which V tends to the origin, and a uniform random walk (of step-size $(\eta\omega_0)/2$) which causes V to diffuse away from the origin. The stationary probability distribution is therefore uni-modal and symmetric about $V = 0$ (figure 5.2). Now for $p < 1$, the random walk becomes biased toward the negative, thus breaking the symmetry of the stationary probability density (figure 5.2).

β is an order parameter for the dynamics. Hence there a critical value, say β_c , such that for $\beta > \beta_c$ the stationary probability distribution is bi-modal, while for $\beta < \beta_c$ is uni-modal.

5.3.2 Fokker–Planck analysis

An approximation to the stationary probability density $u_\infty(V)$ can be found analytically. Define a probability density $u_n(V)$ on the sample space of membrane potentials $V \in [V_1, V_2]$, so that the probability of finding the membrane potential in some interval $[a, b]$ at the n^{th} time-step is

$$P_n(a \leq V(n) \leq b) = \int_a^b u_n(V) dV \quad (5.24)$$

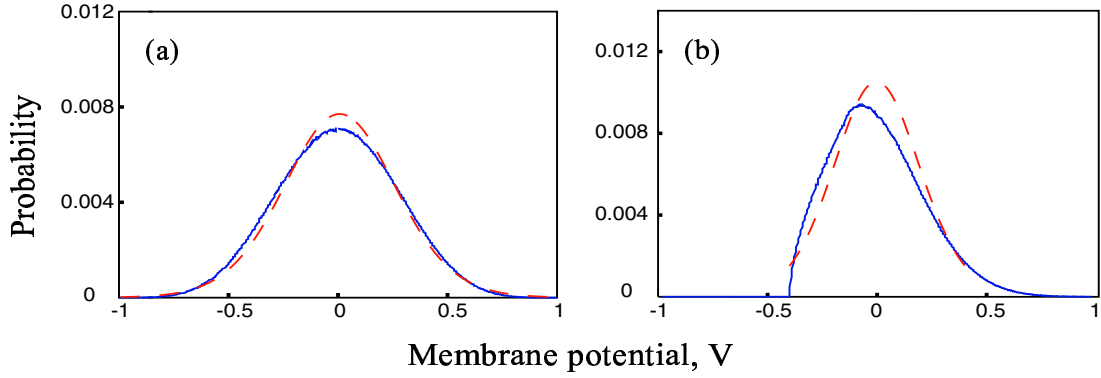


Figure 5.2: Approximations to the stationary probability distribution function $u_\infty(V)$ (bold lines) obtained from numerical iterates of equation (5.20). β small: (a) zero synaptic noise ($p = 1$), (b) non-zero synaptic noise ($p = 0.4$). The dashed lines show the corresponding probability densities obtained from the Fokker–Planck analysis (section 5.3.2). Parameters are: $\kappa = 1$, $\omega = 1$, and $\beta = 0.2$

The noise introduced in section 5.2 lacks temporal correlation and so this system is Markovian (see section 1.2 and appendix B.2). The probability density $u_n(V)$ therefore evolves according to a Chapman–Kolmogorov (CK) equation (recall section 1.2)

$$u_{n+1}(V) = \int_{V_1}^{V_2} \phi(V|V') u_n(V') dV' \quad (5.25)$$

where the transition probability $\phi(V|V')$ is the conditional probability that the system will be found in state V given that it was in V' at the previous time step, and is given by

$$\phi(V|V') = \sum_{\alpha} \Phi_{\alpha}(V') \delta(V - V' - \eta F_{\alpha}(V')) \quad (5.26)$$

recall (equation 1.12) that in the limit $\eta \rightarrow 0$, the discrete–time CK equation may first be transformed to a continuous–time master equation, and then (by way of the Kramers–Moyal

expansion – section 1.3) to a Fokker–Planck equation:

$$\frac{\partial}{\partial t}u(V, t) = -\frac{\partial}{\partial V}D^{(1)}(V)u(V, t) + \frac{1}{2}\frac{\partial^2}{\partial V^2}D^{(2)}(V)u(V, t) \quad (5.27)$$

where the drift and the diffusion coefficients $D^{(1)}$ and $D^{(2)}$ are the first and second moments of $\delta V(n) = V(n+1) - V(n)$ (recall equation (1.24))

$$D^{(1)}(V) = \eta [\omega_0 pP(V) - \kappa V + I_0] \quad (5.28)$$

$$D^{(2)}(V) = \eta^2 [[I_0 - \kappa V]^2 + \omega_0[\omega_0 + 2I_0 - 2\kappa V]pP(V)] \quad (5.29)$$

The 1–dimensional Fokker–Planck equation has a unique stationary solution, $u_{st}(V)$, which satisfies

$$-\frac{\partial}{\partial V}D^{(1)}(V)u_{st}(V) + \frac{1}{2}\frac{\partial^2}{\partial V^2}D^{(2)}(V)u_{st}(V) = 0 \quad (5.30)$$

Define the stationary probability current $\mathcal{J}(V)$, such that

$$\mathcal{J}(V) = \left(-D^{(1)}(V) + \frac{1}{2}\frac{\partial}{\partial V}D^{(2)}(V) \right) u_{st}(V) = \text{constant} \quad (5.31)$$

V_1 and V_2 are *reflecting* boundary conditions and so

$$\mathcal{J}(V_1) = \mathcal{J}(V_2) = \mathcal{J}(V) = 0 \quad (5.32)$$

therefore $u_{st}(V)$ has the form (recall section 1.3.1)

$$u_{st}(V) = N \exp(-\Xi_s(V)) \quad (5.33)$$

where N is a normalization constant such that

$$\int_{V_1}^{V_2} u_{st}(V) = 1 \quad (5.34)$$

and $\Xi_s(V)$ satisfies

$$\Xi_s(V) = \ln D^{(2)}(V) - 2 \int_{V_1}^V \frac{D_1(V')}{D_2(V')} dV' \quad (5.35)$$

$u_{st}(V)$ is the Fokker–Planck approximation to the true stationary density $u_\infty(V)$, and the function $\Xi_s(V)$ is an *effective potential function* for the dynamics. Comparing $u_{st}(V)$ with the histogram of iterates of (5.20) shows that this Fokker–Planck approximation describes well the qualitative and quantitative aspects of the stochastic dynamics (figures 5.1 and 5.2).

5.4 Noisy dynamics in an effective potential

The notion of an effective potential function allows an intuitive description of the neuronal dynamics. More importantly it also permits prediction of the critical value β_c .

5.4.1 Deterministic sub–system and the critical temperature

An estimate of β_c (and also a motivation for the choice for I_0) may be found by considering the stochastic system (5.20) as comprising an underlying deterministic trajectory which is perturbed by small fluctuations. Such an intuitive picture forms the basis of van Kampen’s ‘small fluctuations expansion’ [vK76, vK92].

A deterministic system obeying gradient dynamics has the potential function [vK92]

$$U_d(V) = - \int_V D^{(1)}(V') dV' \quad (5.36)$$

with $D^{(1)}(V)$ given by equation (5.28). First note the identity:

$$\frac{1}{1 + \exp(-\beta V)} \equiv \frac{1}{2} \left(1 + \tanh \left(\frac{\beta V}{2} \right) \right) \quad (5.37)$$

Thus the deterministic potential function (5.36) is

$$\begin{aligned} U_d(V) &= - \int_V [w_0 p P(V') - \kappa V' + I] dV' \\ &= - \int_V \left[\frac{w_0 p}{2} \tanh\left(\frac{\beta V'}{2}\right) - \kappa V' + \left(\frac{w_0 p}{2} + I_0\right) \right] dV' \end{aligned} \quad (5.38)$$

The stationary points of $U_d(V)$ satisfy $D^{(1)}(V) = 0$. This yields an equation identical in form to the Weiss mean field equation for an Ising ferro-magnet at a temperature $T' = 2/\beta$ and subject to an external magnetic field $(I_0 + \frac{1}{2}p w_0)$, see *e.g.* [CL95].

The stationary points can be determined graphically from the intercepts of the straight line

$$y = \kappa V + I_0 + \frac{1}{2} w_0 p \quad (5.39)$$

with the sigmoid

$$y = \frac{1}{2} w_0 p \tanh\left(\frac{\beta V}{2}\right) \quad (5.40)$$

When $I_0 = -\frac{1}{2} w_0 p$ the dynamics displays a phase transition at the critical value $\beta_c = (4\kappa)/(w_0 p)$. Below β_c there is a single intercept at $V = 0$ and $U_d(V)$ has a single minima. However, above β_c there are three intercepts: one at $V = 0$ and two others symmetrically arranged about the origin, and so $U_d(V)$ is bi-stable (figure 5.3(i)). If instead, $I_0 \neq -\frac{1}{2} w_0 p$ then the intercepts (and hence the stable states) become shifted along the V -axis (figure 5.3(ii)). In fact, a large enough I_0 can also induce a phase transition.

5.4.2 The effective potential

The membrane potential of the neuron therefore executes a random walk in an effective potential that is sculpted by the noise parameters. Synaptic noise, p , breaks the symmetry of $\Xi_s(V)$ (figure 5.4(b)), while threshold noise, β , determines $\delta\Xi(\beta)$: the height of the barrier between the minima. As β is increases, so too does $\delta\Xi$ (figure 5.4(a)).

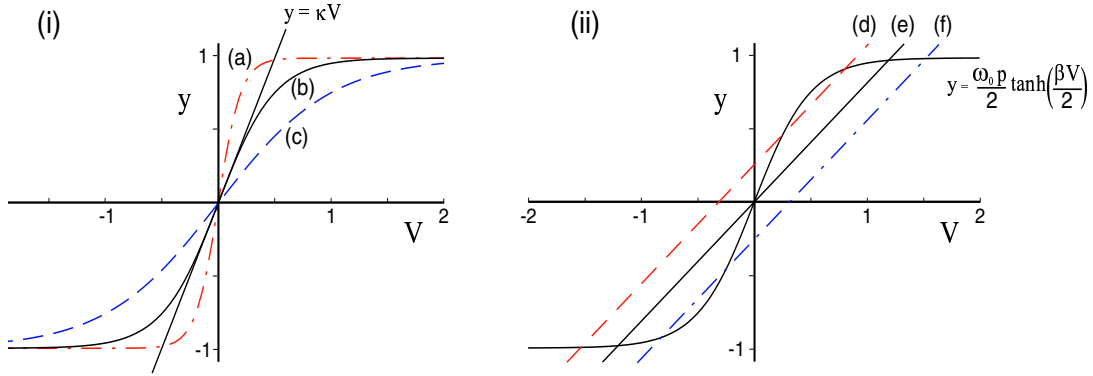


Figure 5.3: Ground states of the deterministic sub-system are determined by the intercepts between $y = \kappa V + I_0 + \frac{1}{2}\omega_0 p$ and $y = \frac{1}{2}\omega_0 p \tanh\left(\frac{\beta V}{2}\right)$. (i) $I_0 = -\frac{1}{2}\omega_0 p$: (a) $\beta > \beta_c$ and U_d is bi-stable (the ferromagnetic phase), (b) $\beta = \beta_c$, (c) $\beta < \beta_c$ and U_d is mono-stable. (ii) $\beta > \beta_c$: (d) $I_0 < -\frac{1}{2}\omega_0 p$ (e) $I_0 = -\frac{1}{2}\omega_0 p$ (f) $I_0 > -\frac{1}{2}\omega_0 p$.

Consider a fixed synaptic noise, with $p \neq 1$, and $\beta > \beta_c$, such that the effective potential is asymmetric and bi-stable. There are two natural time-scales for these dynamics: the mean escape time from the negative global minimum (the silent state) via the barrier $\delta\Xi_{12}$ to the positive meta-stable state (the bursting state); and the mean time for the converse transition over $\delta\Xi_{21}$ (figure 5.4(b)) and both of these time-scales will exhibit an Arrhenius⁴ dependence on their respective barrier heights. Following the bursting paradigm, these two times may be identified with the mean inter-burst interval and the mean burst length respectively. The inter-burst interval therefore depends solely on β and so is solely due to threshold noise, while the burst length is a function of both p and β , and so is determined by both threshold and synaptic noise.

Spike trains obtained from numerical iterates of equation (5.20) confirm this picture. There are long periods during which the neuron fires only occasionally, and at times that are separated intervals of order $1/P(V_1)$. Even rarer are the highly correlated bursts of spikes

⁴Unfortunately, a Kramers' rate (section 1.4) is not computable since it requires derivatives of the potential, and $\Xi(V)$ is obtained from numerical integration of equation (5.35) (see appendix B).

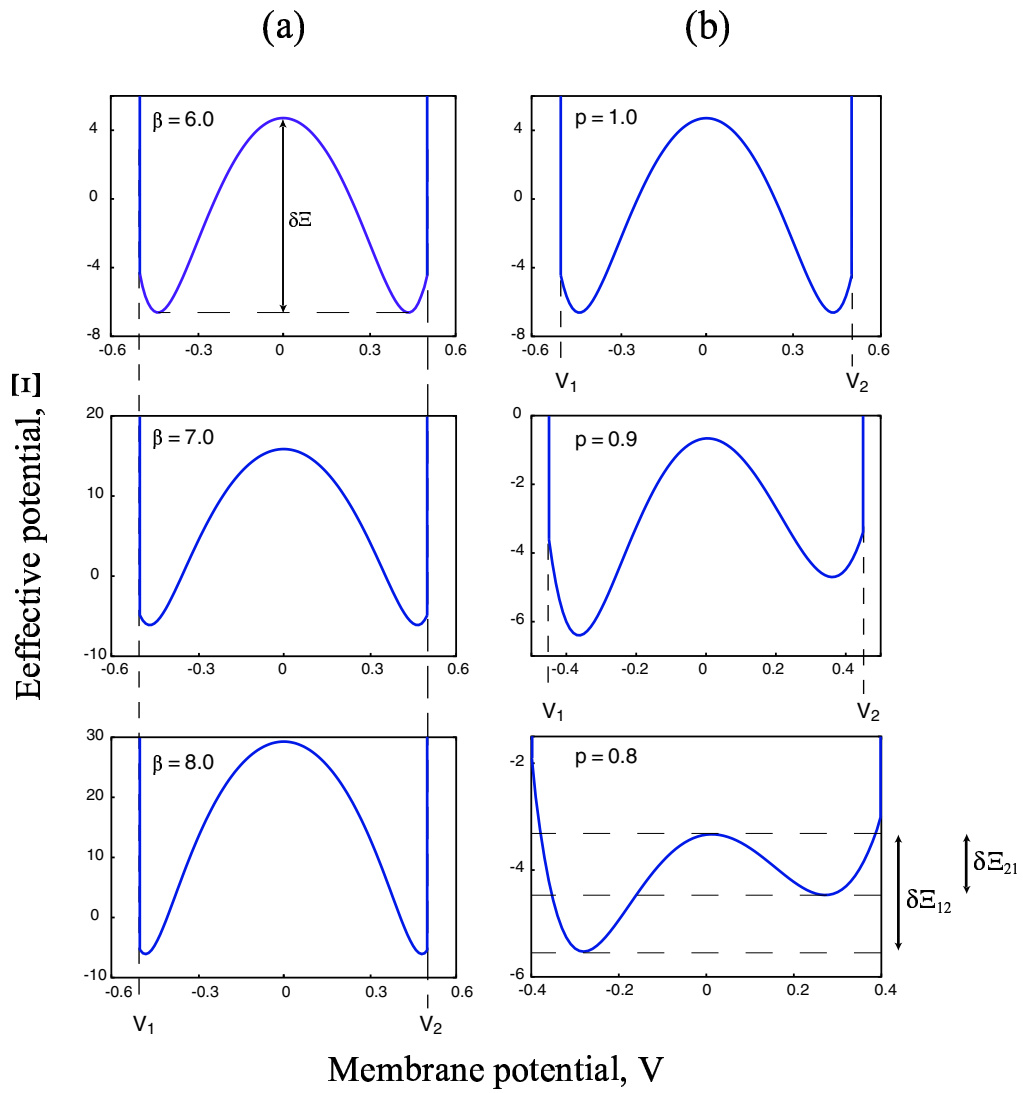


Figure 5.4: The effective potential for various noise strengths: (a) zero synaptic noise ($p = 1$) but varying threshold noise (β). (b) constant threshold noise ($\beta = 6.0$), and varying synaptic noise.

that signify occupation of the depolarized state. The occasional spikes should be considered as spurious background activity, but the bursting states are much more significant. (For example, recall that in chapter 3, bursting was shown to be a useful coding for temperature.) Therefore, how are these bursts distributed in time? An analogous measure to the inter-spike interval histogram is the *inter-burst interval histogram* (IBIH). Assuming that the time spent in the transition region of Ξ is small, this may be found numerically from a large number of trials, each of which consists of taking the initial point $V(0) = V_1$ and iterating equation (5.20) until $V(n) \approx V_2$ for the first time.

If the neuronal input is constant, such a distribution is uni-modal with an exponential tail (figure 5.5).

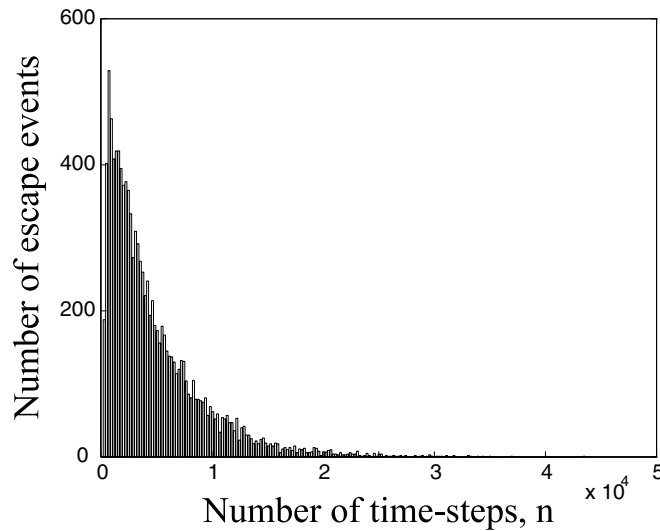


Figure 5.5: *Histogram of escape times (the IBIH) for an asymmetric, bi-stable neuron with constant input.*

5.5 Periodic Modulation and Response

Bulsara *et al.* [BJZ⁺91] have used both analysis and analog simulation to demonstrate that their single effective neuron model will exhibit SR when subject to weak periodic forcing.

To look for commensurate behaviour in this one-vesicle model, first introduce a weak, periodically modulated external input

$$I_E(n) = \xi \sin(\Omega n) \quad (5.41)$$

subject to the adiabatic approximation

$$\frac{2\pi}{\Omega} \gg 1 \quad (5.42)$$

so that equation (5.20) becomes

$$V(n+1) = V(n) + \eta (F_\alpha(V(n)) + \xi \sin(\Omega n)) \quad (5.43)$$

where the $\{F_\alpha(V(n))\}$ are defined by equation (5.21). Furthermore, to ensure that I_E alone is too weak to switch the neuron between quiescent and bursting states, impose

$$\xi \ll \frac{w_0}{\kappa} \quad (5.44)$$

In chapter 3 such input was associated with a slowly oscillating autocatalytic calcium current, but it has a wider range of applicability [Lán97]. For example: a sinusoidal tone applied to an auditory neuron [LBM91]; a periodic tactile stimulus [CIG96]; or even the action of a single pacemaker neuron [CBGC96].

Computation of the IBIH⁵ for various values of threshold noise shows that the escape times from the resting state V_1 can become partially entrained to the periodic signal. The typical multimodal distribution is again apparent: peaks occur at integer multiples of the driving period, and with exponentially decaying heights (*e.g.* figure 5.6).

⁵These histograms are obtained by iterating the neuron equation, (5.20), for a fixed time (of the order of 10 times the forcing period). If the neuron switches into a bursting state then the switch time is noted, if it does not switch within this time then a null result is noted. The neuron is then reset to the quiescent state and restarted. This process is repeated many times to obtain reasonable histograms.

Consider how this entrainment is affected as the noise parameter β is swept through its range. Note first that the condition of maximal threshold noise occurs when $\beta \rightarrow 0$, and furthermore that the deterministic limit derives from $\beta \rightarrow \infty$. For β low (*i.e.* high noise), $\delta\Xi_{12}$ is small and all transitions occur within the first cycle of driving. As β increases (*i.e.* the noise decreases), then so too does $\delta\Xi_{12}$ and higher sub-harmonics of the driving appear. As $\beta \rightarrow \infty$ (deterministic limit) the forcing becomes impotent and escape is prevented.

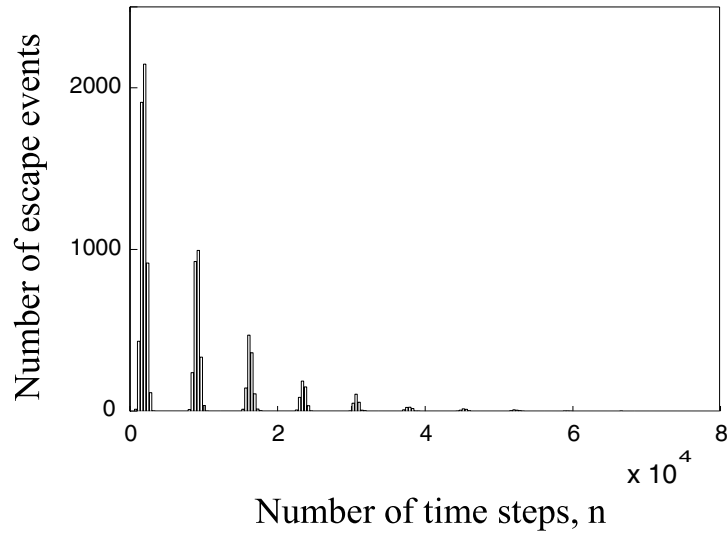


Figure 5.6: *An inter-burst interval histogram for the one-vesicle model subject to weak periodic driving.*

A plot of the area⁶ of each peak versus β , shows a set of resonance conditions: for each peak k , there is a value of β , say β_{max}^k , for which the peak area is maximal (figure 5.7). For $\beta \approx \beta_{max}^1$, the noisy transition rate is comparable to the driving period, and so escape is maximally synchronized to the signal.

⁶The area is computed according to Gammaitoni's prescription [GMS95] (equation (1.48))

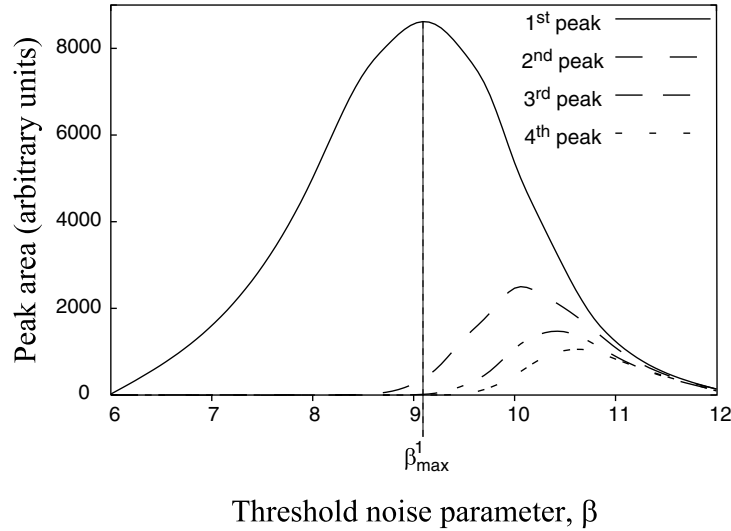


Figure 5.7: *The variation in area under the first four peaks of the IBIH, versus increasing threshold noise. Parameters are: $\kappa = 0.5, \omega = 0.5, \Omega = 0.05$ and $A = 0.05$.*

5.6 Discussion

To conclude, I have shown that a simple stochastic model of a spiking neuron can exhibit a much richer discharge than can its deterministic counterpart. For certain parameter values the neuron can burst, with burst lengths and inter-burst intervals that are Poisson distributed. I have demonstrated that the bursting dynamics may be described by a random walk of the membrane potential in a (possibly asymmetric) bistable potential. I have identified the two minima of this potential with the bursting and quiescent states, and I have shown that noise can cause transitions between these two states. The noise parameters, β and p , therefore *tune* the discharge pattern. Threshold noise controls the forward transition (*i.e.* from quiescence to bursting), and hence determines the inter-burst interval. In contrast, the backward transition (from bursting to rest – *i.e.* the burst length) is determined by both threshold and synaptic noise. I have further shown that when the cell is driven by a weak periodic signal the bursting dynamics become stochastically phase-locked to the forcing, and the neuron exhibits a form of stochastic resonance.

There are obvious limitations to this work: restriction to a single neuron model with feedback has aided the analysis, but represents an extreme oversimplification. However, it is plausible that the feedback mechanisms present within some real neuronal networks may initiate equivalent behaviour. A further difficulty arises from the imposition of the adiabatic condition (5.42). The slow signal is necessary to ensure the system remains near an equilibrium state, and therefore the validity of the analysis. However, the long time period means that the residence times in the bursting state, and hence burst lengths, become unrealistically long: of the order of several hundred spikes per burst.

It should be noted that this choice for the probability distribution for threshold noise, while simplifying the analysis, is not crucial to the behaviour discussed here. Any sigmoidal density will behave comparably.

The main results of this chapter are to appear in [BR99].

Chapter 6

Conclusions

“‘I have done that,’ says my memory. ‘I cannot have done that’ says my pride, and remains adamant. At last – memory yields.”

Nietzsche

It has been said that a thesis is never finished . . . but is only ever abandoned, and unfortunately this work subscribes to that sentiment. It is inevitable that the completion of any piece of work (almost) always suggests a myriad of ways in which it might be continued. With this in mind, after first summarizing what I have achieved, I want to take the time to indicate some ways in which my work should be extended.

Chapter 1: contained some of the necessary mathematical and physical background to this thesis. Specifically I discussed what noise is, and how it may be treated mathematically. I introduced briefly the Langevin equation and discussed its connection to the master equation and to the Fokker–Planck equation. I then showed how to compute the mean rate of escape of a noisy particle from a meta–stable state. I completed the chapter with a brief review of stochastic resonance.

Chapter 2: was a review of the biology of neurons, and a brief summary of the Hodgkin–

Huxley model for action potential generation. I then discussed what various sources of noise contributed to the neural dynamics.

Chapter 3: presented my studies on cold-receptor function. I first showed that complex ionic models could (in the spirit of Ermentrout and Kopell [EK86]) reduce to canonical phase-models which possess qualitatively similar dynamics. I then investigated the phase-model (both numerically and analytically) in the deterministic regime and also when subject to a finite amount of thermal noise. I showed that numerically obtained spike trains and inter-spike interval histograms from the phase model agree well with the experimental data. By way of Floquet analysis and the Mathieu equation, I showed that the temperature dependence of the discharge pattern of these cells might be viewed as a trajectory through the mode-locked solutions of a Strutt map. My investigations also suggest that skipping might be caused by noise and I indicated how both the number of spikes in a burst, and also the skipping rate at any given temperature may be predicted. I studied how altering the noise level affects the dynamics and I showed that the skipping regime may be subdivided: the first part of skipping is caused by noise-induced trapping and the second part is due to noise-induced spiking. Finally, I demonstrated that the phase-model displays a non-monotonic dependence on noise strength, and in fact exhibits both resonant trapping and autonomous stochastic resonance.

Chapter 4: Here I turned to the problem of the perception of ambiguous figures. I first reviewed the psycho-physics of how such figures are interpreted by the brain, and I discussed two experiments that indicate that stochastic resonance might occur at a cognitive level. I proposed Haken's winner-takes-all network as a model for the interpretive process and showed how it might be extended to model the phenomena of reversal. I then investigated how Haken's model might elucidate a mechanism for cognitive stochastic resonance. I then turned to the *diffusive* Haken model (due to Schmutz and Banzhaff [SB92] and Bressloff [Bre95, Bre97]) a model previously proposed to explore how the neural substrate might perform pattern recognition. I showed how this network could also support stochastic resonance but that there was a trade off between the strength of the diffusive coupling between neurons (a factor that determines the network's robustness to the loss, or 'death',

of individual cells) and the amount of noise that the network could support.

Chapter 5: in this chapter I showed how specific noise distributions for synaptic and threshold noise might affect neuronal dynamics. To obtain a framework for the inclusion of noise, I first indicated a method by which the dynamics could be discretized. I then investigated these discrete dynamics first via a master equation and subsequently by means of a Fokker–Planck equation. Using these techniques I was able to show that (for certain parameter regimes) this system may be interpreted as evolving in a generalized bistable potential. I identified residence of the excited stable–state with bursting, and residence of the negative stable–state as being a time of quiescence. I then presented numerical results to show that in the absence of any external input, transitions between these two states, and hence inter–burst intervals, are exponentially distributed. I completed my study by showing that the introduction of a weak, periodic input could (stochastically) entrain the neuron in a manner that is related to stochastic resonance.

Without re–iterating the conclusions of previous chapters, a ‘wish–list’ of future projects and unsolved problems include:

- In this thesis (with the exception of chapter 5) I have considered additive, Gaussian noise. However, as discussed in chapter 1, such noise is a mathematical fiction, and so the most obvious extension to this thesis would be to consider how coloured–noise sources (see *e.g.* [HJ95]) might change the neural dynamics.
- I feel that my work on cold–receptor function holds promise for a deeper understanding of the operation of these cells. However, to achieve this, a concrete identification between the parameters of the model and those of real cells need to be made. Longtin [RBL98] has made some headway with this, but more needs to be done.
- There are few published numerical¹ techniques for obtaining general solutions to the time–dependent Fokker–Planck equation (recall section 3.4.2). Numerical algorithms for the solution to such partial differential equations is a large area of research, and is beyond the scope of this thesis, but this is definitely something that requires attention.

¹Nor are there any analytic approximations.

- Recalling that skipping in the cold-receptor model may be interpreted as a noise-induced crossing of the $j = 0$ and $j = 1$ tongue boundary of the Strutt map. An alternative strategy for computing the skipping rate might therefore be to find the mean first-passage time for this transition (in terms of the variables, a and q , of equation (3.24)).
- Stochastic resonance (in the *bona-fide* sense as discussed in section 1.5) demands that the time-scale matching relation equation (1.46) be fulfilled. However, I have not yet been able to prove an equivalent relation for resonant trapping and autonomous stochastic resonance in the cold-receptor model close to its saddle-node bifurcation. Such a relation first requires that the velocity of a noise-induced passage through a bifurcation be evaluated, and a possible technique for this has been suggested by Sigeti [Sig88].

The most compelling lesson from my work has been to glimpse at the richness of the interaction between noise and dynamical systems. However, much of the current neural computing literature falls into either the *deterministic* camp (*i.e.* investigations of purely-deterministic neural dynamics² such as those described in [HI97]), the *neural-coding and information-theoretic* camp (*e.g.* the book by Rieke *et al.* [RWdRvSB97]) or what might be termed the *mean-field* camp (*i.e.* those that consider noise in large networks, *e.g.* the replica-symmetric standpoint of [Ami89]). Although all of these approaches are extremely valid, there little cross-over between them. It is particularly salutatory that the amongst the many references to noise in the index of Arbib's exhaustive compendium [Arb95], there is no entry pertaining to neuronal noise in the sense considered here. One notable exception to my classification is of course the recent interest in stochastic resonance in neural systems, however this phenomena (SR) is only a small part of the larger field of 'noise in dynamical systems' and there is much of the latter that has a wide applicability for neural modellers.

²In this category I include treatments of, for example: synchronization phenomena, ion channel models, and chaos in neuron models.

Appendix **A**

A Few Theorems

A.1 Floquet's theorem

Floquet's theorem:¹ *The regular system*

$$\dot{x}(t) = Q(t)x \tag{A.1}$$

where the coefficient Q is periodic with minimal period T , has at least one non-trivial solution $x = X(t)$ such that

$$X(t + T) = CX(t), \quad -\infty < t < \infty \tag{A.2}$$

where C is a constant

Proof: [JS87, Gle94] first integrate (A.1), so that

$$X(t) = X_0 \exp \left(\int_0^t Q(s) ds \right) \tag{A.3}$$

¹I present here the scalar case, however generalization to more than one variable is straightforward.

thus obtaining the fundamental matrix $\Psi(t) = \exp\left(\int_0^t \mathcal{Q}(s)ds\right)$, with $X(t) = \Psi(t)X_0$. Furthermore, note that the integral may be split into

$$\int_0^{t+\mathcal{T}} \mathcal{Q}(s)ds = \int_0^{\mathcal{T}} \mathcal{Q}(s)ds + \int_{\mathcal{T}}^{\mathcal{T}+t} \mathcal{Q}(s)ds \quad (\text{A.4})$$

and so

$$\Psi(t + \mathcal{T}) = \exp\left(\int_0^{\mathcal{T}} \mathcal{Q}(s)ds\right) \exp\left(\int_{\mathcal{T}}^{\mathcal{T}+t} \mathcal{Q}(s)ds\right) \quad (\text{A.5})$$

but since $\mathcal{Q}(t) = \mathcal{Q}(t + \mathcal{T})$, we have

$$\int_{\mathcal{T}}^{\mathcal{T}+t} \mathcal{Q}(s)ds = \int_0^t \mathcal{Q}(s)ds \quad (\text{A.6})$$

and therefore

$$\Psi(t + \mathcal{T}) = \Psi(\mathcal{T})\Psi(t) \quad (\text{A.7})$$

and since \mathcal{T} is fixed, $\mathcal{C} = \Psi(\mathcal{T})$ is a constant, and so we have the required periodic solution.

Furthermore, also note

$$\Psi(n\mathcal{T}) = \Psi(\mathcal{T})^n \quad (\text{A.8})$$

The number

$$\Psi(\mathcal{T}) = \exp\left(\int_0^{\mathcal{T}} \mathcal{Q}(s)ds\right) = \exp(\rho\mathcal{T}) \quad (\text{A.9})$$

is called a Floquet multiplier, while ρ is called a Floquet exponent. Note that ρ is only defined up to a constant

$$\rho = \frac{1}{\mathcal{T}} \log(\Psi(\mathcal{T})) + \frac{2n\pi i}{\mathcal{T}} \quad n \in \mathbb{Z} \quad (\text{A.10})$$

$x = 0$ is a stationary point of the system, to investigate its stability define

$$p(t) = \Psi(t) \exp(-\rho t) \tag{A.11}$$

thus

$$p(t + \mathcal{T}) = \Psi(t + \mathcal{T}) \exp(-\rho(t + \mathcal{T})) = \Psi(t) \exp(-\rho t) = p(t) \tag{A.12}$$

and so $p(t)$ is periodic and bounded, and the solution may be written

$$X(t) = \Psi(t)X_0 = p(t) \exp(\rho t)X_0 \tag{A.13}$$

and so if $\Re \rho < 0$ the solutions decay, while for $\Re \rho > 0$ they are unbounded.

A.2 Multistability in networks of weakly coupled bistable units – the anti-continuum limit

The stationary states of a network of *weakly-coupled* bistable units can be shown to be analytic continuations of the stationary states of the network in its de-coupled limit. Following MacKay and Sepulchre [MS95] consider a large (and possibly infinite) network of N bistable oscillators. Suppose that the i^{th} oscillator is described by a state variable x_i and that in the absence of any other oscillator, it evolves according to

$$\dot{x}_i = f(x_i) \tag{A.14}$$

where the function $f(\dots)$ is C^1 and has two stable states corresponding to $x_i = x^{(n)}$, ($n = 1, 2$).

The state of the network may be written as the N -dimensional vector \mathbf{X} , with components x_i , ($i = 1, \dots, N$). \mathbf{X} is assumed to evolve according to

$$\dot{\mathbf{X}} = F(\mathbf{X}) + \mu K(\mathbf{X}) \equiv G(\mathbf{X}, \mu) \tag{A.15}$$

where F is the map

$$F(\mathbf{X}) = (f(x_i))_{i \in N} \tag{A.16}$$

$K(\dots)$ is some C^1 function that describes interactions between units, and μ describes the strength of the coupling.

When $\mu = 0$ the network exhibits 2^N stationary states $\mathbf{X}_0^{(j)}$, ($j = 0 \dots 2^N$), each of which satisfy $F(\mathbf{X}_0^{(j)}) = 0$, and hence also $G(\mathbf{X}_0^{(j)}, 0) = 0$. As a consequence of the implicit function theorem (see *e.g.* [Gle94]), the zero $(\mathbf{X}_0^{(j)}, 0)$ of G has a local continuation (termed the anti-continuum limit [Aub95]) about $\mu = 0$ if (i) G is C^1 and (ii) the Jacobian of G

(taken with respect to \mathbf{X}) is invertible at $(\mathbf{X}_0^{(j)}, 0)$ with a bounded inverse. These continued solutions are therefore delocalizations of the original ground states $\mathbf{X}_0^{(j)}$.

A.2.1 Continued solutions of the diffusive Haken model

With reference to the diffusive Haken model discussed in chapter 4, denote the state of the network by $Q(\mu, \mathcal{Z})$ where $\mathcal{Z} \equiv \mathcal{Z}(\mu)$ is now implicitly a function of the coupling strength μ . Stationary states satisfy

$$(1 - 2\mathcal{Z})q_i + q_i^3 + \mu \sum_{\langle j,i \rangle} (q_j - q_i) \equiv [G(Q, \mu, \mathcal{Z})]_i = 0 \quad (\text{A.17})$$

where \mathcal{Z} is determined self-consistently from (equation (4.9))

$$\mathcal{Z}(\mathbf{q}) = \sum_i q_i^2 \quad (\text{A.18})$$

The introduction of this self-consistency complicates the stability of the continued solutions. First consider \mathcal{Z} fixed, *e.g.* $\mathcal{Z} \equiv \mathcal{Z}_0$, such that $\mathcal{Z}_0 > \frac{1}{2}$, and for $\mu = 0$ the equilibria of (A.17) satisfy

$$\bar{q}_i = 0 \quad \text{or} \quad \bar{q}_i = \pm \sqrt{2\mathcal{Z}_0 - 1} \neq 0 \quad (\text{A.19})$$

(if negative solutions are included). Denote the Jacobian $\partial G / \partial Q$ by δG . Since

$$[\delta G(\bar{Q}, 0, \mathcal{Z}_0)]_{ij} = \delta_{i,j} \chi_i \quad (\text{A.20})$$

where $\bar{Q} \equiv Q(0, \mathcal{Z}_0)$ is a zero of $G(\dots)$, $\chi_i = -(2\mathcal{Z}_0 - 1)$ if $\bar{q}_i = 0$ and $\chi_i = 2(2\mathcal{Z}_0 - 1)$ if $\bar{q}_i \neq 0$. δG is invertible at the stationary point $(\bar{Q}, 0, \mathcal{Z})$, and so from the implicit function theorem (IFT) there exists a sufficiently small coupling μ for which there exist local continuations of each \bar{Q} [Bre95].

Now let \mathcal{Z} be no longer fixed, but instead determined by the self-consistency condition equation (A.18) (equation (4.9)). By a second application of the IFT it is possible to show [Bre95] that there exists μ_0 such that for $|\mu| < \mu_0$, there is a locally unique continuation of $\mathcal{Z}(\mu)$ and of the network state $Q(\mu, \mathcal{Z}(\mu))$ such that

$$\delta G(Q(\mu, \mathcal{Z}(\mu)), \mu, \mathcal{Z}(\mu)) = 0 \tag{A.21}$$

and so these continued states are also delocalizations of the original ground states of the network.

Appendix **B**

Numerical Issues

“The purpose of computing is insight, not numbers.” [Ham73]

All of the numerical data in this thesis derives from software written by myself in C. Data was analysed with both MATLAB (version 4.2) and with Microsoft EXCEL (version 7). The Mathieu functions in chapter 3 were computed with MATHEMATICA (version 3.0), and the generalised potential (equation (5.35)) in chapter 5 was numerically integrated with MAPLE (version V release 4), using their proprietary algorithms.

B.1 Random and pseudo-random number generators

For a working definition of randomness, consider the sequence of numbers $\mathcal{R} = \{x_n\}$, with $x_n \in [a, b] \forall n$. \mathcal{R} is called a *random sequence* (or sequence of uniform deviates) if:

- (i) every element of \mathcal{R} is independent of every other element
- (ii) the elements of \mathcal{R} are equi-distributed on the interval $[a, b]$.

Computer generated random numbers are rarely truly random, since there's usually a trade-off between computational efficiency and how 'random' a sequence must be for a given task. Thus, computer generated random numbers are more properly called *pseudo-random*. There is no 'best' random number generator (RNG) and in fact the ANSI¹ standard for the C language merely gives an example of an RNG. Thus, RNG implementations are usually machine and compiler dependent. A typical algorithm is the *linear congruential generator*, which generates a sequence of numbers according to

$$x_{n+1} = ax_n + c \pmod{m} \quad a, c, m \in \mathbb{Z}^+ \quad (\text{B.1})$$

where a , c , and m are called the multiplier, the increment and the modulus, respectively. Random numbers are generated by supplying an initial 'seed', x_0 , (*e.g.* an integer composed from a reading of the system clock) and iterating the generator. However, since m is an integer, the generator is actually periodic with maximal² period m . In consequence, poor implementations of (B.1) (*e.g.* those with small values of m) can give dangerous results³.

An even simpler RNG is the *simple multiplicative congruential* (SMC) algorithm

$$x_{n+1} = ax_n \pmod{m} \quad a, m \in \mathbb{Z}^+ \quad (\text{B.2})$$

provided that a and m are chosen very carefully and that $x_0 \neq 0$, then this generator can perform as effectively as, and is generally faster than, most other algorithms [PTVF92]. Park and Miller [PM88] recommend

$$a = 7^5 \quad \text{and} \quad m = 2^{31} - 1 \quad (\text{B.3})$$

which has a period of $2^{31} - 2 \approx 2.1 \times 10^9$.

¹American National Standards Institute

²(B.1) has its maximal period when m is prime.

³[PTVF92] is particularly scathing about how such generators are implemented (note the emphasis on implementation) in most commercial compilers.

However, there is a complication when using the SMC algorithm to create a sequence of random numbers. First note that successive iterates of (B.2) differ only by a multiple of $\sim 1.7 \times 10^4$ (out of a total modulus of $\sim 2.1 \times 10^9$). Thus when the SMC generates a very small number, its immediate successor in the sequence will be another small number. For example, if the SMC algorithm returns $x_j = 10^{-7}$, then x_{j+1} will be of order 1.7×10^{-3} .

Such sequential correlations can be removed by means of a *shuffling algorithm* due to Bays and Durham (see *e.g.* [PTVF92]). When the RNG algorithm is first called, the shuffle routine creates a table of, say 32, random numbers (see figure B.1). Although the elements, b_i , of the table will be serially correlated, an un-correlated sequence may be created by selecting members at random from the table. The method proceeds as follows: each time the algorithm is called, the random number b_0 is used to choose an element, say b_4 , from the table which is then output. b_4 is now copied into b_0 for use during the next iteration, and a new element b_4 is created by the RNG.

B.1.1 Transformation methods and non-uniform deviates

Uniform deviates are all well and good, but random numbers drawn from other distributions are required more frequently.

To transform one distribution into another [PTVF92], consider first the function $y(x)$ of the uniform deviate x . If x has a probability density $p(x)$, then if $y(x)$ will have a probability density

$$p(y) = p(x) \left| \frac{dx}{dy} \right| \quad (\text{B.4})$$

However, for a uniform deviate on the interval (0,1)

$$p(x) dx = \begin{cases} dx & \text{if } 0 < x < 1 \\ 0 & \text{otherwise} \end{cases} \quad (\text{B.5})$$

therefore, any arbitrary distribution of y 's, say $p(y) = \mathcal{F}(y)$, can be found from solving

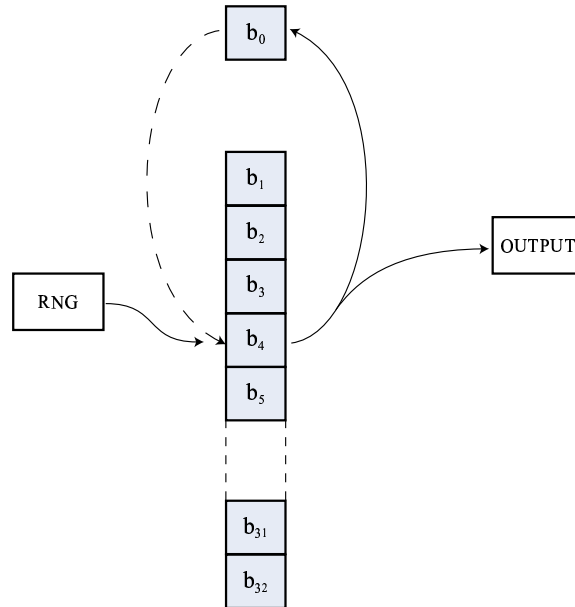


Figure B.1: *The Bays and Durham shuffle algorithm for removing serial correlations in a sequence of iterates of the simple multiplicative congruential generator (equation (B.2)). Each time the algorithm is called, the random number b_0 is used to choose an element, say b_4 , from the table which is then output. b_4 is now copied into b_0 for use during the next iteration, and a new element b_4 is created by the RNG (see e.g. [PTVF92]). [After [PTVF92]].*

(B.4), subject to (B.5), so that

$$x = F(y) = \int_0^y \mathcal{F}(y) dy \quad (\text{B.6})$$

and so the transform from a uniform distribution to an arbitrary one is given by

$$y(x) = F^{-1}(x) \quad (\text{B.7})$$

provided the inverse of F , F^{-1} , exists.

This procedure has an intuitive geometrical interpretation [PM88] (figure B.2). Note first

that $F(y)$ is the area to the left of y under the distribution curve $\mathcal{F}(y)$. Therefore, the procedure is to pick a uniform deviate x and then to find the value y corresponding to a fraction x of the area to the left under the distribution curve.

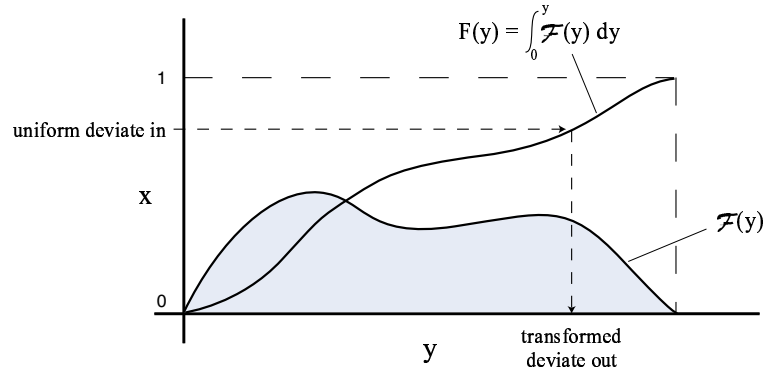


Figure B.2: *Geometric interpretation of the transformation method for generating non-uniform deviates. Given a uniform deviate, x , and a (non-uniform) distribution, $\mathcal{F}(y)$, the required non-uniform deviate, y , is the point corresponding to a fraction x of the area to the left under the distribution curve. [After [PTVF92]].*

Normal deviates and the Box–Muller algorithm

The transformation method generalizes to more than one dimension, and is used in an efficient algorithm (due to Box and Muller – see [PM88]) for generating normal deviates.

step 1 Generate two deviates distributed uniformly on the unit circle. This may be achieved by first transforming two iterates, x_i ($i = 1, 2$), of the LCM generator, so that $(2x_i - 1) \rightarrow z_i$. If $Z \equiv \sum_i z_i^2 \geq 1$ then these two are rejected, two new x_i are generated and the process is repeated.

step 1 The Box–Muller transformation. The two deviates, z_i , are now transformed to normal deviates according to

$$y_1 = z_1 \sqrt{-\frac{2 \ln(Z)}{Z}} \quad \text{and} \quad y_2 = z_2 \sqrt{-\frac{2 \ln(Z)}{Z}} \quad (\text{B.8})$$

B.2 Numerical simulation of noisy dynamical systems

Consider the stochastic differential equation (SDE)

$$\frac{d}{dt}\mathcal{X}(t) = F(\mathcal{X}, t) + \eta(t) \quad (\text{B.9})$$

where $\eta(t)$ is a zero-mean white noise process⁴. The random process $\mathcal{X}(t)$ is *Markovian* [Gil96a], and so

- (i) $\mathcal{X}(t + dt)$ depends solely on t , dt and $\mathcal{X}(t)$, *i.e.* $\mathcal{X}(t)$ has no *memory*.
- (ii) the increment

$$\mathcal{D}(dt; \mathcal{X}(t), t) = \mathcal{X}(t + dt) - \mathcal{X}(t) \quad (\text{B.10})$$

is a smooth function of its arguments.

- (iii) $\mathcal{X}(t)$ is a continuous function of t , in the sense that $\mathcal{D}(dt; \mathcal{X}(t), t) \rightarrow 0$ as $dt \rightarrow 0$, $\forall x, t$.

To numerically integrate an SDE, one must first decide upon a satisfactory discretization [Gil96a]. First write (B.9) as an integral equation

$$\mathcal{X}(t + \Delta t) = \mathcal{X}(t) + \int_t^{t+\Delta t} F(\mathcal{X}, t) dt + \int_t^{t+\Delta t} \eta(t) dt \quad (\text{B.11})$$

in the absence of the last term, a simple Euler scheme could be used. Setting the time-step Δt to be small but finite, (B.11) would therefore become

$$\mathcal{X}_{m+1} = \mathcal{X}_m + F_m \Delta t$$

⁴Any non-zero mean, *i.e.* $\langle \eta(t) \rangle \equiv \bar{\eta} \neq 0$, can be incorporated into the function $F(x, t)$ to leave the zero-mean process $\eta'(t) = \eta(t) - \bar{\eta}$.

where

$$\mathcal{X}_m \equiv x(t) |_{t=t'}, \quad \mathcal{X}_{m+1} \equiv \mathcal{X}(t) |_{t=t'+\Delta t} \quad \text{and} \quad F_m \equiv F(\mathcal{X}, t) |_{t=t'}$$

However, since $\eta(t)$ is non-differentiable, care must be taken when discretizing the corresponding random process. Consider first dividing the interval $[t, t + \Delta t)$ into $n > 1$ sub-intervals of equal length $\Delta t/n$ such that $t_i = t + i(\Delta t/n)$, ($i = 0 \dots n$). We then have

$$\mathcal{X}(t + \Delta t) - \mathcal{X}(t) = \mathcal{X}(t_n) - \mathcal{X}(t_0) = \sum_{i=1}^n [\mathcal{X}(t_i) - \mathcal{X}(t_{i-1})] \quad (\text{B.12})$$

$$\begin{aligned} &= \sum_{i=1}^n [\mathcal{X}(t_{i-1} + \Delta t/n) - \mathcal{X}(t_{i-1})] \quad (\text{B.13}) \\ &\equiv \mathcal{D}(\Delta t; \mathcal{X}(t), t) \end{aligned}$$

therefore

$$\mathcal{D}(\Delta t; \mathcal{X}(t), t) = \sum_{i=1}^n \mathcal{D}(\Delta t/n; \mathcal{X}(t_{i-1}), t_{i-1}) \quad (\text{B.14})$$

As a consequence of conditions (i) and (ii) (above), Δt can be made so small that all of the t_i 's are arbitrarily close to t . Thus, to lowest order in Δt we can replace

$$t_{i-1} \rightarrow t \quad \text{and} \quad \mathcal{X}(t_{i-1}) \rightarrow \mathcal{X}(t) \equiv x \quad (\text{B.15})$$

and so, to lowest order in Δt and for all $n > 1$,

$$\mathcal{D}(\Delta t; x, t) = \sum_{i=1}^n \mathcal{D}_i(\Delta t/n; x, t) \quad (\text{B.16})$$

and from the Markov condition (i) above, the $\mathcal{D}_i()$ are n statistically-independent copies of the random variable $\mathcal{D}(\Delta t/n; x, t)$. Furthermore, the mean and variance of each of the $\mathcal{D}_i()$ are finite due to condition (iii). Therefore, if n is allowed to become arbitrarily large,

the central limit theorem may be invoked to show that the sum $\mathcal{D}(\Delta t; \mathcal{X}(t), t)$ is normally distributed. Furthermore, so too are the n statistically-independent random quantities $\mathcal{D}(\Delta t/n; \mathcal{X}(t), t)$. Thus, the mean and variance are given by

$$\begin{aligned}\langle \mathcal{D}(\Delta t; \mathcal{X}(t), t) \rangle &= \sum_{i=1}^n \langle \mathcal{D}_i(\Delta t/n; x, t) \rangle \\ &= n \times \langle \mathcal{D}(\Delta t/n; x, t) \rangle\end{aligned}\tag{B.17}$$

$$\begin{aligned}\langle \mathcal{D}^2(\Delta t; \mathcal{X}(t), t) \rangle &= \sum_{i=1}^n \langle \mathcal{D}_i^2(\Delta t/n; x, t) \rangle \\ &= n \times \langle \mathcal{D}^2(\Delta t/n; x, t) \rangle\end{aligned}\tag{B.18}$$

Now, a smooth function $h(y)$ can only satisfy $h(y) = n \times h(y/n)$, $\forall n \in \mathbb{Z}^+$ if it is a linear function of y , *i.e.* $h(y) = \mathcal{B}y$ where \mathcal{B} is a constant. Thus

$$\begin{aligned}\langle \mathcal{D}(\Delta t; \mathcal{X}(t), t) \rangle &= A(x, t)\Delta t \\ \langle \mathcal{D}^2(\Delta t; \mathcal{X}(t), t) \rangle &= D(x, t)\Delta t\end{aligned}\tag{B.19}$$

therefore, since $\mathcal{D}()$ is normal,

$$\mathcal{D}(\Delta t; \mathcal{X}(t), t) = \mathbb{N}(A(x, t)\Delta t, D(x, t)\Delta t) \equiv A(x, t)\Delta t + \sqrt{D(x, t)\Delta t} \mathbb{N}(0, 1)\tag{B.20}$$

and so the noise term is proportional to the square root of the time-step. The discretization therefore becomes

$$\mathcal{X}_{m+1} = \mathcal{X}_m + F_m \Delta t + \eta_m \sqrt{\Delta t}\tag{B.21}$$

where $\eta_m = \eta|_{t=t'}$.

The Euler scheme therefore generalizes to numerical integration of (B.9), subject to the initial condition, say $\mathcal{X}(t=0) = \mathcal{X}_0$. (B.21) is iterated by choosing a noise term, η_m , at every time-step, according to the Box-Muller algorithm (B.8).

As with the numerical integration of ordinary differential equations, the Euler scheme is far from being the most accurate (for a review and comparison of numerical techniques for the integration of SDEs see [Man89, Man97]). However, provided that the time-step Δt is chosen to be small enough, it is generally fairly reliable [Man97]. In the simulations performed for this thesis, stability and convergence were confirmed by trying several different time-steps. It was generally found that $\Delta = 0.1$ gave accurate results, while also allowing fast integration.

Bibliography

- [AB85] W.B. Adams and J.A. Benson. The generation and modulation of endogenous rhythmicity in the *aplysia* bursting neurone R15. *Progress in Biophysics and Molecular Biology*, 46:1–49, 1985.
- [AGMS94] F. Apostolico, L. Gammaitoni, F. Marchesoni, and S. Santucci. Resonant trapping: a failure mechanism in switch transitions. *Physical Review E*, 55(1):36–39, January 1994.
- [Ami89] D.J. Amit. *Modeling Brain Function – the world of attractor neural networks*. Cambridge University Press, 1989.
- [Arb95] M. Arbib, editor. *Handbook of Brain Theory and Neural Networks*. MIT University Press, 1995.
- [Att71] F. Attneave. Multistability in perception. *Scientific American*, 225(6):62–71, 1971.
- [Att85] J. Attali. *Noise: The Political Economy of Music*. University of Minnesota Press, 1985.
- [ATT90] K. Aihara, T. Takabe, and M. Toyoda. Chaotic neural networks. *Physics Letters A*, 144(6/7):333–340, March 1990.

- [Aub95] S. Aubry. Anti-integrability in dynamical and variational problems. *Physica D*, 86:284–296, 1995.
- [Bar95] M.F. Barnsley. *Fractals Everywhere*. Academic Press, New York, second edition, 1995.
- [BBH80] H.A. Braun, H. Bade, and H. Hensel. Static and dynamic discharge patterns of bursting cold fibres related to hypothetical receptor mechanisms. *Pflügers Archiv – European Journal of Physiology*, 386:1–9, 1980.
- [BBJ89] A.R. Bulsara, R.D. Boss, and E.W. Jacobs. Noise effects in an electronic model of a single neuron. *Biological Cybernetics*, 61:211–222, 1989.
- [BC97] P.C. Bressloff and S. Coombes. Physics of the extended neuron. *International Journal of Modern Physics B*, 11(20):2343–2392, 1997.
- [BCR⁺82] A. Borsellino, F. Carlini, M. Riani, M.T. Tuccio, A. DeMarco, P. Penengo, and A. Trabucco. Effects of visual angle on perspective reversal for ambiguous patterns. *Perception*, 11:263–273, 1982.
- [BDA⁺72] A. Borsellino, A. DeMarco, A. Allazetta, S. Rinesi, and B. Bartolini. Reversal time distribution in the perception of visual ambiguous stimuli. *Kybernetik*, 10:139–144, 1972.
- [BG96] A.R. Bulsara and L. Gammaitoni. Tuning in to noise. *Physics Today*, pages 39–45, March 1996.
- [BHD⁺98] H.A. Braun, M.T. Huber, M. Dewald, K. Schäffer, and K. Voigt. Computer simulations of neuronal signal transduction: The role of nonlinear dynamics and noise. *International Journal of Bifurcation and Chaos*, 8(5):881–889, 1998.
- [BJS90] A.R. Bulsara, E.W. Jacobs, and W.C. Schieve. Noise effects in a nonlinear dynamic system: the rf Superconducting Quantum Interference Device. *Physical Review A*, 42:4614–4621, 1990.

- [BJZ⁺91] A. Bulsara, E.W. Jacobs, T. Zhou, F. Moss, and L. Kiss. Stochastic resonance in a single neuron model: theory and analog simulation. *Journal of Theoretical Biology*, 152:531–555, 1991.
- [BPSV82] R. Benzi, G. Parisi, A. Sutera, and A. Vulpiani. Stochastic resonance in climatic change. *Tellus*, 34(1):10–16, 1982.
- [BR98] P.C. Bressloff and P. Roper. Stochastic dynamics of the diffusive Haken model with subthreshold periodic forcing. *Physical Review E*, 58(2):2282–2287, August 1998.
- [BR99] P.C. Bressloff and P. Roper. Stochastic resonance and bursting in a binary-threshold neuron with intrinsic noise. In R. Baddeley, P. Hancock, and P. Földiák, editors, *Information Theory and the Brain*. Cambridge University Press, 1999. In press.
- [Bre92] P.C. Bressloff. Analysis of quantal synaptic noise in neural networks using iterated function systems. *Physical Review A*, 45(10):7549–7559, May 1992.
- [Bre95] P.C. Bressloff. Neural networks, lattice instantons, and the anti-integrable limit. *Physical Review Letters*, 75(5):962–965, July 1995.
- [Bre97] P.C. Bressloff. A self-organizing network in the weak-coupling limit. *Physica D*, 110(3–4):195–208, 1997.
- [BS90] P.C. Bressloff and J. Stark. Neuronal dynamics based on discontinuous circle maps. *Physics Letters A*, 150(3,4):187–195, 1990.
- [BSV⁺97] H.A. Braun, K. Schäffer, K. Voigt, R. Peters, F. Bretschneider, X. Pei, L. Wilkens, and F. Moss. Low-dimensional dynamics in sensory biology 1: Thermally sensitive electroreceptors of the catfish. *Journal of Computational Neuroscience*, 4:335–347, 1997.
- [BSW90] H.A. Braun, K. Schäfer, and H. Wissing. Theories and models of temperature transduction. In J. Blich and K. Voigt, editors, *Thermoreception and Thermal Regulation*, pages 18–29. Springer-Verlag, 1990.

- [BSWH84] H.A. Braun, K. Schäfer, H. Wissing, and H. Hensel. Periodic transduction processes in thermosensitive receptors. In J. Blich and K. Voigt, editors, *Sensory Receptor Mechanisms*, pages 18–29. World Scientific Publishing, 1984.
- [BT90] P.C. Bressloff and J.G. Taylor. Random iterative networks. *Physical Review A*, 41(2):1126–1137, January 1990.
- [BT91] P.C. Bressloff and J.G. Taylor. Discrete-time leaky integrator network with synaptic noise. *Neural Networks*, 4(6):789–801, 1991.
- [BW86] K.L. Babcock and R.M. Westervelt. Stability and dynamics of simple electronic neural networks with added inertia. *Physica D*, 23:464–469, 1986.
- [BW87] K.L. Babcock and R.M. Westervelt. Dynamics of simple electronic neural networks. *Physica D*, 28:305–316, 1987.
- [BWSH94] H.A. Braun, H. Wissing, K. Schäfer, and M.C. Hirsch. Oscillation and noise determine signal transduction in shark multimodal sensory cells. *Nature*, 367:270–273, January 1994.
- [CA68] D.O. Carpenter and B.O. Alving. A contribution of an electrogenic Na^+ pump to membrane potential in *aplysia* neurons. *Journal of General Physiology*, 52(1):1–21, 1968.
- [CA93] D.R. Chialvo and A.V. Apkarian. Modulated noisy biological dynamics: three examples. *Journal of Statistical Physics.*, 70(1/2):375–391, 1993.
- [Car67] D.O. Carpenter. Temperature effects on pacemaker generation, membrane potential, and critical firing threshold in *aplysia* neurons. *Journal of General Physiology*, 50(6):1469–1484, 1967.
- [CBGC96] F. Chapeau-Blondeau, X. Godiver, and N. Chambert. Stochastic resonance in a neuron model that transmits spike trains. *Physical Review E*, 53(1):(1–6), January 1996.

- [CCB91] C.C. Canavier, J.W. Clark, and J.H. Byrne. Simulation of the bursting activity of neuron R15 in *aplysia*: Role of ion currents, calcium balance, modulatory transmitters. *Journal of Neurophysiology*, 66:2107–2124, 1991.
- [CFJ98] M.H. Choi, R.F. Fox, and P. Jung. Quantifying stochastic resonance in bistable systems: response vs residence time distributions. *Physical Review E*, 57(6):6335–6344, June 1998.
- [CIG96] J.J. Collins, T.T. Imhoff, and P. Grigg. Noise enhanced tactile sensation. *Nature*, 383:770, 1996.
- [CL55] E.A. Coddington and N. Levinson. *Theory of ordinary differential equations*. Mc-Graw-Hill Book Company, New York, 1955.
- [CL95] P.M. Chaikin and T.C. Lubensky. *Principles of condensed matter physics*. Cambridge University Press, 1995.
- [CM94] J.M. Casado and M. Morillo. Distribution of escape times in a driven stochastic model. *Physical Review E*, 49(2):1136–1139, 1994.
- [DeF81] L.J. DeFelice. *Introduction to Membrane Noise*. Plenum, New York, 1981.
- [DH89] T. Ditzinger and H. Haken. Oscillations in the perception of ambiguous figures – a model based on synergetics. *Biological Cybernetics*, 61:279–287, 1989.
- [DWPM93] J.K. Douglass, L. Wilkens, E. Pantazelou, and F. Moss. Noise enhancement of information transfer in crayfish mechanoreceptors by stochastic resonance. *Nature*, 365:337–340, 1993.
- [EK86] G.B. Ermentrout and N. Kopell. Parabolic bursting in an excitable system coupled with a slow oscillation. *SIAM Journal of Applied Mathematics*, 46(2):233–253, April 1986.
- [ES78] S.R. Ellis and L. Stark. Eye movements during the viewing of Necker cubes. *Perception*, 7:575–581, 1978.

- [Fis67] G.H. Fisher. Measuring ambiguity. *American Journal of Psychology*, 46(2):233–253, April 1967.
- [Fit61] R. FitzHugh. Impulses and physiological states in theoretical models of nerve membrane. *Biophysical Journal*, 1:445–466, 1961.
- [FK50] P. Fatt and B. Katz. Some observations on biological noise. *Nature*, 166:597–598, 1950.
- [FK52] P. Fatt and B. Katz. Spontaneous subthreshold activity at motor nerve endings. *Journal of Physiology*, 117:109–128, 1952.
- [Fre91] W.J. Freeman. The physiology of perception. *Scientific American*, 264(2):34–41, February 1991.
- [FY95] P. Földiák and M. P. Young. Sparse coding in the primate cortex. In M. Arbib, editor, *Handbook of Brain Theory and Neural Networks*, pages 895–898. MIT Press, 1995.
- [Gar85] C.W. Gardiner. *Handbook of Stochastic Methods*. Springer Verlag, New York, second edition, 1985.
- [GDNH93] H. Gang, T. Ditzinger, C.Z. Ning, and H. Haken. Stochastic resonance without external periodic force. *Physical Review Letters*, 71(6):807–810, August 1993.
- [GHJM98] L. Gammaitoni, P. Hänggi, P. Jung, and F. Marchesoni. Stochastic resonance. *Reviews of Modern Physics*, 70(1):223–286, January 1998.
- [GHT82] A.L.F. Gorman, A. Herman, and M.V. Thomas. Ionic requirements for membrane oscillations and their dependence on the calcium concentration in a molluscan pace-maker neuron. *Journal of Physiology*, 327:185–217, 1982.
- [Gil96a] D.T. Gillespie. The mathematics of brownian motion and johnson noise. *American Journal of Physics*, 64(3):225–240, March 1996.

- [Gil96b] D.T. Gillespie. The multi-variate langevin and fokker-planck equations. *American Journal of Physics*, 64(10):1246–1257, October 1996.
- [Gla95] L. Glass. Chaos in neural systems. In M. Arbib, editor, *Handbook of Brain Theory and Neural Networks*, pages 186–189. MIT Press, 1995.
- [Gle94] P. Glendinning. *Stability, instability and chaos*. Cambridge University Press, 1994.
- [GM64] G.L. Gerstein and B. Mandelbrot. Random walk models for the spike activity of a single neuron. *Biophysical Journal*, 4:41–68, 1964.
- [GMS95] L. Gammaitoni, F. Marchesoni, and S. Santucci. Stochastic resonance as a *bona fide* resonance. *Physical Review Letters*, 74(7):1052–1055, February 1995.
- [GNN+96] B.J. Gluckman, T.I. Netoff, E.J. Neel, W.L. Ditto, M.L. Spano, and S. J. Schiff. Stochastic resonance in a neuronal network from a mammalian brain. *Physical Review Letters*, 77(19):4098–4101, November 1996.
- [Hak87] H. Haken. Synergetic computers for pattern recognition and associative memory. In H. Haken, editor, *Computational Systems – Natural and Artificial*, pages 2–22. Springer-Verlag, 1987.
- [Hak91] H. Haken. *Synergetic Computers and Cognition*. Springer-Verlag, 1991.
- [Ham73] R. Hamming. *Numerical methods for scientists and engineers*. McGraw-Hill, second edition, 1973.
- [HCC+96] C. Heneghan, C.C. Chow, J.J. Collins, T.T. Imhoff, S.B. Lowen, and M.C. Teich. Information measures quantifying aperiodic stochastic resonance. *Physical Review E*, 54(3):R2228–R2231, 1996.
- [HH52] A.L. Hodgkin and A.F. Huxley. A quantitative description of membrane current and its application to conduction and excitation in nerve. *Journal of Physiology (London)*, 117:500–544, 1952.

- [HI97] F.C. Hoppensteadt and E.M. Izhikevich. *Weakly Connected Neural Networks*, volume 126 of *Applied Mathematical Sciences*. Springer–Verlag, New York, 1997.
- [HJ95] P. Hänggi and P. Jung. Colored noise in dynamical systems. *Advances in Chemical Physics*, 89:239–326, 1995.
- [HKP91] J. Hertz, A. Krogh, and R.G. Palmer. *Introduction to the theory of neural computation*. Addison–Wesley, 1991.
- [HLQ69] J.I. Hubbard, R. Llinás, and D.M.J. Quastel. *Electrophysiological Analysis of Synaptic Transmission*, volume 19 of *Monographs of the Physiological Society*. Camelot Press, London, 1969.
- [Hol76] A.V. Holden. *Models of the stochastic activity of neurons*, volume 12 of *Lecture Notes in Biomathematics*. Springer–Verlag, Berlin, 1976.
- [Hop82] J.J. Hopfield. Neural networks and physical systems with emergent collective computational abilities. *Proceedings of the National Academy of Science USA.*, 79:2554–2558, April 1982.
- [HR84] J.L. Hindmarsh and R.M. Rose. A model of neuronal bursting using 3 coupled 1st order differential equations. *Proceedings of the Royal Society of London Series B–Biological Sciences*, 221(1222):87–102, 1984.
- [HTB90] P. Hänggi, P. Talkner, and M. Borkovec. Reaction–rate theory: fifty years after Kramers. *Reviews of Modern Physics*, 62(2):251–341, April 1990.
- [Iva90] K.P. Ivanov. The location and function of different skin thermoreceptors. In J. Bligh and K. Voigt, editors, *Thermoreception and Thermal Regulation*, pages 37–43. Springer–Verlag, 1990.
- [JNT75] J.J.B. Jack, D. Noble, and R.W. Tsien. *Electric Current Flow in Excitable Cells*. Clarendon Press, Oxford, 1975.

- [JS87] D.W. Jordan and P. Smith. *Nonlinear Ordinary Differential Equations*. Oxford Applied Mathematics and Computing Science Series. Clarendon Press, Oxford, second edition, 1987.
- [Kan89] E.R. Kandel. Small systems of neurons. In R.R. Llinas, editor, *The biology of the brain from neurons to networks*, pages 70–86. Scientific American, 1989.
- [Kat66] B. Katz. *Nerve, muscle and synapse*. McGraw–Hill, New York, 1966.
- [KF87] H. Korn and D.S. Faber. Regulation and significance of probabilistic mechanisms at central synapses. In W.M. Edelman, W. Gall, and W.M. Cowan, editors, *Synaptic functions*, pages 57–108. John Wiley and Sons, 1987.
- [KM72] B. Katz and R. Miledi. The statistical nature of the acetylcholine potential and its molecular components. *Journal of Physiology*, 224:665–700, 1972.
- [KNS⁺79] J.H. Kaas, R.J. Nelson, M. Sur, C.S. Lin, and M.M. Merzenich. Multiple representations of the body within the primary somatosensory cortex of primates. *Science*, 204:521–523, May 1979.
- [Koh82] T. Kohonen. Self–organized formation of topologically correct feature maps. *Biological Cybernetics*, 43(1):59–69, 1982.
- [Koh84] T. Kohonen. *Self organisation and Associative Memory*. Springer–Verlag, 1984.
- [KSJ91] E.R. Kandel, J.H. Schwartz, and T.M. Jessel. *Principles of Neural Science*. Elsevier Science, New York, third edition, 1991.
- [Lán97] P. Lánský. Sources of periodical force in noisy integrate–and–fire models of neuronal dynamics. *Physical Review E*, 55(2):2040–2043, February 1997.
- [Lap07] L. Lapicque. Recherches quantitatives sur l’excitation électrique des nerfs traitée comme une polarisation. *Journal de Physiologie et de Pathologie Generale*, 9:620–635, 1907.

- [LBM91] A. Longtin, A.R. Bulsara, and F. Moss. Time-interval sequences in bistable systems and the noise-induced transmission of information by sensory neurons. *Physical Review Letters*, 67(52):656–659, July 1991.
- [LH96] A. Longtin and K. Hinzer. Encoding with bursting, subthreshold oscillations, and noise in mammalian cold receptors. *Neural Computation*, 8:215–255, 1996.
- [Lis97] J.E. Lisman. Bursts as a reliable unit of neural information: making unreliable synapses reliable. *Trends in Neuroscience*, 20(1):38–43, January 1997.
- [Lit74] W.A. Little. The existence of persistent states in the brain. *Mathematical Biosciences*, 19:101–120, 1974.
- [LM74] I. Lundström and D. McQueen. A proposed 1/f noise mechanism in nerve cell membranes. *Journal of Theoretical Biology*, 45:405–409, 1974.
- [LM96] J.E. Levin and J.P. Miller. Broadband neural encoding in the cricket cercal sensory system enhanced by stochastic resonance. *Nature*, 380:165–168, March 1996.
- [LMD⁺95] J.F. Lindner, B.K. Meadows, W.L. Ditto, M.E. Inchiosa, and A.R. Bulsara. Array enhanced stochastic resonance and spatiotemporal synchronization. *Physical Review Letters*, 75(1):3–6, July 1995.
- [LN71a] H. Lecar and R. Nossal. Theory of threshold fluctuations in nerves: II analysis of various sources of membrane noise. *Biophysical Journal*, 11:1068–1084, 1971.
- [LN71b] H. Lecar and R. Nossal. Theory of threshold fluctuations in nerves: II relationships between electrical noise and fluctuations in axon firing. *Biophysical Journal*, 11:1048–1067, 1971.
- [Lon97] A. Longtin. Autonomous stochastic resonance in bursting neurons. *Physical Review E*, 55(1):868–876, January 1997.

- [Man89] R. Mannella. Computer experiments in nonlinear stochastic physics. In F. Moss and P.V.E. McClintock, editors, *Noise in nonlinear dynamical systems: Experiments and simulations*, volume 3, pages 189–217. Cambridge University Press, 1989.
- [Man97] R. Mannella. Numerical integration of stochastic differential equations. Unpublished, 1997.
- [McL47] N.W. McLachlan. *Theory and Application of Mathieu Functions*. Clarendon Press, Oxford, 1947.
- [Mel94] B.W. Mel. Information processing in dendritic trees. *Neural Computation*, 6:1031–1085, 1994.
- [MK78] G. Matsumoto and T. Kunisawa. Critical slowing down near the transition region from the resting to time-ordered states in giant squid axons. *Journal of the Physical Society of Japan*, 44(3):1047–1048, March 1978.
- [Mos94] F. Moss. Stochastic resonance: from the ice ages to the monkey’s ear. In G.H. Weiss, editor, *Contemporary problems in Statistical Physics.*, chapter 5, pages 205–253. SIAM, Philadelphia, 1994.
- [MPO94] F. Moss, D. Pierson, and D. O’Gorman. Stochastic resonance: tutorial and update. *International Journal of Bifurcation and Chaos*, 4(6):1383–1397, 1994.
- [MS95] R.S. MacKay and J. A. Sepulchre. Multistability in networks of weakly coupled bistable units. *Physica D*, 82:243–254, 1995.
- [MS96a] R.S. Maier and D.L. Stein. The weak-noise characteristic boundary exit problem: old and new results. In M. Millonas, editor, *Fluctuations and Order: The New Synthesis*, pages 109–118. Springer-Verlag, 1996.
- [MS96b] R.N. Mantegna and B. Spagnolo. Noise enhanced stability in an unstable system. *Physical Review Letters*, 76(4):563–566, January 1996.

- [MW89] B. McNamara and K. Wiesenfeld. Theory of stochastic resonance. *Physical Review A*, 39(9):4854–4869, May 1989.
- [Nec32] L.A. Necker. Observations on some remarkable phenomenon which occurs on viewing a figure of a crystal or geometrical solid. *The London and Edinburgh Philosophical Magazine and Journal of Science*, 3:329–337, 1832.
- [NK86] S.T. Neely and D.O. Kim. A model for active elements in cochlear biomechanics. *Journal of the Acoustical Society of America*, 79(5):1472–1480, 1986.
- [NM95] A.H. Nayfeh and D.T. Mook. *Nonlinear Oscillations*. Wiley Classics Library. John Wiley and Sons, 1995.
- [NS72] J. Nagumo and S. Sato. On a response characteristic of a mathematical neuron model. *Kybernetik*, 10:155–164, 1972.
- [NSS97] A. Neiman, P.I. Sapsin, and L. Stone. Coherence resonance at noisy precursors of bifurcations in nonlinear system. *Physical Review E*, 56(1):270–273, July 1997.
- [OC93] T. Ohira and J. Cowan. Master equation approach to stochastic neurodynamics. *Physical Review E*, 48:2259–2266, 1993.
- [OC95] T. Ohira and J. Cowan. Stochastic single neurons. *Neural Computation*, 7:518–528, 1995.
- [Pec39] Ch. Pecher. La fluctuation d’excitabilité de la fibre nerveuse. *Archives Internationales de Physiologie*, 49:129–152, 1939.
- [Per92] P. Peretto. *An Introduction to the Modelling of Neural Networks*. Monographs and Texts in Statistical Physics. Cambridge University Press, 1992.
- [Pla81] R.E. Plant. Bifurcation and resonance in a model for bursting nerve-cells. *Journal of Mathematical Biology*, 11(15):15–32, 1981.

- [PM88] S. Park and K. Miller. Random number generators: Good ones are hard to find. *Communications of the Association for Computing Machinery*, 31(10):1192–1201, 1988.
- [PTVF92] W.H. Press, S.A. Teukolsky, W.T. Vetterling, and B.P. Flannery. *Numerical Recipes in C: the Art of Scientific Computing*. Cambridge University Press, second edition, 1992.
- [RBL98] P. Roper, P.C. Bressloff, and A. Longtin. A phase model of temperature-dependent mammalian cold receptors. *Neural Computation*, 1998. Submitted.
- [Rei98] L. Reichl. *A Modern Course in Statistical Physics*. Wiley–Interscience, New York, second edition, 1998.
- [Ric54] S.O. Rice. Mathematical analysis of random noise. In N. Wax, editor, *Selected Papers on Noise and Stochastic Processes*, pages 133–294. Dover Publications, 1954.
- [Ric95] L.M. Ricciardi. Diffusion models of neuron activity. In M. Arbib, editor, *Handbook of Brain Theory and Neural Networks*, pages 299–304. MIT Press, 1995.
- [Rin87] J. Rinzel. A formal classification of bursting mechanisms in excitable systems. In E. Teramoto and M. Yamaguti, editors, *Mathematical Topics in Population Biology, Morphogenesis and Neurosciences*, number 71 in Lecture Notes in Biomathematics, pages 267–281. Springer–Verlag, 1987.
- [Ris89] H. Risken. *The Fokker–Planck Equation*. Springer Verlag, New York, second edition, 1989.
- [RL87] J. Rinzel and Y.S. Lee. Dissection of a model for neuronal parabolic bursting. *Journal of Mathematical Biology*, 25:653–675, 1987.
- [RL93] J.P. Rospars and P. Lánský. Stochastic model neuron without resetting of dendritic potential: application to the olfactory system. *Biological Cybernetics*, 69:283–294, 1993.

- [RS94a] W. Rappel and S.H. Strogatz. Stochastic resonance in an autonomous system with a nonuniform limit cycle. *Physical Review E*, 50(4):3249–3250, 1994.
- [RS94b] M. Riani and E. Simonotto. Stochastic resonance in the perceptual interpretation of ambiguous figures – a neural-network model. *Physical Review Letters*, 72(19):3120–3123, 1994.
- [RS95] M. Riani and E. Simonotto. Periodic perturbation of ambiguous figure – a neural-network model and a non-simulated experiment. *Il Nuovo Cimento D*, 17(7–8):903–913, 1995.
- [RSMH86] D.E. Rumelhart, P. Smolensky, J.L. McClelland, and G.E. Hinton. *Parallel Distributed Processing.*, volume 2. MIT Press, 1986.
- [RWdRvSB97] F. Rieke, D. Warland, Rob de Ruyter van Steveninck, and W. Bialek. *Spikes – exploring the neural code.* MIT Press, 1997.
- [SB90] K. Schäfer and H.A. Braun. Modulation of periodic cold receptor activity by ouabain. *Pflügers Archiv – European Journal of Physiology*, 417:91–99, 1990.
- [SB92] M. Schmutz and W. Banzhaf. Robust competitive networks. *Physical Review A*, 45(6):4132–4145, March 1992.
- [SBD91] W.C. Schieve, A.R. Bulsara, and G.M. Davis. Single effective neuron. *Physical Review A*, 43(6):2613–2623, March 1991.
- [SBH82] K. Schäfer, H.A. Braun, and H. Hensel. Static and dynamic activity of cold receptors at various calcium levels. *Journal of Neurophysiology*, 47(6):1017–1028, June 1982.
- [SBR88] K. Schäfer, H.A. Braun, and L. Rempe. Classification of a calcium conductance in cold receptors. *Progress in Brain Research*, 74:29–36, 1988.

- [SBR90] K. Schäfer, H.A. Braun, and L. Rempe. Mechanisms of sensory transduction in cold receptors. In J. Bligh and K. Voigt, editors, *Thermoreception and Thermal Regulation*, pages 30–36. Springer–Verlag, 1990.
- [SH95] G. Schöner and H. Hock. Concepts for a dynamic theory of perceptual organization: an example from apparent motion. In P. Kruse and M. Stadler, editors, *Ambiguity in Mind and Nature*, pages 275–310. Springer Verlag, 1995.
- [She87] R.N. Shepherd. Towards a Universal Law of Generalization for psychological science. *Science*, 237:1317–1323, September 1987.
- [She94] G.M. Shepherd. *Neurobiology*. Oxford University Press, third edition, 1994.
- [Sig88] D.E. Sigesti. *Universal results for the effects of noise on dynamical systems*. PhD thesis, Department of Physics, The University of Texas at Austin, 1988.
- [SK86] S. Shimonoto and Y. Kuramoto. Phase transitions in active rotator systems. *Progress of Theoretical Physics*, 75(5):1105–1110, 1986.
- [SK95] M. Stadler and P. Kruse. The function of meaning in cognitive order formation. In P. Kruse and M. Stadler, editors, *Ambiguity in Mind and Nature*, pages 5–21. Springer Verlag, 1995.
- [Str94] S.H. Strogatz. *Nonlinear Dynamics and Chaos*. Addison–Wesley, Reading, MA, 1994.
- [Swi96] N.V. Swindale. The development of topography in the visual–cortex – a review of models. *Network – Computation In Neural Systems*, 7(2):161–247, 1996.
- [TLM⁺88] R.W. Tsien, D. Lipscombe, D.V. Madison, K.R. Bley, and A.P. Fox. Multiple types of neuronal calcium channels and their selective modulation. *Trends in Neuroscience*, 11(10):431–437, 1988.

- [Tuc88] H.C. Tuckwell. *Introduction to Theoretical Neurobiology*, volume 1 of *Cambridge Studies in Mathematical Biology*. Cambridge University Press, 1988.
- [VD68] A.A. Verveen and H.E. Derksen. Fluctuation phenomena in nerve membrane. *Proceedings of the IEEE.*, 56(6):906–916, June 1968.
- [vdM73] C. von der Malsburg. Self-organization of orientation sensitive cells in the striate cortex. *Kybernetik*, 14:85–100, 1973.
- [Ver61] A.A. Verveen. *Fluctuations in Excitability: Research Report on Signal Transduction in Nerve Fibres*. PhD thesis, Netherlands Central Institute for Brain Research, Amsterdam, 1961.
- [vK76] N.G. van Kampen. The expansion of the master equation. *Advances in Chemical Physics*, 34:245–309, 1976.
- [vK92] N.G. van Kampen. *Stochastic processes in Physics and Chemistry*. North-Holland, 1992.
- [Wal91] P.M.B. Walker. *Chambers Science and Technology Dictionary*. Chambers, Edinburgh, 1991.
- [WC82] M.L. Wiederhold and D.O. Carpenter. Possible role of pacemaker mechanisms in sensory systems. In D.O. Carpenter, editor, *Cellular Pacemakers*, volume 2, pages 27–58. Wiley-Interscience, 1982.
- [WC94] C.W. Wu and L.O. Chua. Symbolic dynamics of piecewise-linear maps. *IEEE Transactions on Circuits and Systems II – Analog and Digital Signal Processing*, 41(6):420–424, 1994.
- [WGC74] J.A. Willis, G.L. Gaubatz, and D.O. Carpenter. The role of the electrogenic pump in modulation of pacemaker discharge of *aplysia* neurons. *Journal of Cellular Physiology*, 84:463–471, 1974.
- [Wie85] K. Wiesenfeld. Noisy precursors of nonlinear instabilities. *Journal of Statistical Physics*, 38(5/6):1071–1097, 1985.

-
- [WJ98] K. Wiesenfeld and F. Jaramillo. Minireview of stochastic resonance. *Chaos*, 8(3):539–548, September 1998.
- [WM95] K. Wiesenfeld and F. Moss. Stochastic resonance and the benefits of background noise: from ice ages to crayfish and squids. *Nature*, 373:33–36, January 1995.
- [WR95] X.J. Wang and J. Rinzel. Oscillatory and bursting properties of neurons. In M. Arbib, editor, *Handbook of Brain Theory and Neural Networks*. MIT Press, 1995.
- [WW74] W.A. Wilson and H. Wachtel. Negative resistance characteristic essential for the maintenance of slow oscillations in bursting neurons. *Science*, 186:932–934, 1974.
- [ZMJ90] T. Zhou, F. Moss, and P. Jung. Escape-time distributions of a periodically modulated bistable system with noise. *Physical Review A*, 42(6):3161–3169, September 1990.